



Publicly Accessible Penn Dissertations

1-1-2013

Mechanistic Studies of the Elongation Cycle of Protein Synthesis

Wei Liu

University of Pennsylvania, weiliu@sas.upenn.edu

Follow this and additional works at: <http://repository.upenn.edu/edissertations>

 Part of the [Biochemistry Commons](#)

Recommended Citation

Liu, Wei, "Mechanistic Studies of the Elongation Cycle of Protein Synthesis" (2013). *Publicly Accessible Penn Dissertations*. 887.
<http://repository.upenn.edu/edissertations/887>

This paper is posted at ScholarlyCommons. <http://repository.upenn.edu/edissertations/887>
For more information, please contact libraryrepository@pobox.upenn.edu.

Mechanistic Studies of the Elongation Cycle of Protein Synthesis

Abstract

During translation elongation, amino acid residues are repetitively added to the growing nascent peptide chain, directed by the mRNA sequence and facilitated by two elongation factors, EF-Tu and EF-G. In this thesis, translation elongation is investigated from two new perspectives to further explore the underlying mechanisms.

In the first approach, a functional EF-Tu derivative labeled with a fluorescence quencher was prepared and used for the development of two fluorescent assays to study EF-Tu:L11 and EF-Tu:tRNA FRET signals. Application of these two assays revealed the tRNA discrimination on the ribosomal A-site, the effects of error-inducing antibiotics on tRNA selection, and tRNA release from EF-Tu on the ribosome regulated by EF-Tu:tRNA affinity. In combination with other assays measuring pre-translocation complex formation, ensemble and single molecule FRET studies of the EF-Tu:L11:tRNA triangle indicated that EF-Tu:L11 separation occurs concurrently with inorganic phosphate release and tRNA accommodation, but prior to EF-Tu separation from tRNA and dissociation from the ribosome. The latter process proceeds through two possible pathways, rapid but reversible dissociation followed by a conformational change off the ribosome versus slow conformational change on the ribosome followed by rapid dissociation.

Translation elongation was also studied using mRNAs specifically modified with fluorescent isomorphous nucleoside mimetics. These modified mRNAs maintain considerable functionalities in the formation of initiation, pre-translocation and post-translocation complexes, although with different efficiencies, and show fluorescence changes in different patterns upon ribosomal complex conversion. Pre-steady state measurements of these fluorescence changes demonstrate the responses of modified mRNAs to codon:anticodon interaction occurring after ternary complex initial binding to the ribosome but before tRNA accommodation into the A-site, and mRNA movements on the ribosome during translocation.

Degree Type

Dissertation

Degree Name

Doctor of Philosophy (PhD)

Graduate Group

Chemistry

First Advisor

Barry S. Cooperman

Keywords

EF-Tu, fluorescence, kinetics, mRNA, Ribosome

Subject Categories

Biochemistry

**MECHANISTIC STUDIES OF THE ELONGATION CYCLE
OF PROTEIN SYNTHESIS**

Wei Liu

A DISSERTATION

in

Chemistry

Presented to the Faculties of the University of Pennsylvania

in

Partial Fulfillment of the Requirements for the

Degree of Doctor of Philosophy

2013

Supervisor of Dissertation

Dr. Barry S. Cooperman

Professor of Chemistry

Graduate Group Chairperson

Dr. Gary A. Molander, Professor of Chemistry

Dissertation Committee

Dr. Ivan J. Dmochowski, Associate Professor of Chemistry

Dr. Christopher B. Murray, Professor of Chemistry and Materials Science and
Engineering

Dr. E. James Petersson, Assistant Professor of Chemistry

MECHANISTIC STUDIES OF THE ELONGATION CYCLE OF PROTEIN
SYNTHESIS

COPYRIGHT

2013

Wei Liu

Dedicated to my wife Ji Qi, my father Zhiqun Liu, and my mother Darong Wang.

ACKNOWLEDGMENTS

Six years ago, I came to U.S. after I obtained my Master's Degree, with my dissertation focusing on canonical coordination chemistry. I wanted to do something different from what I did in China, and joined Professor Barry S. Cooperman's laboratory. Six years later, at the moment of finishing my Ph.D. degree, I want to express my great gratitude to Dr. Cooperman, for his guidance and support throughout my study in Penn Chemistry. With his supervision, I have learned how to critically think of research and to religiously treat scientific problems. His inspiration and immense knowledge make possible the accomplishment of this dissertation and my successful transition from a chemist to a biochemist. After the working of full delight in Dr. Cooperman's lab, I find where my interest is and how I should pursue my future career.

I feel greatly proud to complete my dissertation under the help of all of my committee members, Prof. Ivan J. Dmochowski, Prof. Christopher B. Murray and Prof. E. James Petersson. I learned how to look into my research from multiple perspectives from the communication with all of them on my annual committee meetings. The accomplishment of my dissertation would become impossible without their kindhearted support and important advices.

I also want to thank all of my collaborators for their support for my experiments. Dr. Yale E. Goldman at School of Medicine of University of Pennsylvania helped me

on smFRET studies of my research. His inspiration and helpful suggestions make significant contributions to my research projects. Prof. Wlodek Mandecki and Dr. Joanna Perła-Kaján at University of Medicine & Dentistry of New Jersey provided plasmids for EF-Tu variants. Prof. Olke C. Uhlenbeck and Dr. Jared M. Schrader at Northwestern University provided tRNA^{Val2B} variants and helped on EF-Tu:tRNA interface studies. Prof. Charlotte R. Knudsen and Dr. Darius Kavaliauskas at Aarhus University collaborated with me and provided useful comments on EF-Tu project. Prof. Yitzhak Tor and Dr. Dongwon Shin at University of California, San Diego provided modified mRNAs and collaborated with me on that project. I also got useful advice and interesting ideas from meeting with Prof. Akira Kaji at School of Medicine of University of Pennsylvania.

My growth to a biochemist benefits from pleasant working with all the past and present group members. Dr. Ian Farrell led my first step into biochemistry world by teaching me many basic biochemical techniques, and helped me on tRNA purification. Dr. Jaskiran Kaur taught me how to deal with tRNA and label them with small molecules. I learned how to perform kinetic experiments and analyze kinetic data from Dr. Hanqing Liu, and she also generously shared her talented experience in kinetic data fitting with me. Dr. Chunlai Chen helped me on single molecule experiments, taught me how to mathematically and statistically manipulate single molecule data, and provided helpful comments on my research. I work closely with Dr. Dulce Alonso to investigate labeling tRNA with transitional metal for translation imaging. Dr. Haiou Qin taught me FRET technique and Mr. Michael Reiche provided

mRNA sequence for my studies. Ms. Nora Zuno and Dr. Rajani Shetty provided me ribosome and other components for my studies. I also obtained many suggestion and ideas from the helpful discussion with Dr. Gabriel Rosenblum, Ms. Rong Shen, Mr. Yuanwei Chen and Mr. Martin Ng.

Finally, I would like to express my deep gratitude to my family, for their sacrifice in supporting my study and research. I want to specially thank my wife Ji Qi. We met and got married during my Ph.D.study, and this was my greatest achievement in the last six years, of proud and happiness. Whatever happened to me, excited and frustrated, happy and sorrowful, she always stood besides me, with encouragement and support. I enjoyed every talk with her, receiving selfless advices on both science and life. I also want to thank my parents, who sacrificed the time for family reunion to support my research. Their guidance and suggestions removed the confusion standing in front of me and highlighted the pathway for my future career development.

Only because of the support and help from everyone at every respect in the last six years, can I successfully perform my research and complete this dissertation.

ABSTRACT

MECHANISTIC STUDIES OF THE ELONGATION CYCLE OF PROTEIN SYNTHESIS

Wei Liu

Barry S. Cooperman

During translation elongation, amino acid residues are repetitively added to the growing nascent peptide chain, directed by the mRNA sequence and facilitated by two elongation factors, EF-Tu and EF-G. In this thesis, translation elongation is investigated from two new perspectives to further explore the underlying mechanisms.

In the first approach, a functional EF-Tu derivative labeled with a fluorescence quencher was prepared and used for the development of two fluorescent assays to study EF-Tu:L11 and EF-Tu:tRNA FRET signals. Application of these two assays revealed the tRNA discrimination on the ribosomal A-site, the effects of error-inducing antibiotics on tRNA selection, and tRNA release from EF-Tu on the ribosome regulated by EF-Tu:tRNA affinity. In combination with other assays measuring pre-translocation complex formation, ensemble and single molecule FRET studies of the EF-Tu:L11:tRNA triangle indicated that EF-Tu:L11 separation occurs concurrently with inorganic phosphate release and tRNA accommodation, but prior to EF-Tu separation from tRNA and dissociation from the ribosome. The latter process

proceeds through two possible pathways, rapid but reversible dissociation followed by a conformational change off the ribosome versus slow conformational change on the ribosome followed by rapid dissociation.

Translation elongation was also studied using mRNAs specifically modified with fluorescent isomorphous nucleoside mimetics. These modified mRNAs maintain considerable functionalities in the formation of initiation, pre-translocation and post-translocation complexes, although with different efficiencies, and show fluorescence changes in different patterns upon ribosomal complex conversion. Pre-steady state measurements of these fluorescence changes demonstrate the responses of modified mRNAs to codon:anticodon interaction occurring after ternary complex initial binding to the ribosome but before tRNA accommodation into the A-site, and mRNA movements on the ribosome during translocation.

TABEL OF CONTENTS

ACKNOWLEDGMENT	IV
ABSTRACT.....	VII
LIST OF TABLES.....	XV
LIST OF ILLUSTRATIONS.....	XVI
CHAPTER 1. INTRODUCTION.....	1
1.1 Gene expression and the central dogma	2
1.2 Prokaryotic ribosome	3
1.3 Translation cycle	4
1.4 Crystallographic studies of the ribosome.....	8
1.5 Kinetic studies examing ribosome function	10
1.6 Monitoring ribosomal translation with smFRET	12
1.7 EF-Tu in translation elongation	14
1.8 Fidelity control throughout protein synthesis and antibiotics	16
1.9 Emissive nucleoside mimetics	18
1.10 Frameshifting in translation	19
CHAPTER 2. MATERIALS AND METHODS	28
2.1 Materials	29
2.1.1 Buffers.....	29
2.1.2 Reagents.....	31
2.2 Methods.....	32
2.2.1 Preparation of proteins.....	33

2.2.1.1 Purification of IF3.....	33
2.2.1.2 Purification and labeling of L11(C38S/S87C)	34
2.2.2 Preparation of EF-Tu variants and their derivatives	35
2.2.2.1 Purification of EF-Tu variants.....	35
2.2.2.2 Labeling of EF-Tu with quencher or fluorophore	36
2.2.2.3 Functional analysis of EF-Tu variants	37
2.2.3 Preparation of mRNAs	38
2.2.3.1 Preparation of mRNA 022 MFTI and 022 CUC	39
2.2.3.2 Preparation of mRNA MRF and MVF	39
2.2.3.3 Preparation of mRNA MVYF and MKF	40
2.2.4 Preparation of tRNAs	41
2.2.4.1 Preparation of formyl donor	41
2.2.4.2 Purification of <i>E. coli</i> tRNA ^{fMet} from bulk tRNAs	42
2.2.4.3 Formylaminoacylation of tRNA ^{fMet}	43
2.2.4.4 Aminoacylation of tRNA ^{Phe}	44
2.2.4.5 Preparation of yeast AcPhe-tRNA ^{Phe}	45
2.2.4.6 Aminoacylation of <i>E.coli</i> tRNA ^{Val} , tRNA ^{Arg} and tRNA ^{Lys}	46
2.2.4.7 Aminoacylation of tRNA ^{Val2B} variants	46
2.2.4.8 tRNA labeling with proflavin.....	46
2.2.4.9 tRNA ^{Phe} labeling with Cy3	47
2.2.4.10 Preparation of highly labeled tRNA ^{Phe} with Cy5	48
2.2.5 Preparation of the 70S ribosomal complex and ternary complex	48
2.2.5.1 Preparation of the 70S ribosome labeled with Cy3 or Cy5	49
2.2.5.2 Preparation of ribosomal complex and ternary complex.....	49
2.2.5.3 Purification of ternary complex.....	53

2.2.6 Fluorescence experiments	53
2.2.6.1 Static fluorescence experiments.....	53
2.2.6.2 Stopped-slow experiments.....	54
2.2.6.3 Single-molecule experiments.....	55
2.2.7 Quenched-flow experiments.....	56

CHAPTER 3. LABELED EF-TUS FOR RAPID KINETIC STUDIES OF PRE-TRANSLOCATION COMPLEX FORMATION.....61

3.1 Abstract.....	62
3.2 Introduction.....	63
3.3 Results	65
3.3.1 Nomenclature	65
3.3.2 Probe-labeled EF-Tu variants and their formation of TCs with Phe-tRNA ^{Phe}	65
3.3.3 Interaction of TCs containing labeled EF-Tu with 70SICs.....	68
3.3.4 Kirromycin and GTP hydrolysis effects on TC interaction with 70SIC.....	69
3.3.5 tRNA misreading	70
3.3.6 Altering EF-Tu:aa-tRNA interaction.....	73
3.4 Discussion	76
3.5 Conclusions.....	83

CHAPTER 4. EF-TU DYNAMICS DURING PRE-TRANSLOCATION COMPLEX FORMATION: EF-TU.GDP DISSOCIATIONS VIA TWO DIFFERENT PATHWAYS99

4.1 Abstract.....	100
4.2 Introduction.....	101
4.3 Results	102
4.3.1 Labeled component nomenclature	102

4.3.2 Ensemble experiments	103
4.3.3 Single molecule FRET studies of PRE complex formation	105
4.3.4 A simplified quantitative model for TC interaction with 70SIC leading to PRE complex formation	106
4.3.5 The timing of EF-Tu conformational change	109
4.4 Discussion	110
4.5 Conclusions.....	114
CHAPTER 5. MONITORING TRANSLATION WITH MODIFIED MRNAS STRATEGICALLY LABELED WITH ISOMORPIC FLUORESCENT NUCLEOSIDE MIMETICS	128
5.1 Abstract.....	129
5.2 Introduction.....	130
5.3 Results	132
5.3.1 Modified mRNAs	132
5.3.2 Formation of functional initiation and elongation complexes.....	133
5.3.3 Fluorescence changes on functional complex formation	133
5.3.3.1 Fluorescence changes of mRNA binding to the ribosome	134
5.3.3.2 Fluorescence changes of 70SIC conversion to PRE complex	134
5.3.3.3 Fluorescence changes of PRE conversion to POST complex	135
5.3.4 Kinetics of PRE complex formation	136
5.3.4.1 th G4- and th G6-programmed ribosomes	137
5.3.4.2 th G5-programmed ribosomes	139
5.3.4.3 th A4- and th A6-programmed ribosomes	139
5.3.4.4 th A1-programmed ribosomes	140
5.3.4.5 th A5-programmed ribosomes	141

5.3.5 Kinetics of POST complex formation.....	143
5.3.5.1 th G-programmed ribosomes	143
5.3.5.2 th A-programmed ribosomes	144
5.4 Discussion	145
5.4.1 Functional activities	145
5.4.2 Fluorescence changes.....	146
5.4.3 Kinetics	147
5.4.4 Substitution at the middle codon position – Effects on PRE complex formation .	149
5.5 Conclusions.....	152

APPENDIX I. MONITORING TRANSLATION WITH MODIFIED MRNAS STRATEGICALLY LABELED WITH ISOMORPHIC FLUORESCENT URIDINE AND CYTIDINE MIMETICS176

I.1 Abstract.....	177
I.2 Introduction	178
I.3 Results	177
I.3.1 Modified mRNAs.....	178
I.3.2 Formation of functional initiation and elongation complexes	179
I.3.3 Fluorescence changes on functional complex formation.....	179
I.3.4 Kinetics of PRE complex formation	180
I.4 Experimental.....	181
I.5 Conclusions	182

APPENDIX II. RIBOSOME LABELING WITH GOLD PARTICLE FOR TRANSLATION IMAGING189

II.1 Abstract	190
II.2 Introduction.....	190

II.3 Results	191
II.3.1 L1 labeling with Au particle	191
II.3.2 Reconstitution of functional 50S ribosome	192
II.4 Experimental	193
II.4.1 Purification of L1 variants	193
II.4.2 Labeling of L1(S40C) and the 50S subunit with Au particle	194
II.4.3 Activity of Au labeled ribosome in poly(phe) synthesis.....	195
II.5 Conclustions	196
 BIBLIOGRAPHY	 201

LIST OF TABLES

Tabel 1.1. Components of <i>E. coli</i> ribosomes	21
Tabel 3.1. Labeled protein synthesis components	85
Tabel 3.2. Labeling stoichiometries of EF-Tu variants.....	86
Tabel 3.3. Kinetic parameters for EF-Tu:L11 or EF-Tu:tRNA FRET experiments	87
Tabel 3.4. Thermodynamic and kinetic parameters for tRNA^{Val2B} variants.....	89
Tabel 4.1. Labeled Ternary Complexes (TCs).....	115
Tabel 4.2. Comparison of apparent rate constants between TC^{QSY9/Cy3} and fMet-tRNA^{fMet}(prf).....	116
Tabel 4.3. Fitted rate constants for Scheme	117
Tabel 5.1. Static fluorescence intensity changes during conversions between different ribosome complexes	153
Tabel 5.2. Apparent rate constants for reactions between 70SIC programmed with thG-containing mRNAs and TC	154
Tabel 5.3. Apparent rate constants for reactions between 70SIC programmed with thA-containing mRNAs and TC.....	156
Tabel 5.4. Microscopic rate constants (s⁻¹) for 70SIC reaction with TC	158
Tabel 5.5. Apparent rate constants for POST complex formation on reaction of PRE complex programmed with thG- and thA-containing mRNAs and EF-G.GTP	159
Tabel I.1. Apparent rate constants for reactions between 70SIC programmed with thU- and thC-containing mRNAs and TC	183

LIST OF ILLUSTRATIONS

Figure 1.1. Central dogma of molecular biology	22
Figure 1.2. Three-dimensional structures of the two ribosomal subunits.....	23
Figure 1.3. Overview of translation cycle.....	24
Figure 1.4. mRNA bound to the ribosome initiation complex.....	25
Figure 1.5. Representative scheme of peptide bond formation and translocation	26
Figure 1.6. Emissive RNA alphabet.....	27
Figure 2.1. Electrophoretic analysis of purified mRNA	58
Figure 2.2. Unmodified mRNA sequence.....	60
Figure 3.1. Distances within EF-Tu:L11:aa-tRNA triangle	90
Figure 3.2. Characterization of ternary complexes (TCs) formed by labeled EF-Tus ..	91
Figure 3.3. FRET in TCs formed from E348C-EF-Tu ^{QSY9} variants and Phe-tRNA ^{Phe} (Cy3).....	92
Figure 3.4. Dipeptide formation of E348C-EF-Tu ^{QSY9}	93
Figure 3.5. Labeled TC Interaction with 70SIC ^{Cy3}	94
Figure 3.6. Interaction of double-labeled TC with 70SIC	95
Figure 3.7. Transfer RNA selection and antibiotic effects.....	96
Figure 3.8. Effects of tRNA ^{Val2B} mutation	97
Figure 3.9. Concentration dependent EF-Tu:L11 FRET of tightly coupled ternary complex	98
Figure 4.1. Ensemble studies of TC ^{QSY9} reaction with 70SIC ^{Cy3}	118
Figure 4.2. Concentration dependence of EF-Tu:L11 FRET.....	119
Figure 4.3. Ensemble studies of TC ^{QSY9/Cy3} reaction with 70SIC.....	121

Figure 4.4. Real-time courses of single molecule fluorescence intensities and FRET ..	122
Figure 4.5. Synchronized smFRET values	124
Figure 4.6. Association and dissociation times and rate constants for TC interaction with immobilized 70SIC	126
Figure 4.7. A simplified quantitative model for TC interaction with 70SIC	127
Figure 5.1. mRNAs labeled with isomorphous fluorescent nucleoside mimetics	160
Figure 5.2. Activities of mRNAs containing thG	162
Figure 5.3. Activities of mRNAs containing thA.....	163
Figure 5.4. Excitation and emission spectra of thG- and thA-containing mRNAs	165
Figure 5.5. Fluorescence changes of thG-containing mRNAs	167
Figure 5.6. Fluorescence changes of thA-containing mRNAs.....	169
Figure 5.7. Lack of fluorescence change on adding non-cognate TCs to 70SICs programmed with thG-containing mRNAs	170
Figure 5.8. Lack of fluorescence change on adding non-cognate TCs to 70SICs programmed with thA-containing mRNAs.....	171
Figure 5.9. Kinetics of PRE complex formation of thG-containing mRNAs	172
Figure 5.10. Kinetics of PRE complex formation of thA-containing mRNAs.....	173
Figure 5.11. Kinetics of POST complex formation of thG-containing mRNAs.....	174
Figure 5.12. Kinetics of POST complex formation of thA-containing mRNAs	175
Figure I.1. mRNAs labeled with isomorphous fluorescent nucleoside mimetics.....	184
Figure I.2. Activities of mRNAs containing thU or thC	185
Figure I.3. Determination of excitation wavelength for thU- or thC-containing mRNAs	186
Figure I.4. Fluorescence changes of thU- and thC-containing mRNAs	187
Figure I.5. Kinetics of PRE complex formation of thU- and thC-containing mRNAs ...	188

Figure II.1. Specific and stoichiometric labeling of L1 with Au nanoparticle.....	197
Figure II.2. Reconstitution of 50S^{Au} from L1(S40C)^{Au}	198
Figure II.3. Semi-quantifying of 50S^{Au} labeling efficiency	199
Figure II.4. Function of Au labeled ribosome subunit in peptide synthesis.....	200

CHAPTER 1

INTRODUCTION

1.1 Gene expression and the central dogma

For the propagation of all three kingdoms of life, except for some viruses, heredity information is exclusively stored in genes made up of deoxyribonucleic acids (DNAs). During propagation, the double-helical structure of DNA allows gene replication by nucleotide polymerization using one DNA strand as a template according to Watson-Crick base pairing (Figure 1.1) (Watson and Crick, 1953a; Watson and Crick, 1953b; Crick, 1970). Within the living organism, the achievement of most of the biological functions depends on transcription of genes into ribonucleic acids (RNAs) and further translation of a portion of RNAs into proteins.

The transcription of DNA is performed by RNA polymerase using four ribonucleosides as substrates (adenosine, A; guanosine, G; cytidine, C; uridine, U) (Kornberg, 2007). Biosynthesized RNAs are classified according to their diverse functions. Messenger RNA (mRNA) further serves as the template of translation to direct protein biosynthesis. Transfer RNAs (tRNAs) act as an information bridge between mRNA and protein. Ribosomal RNAs (rRNAs), accounting for ~80% of the RNAs in prokaryote, is the major components of ribosome, the protein synthesis machine. In eukaryotic cells, additional small non-coding RNAs are also transcribed for various regulation purposes (Lee and Dutta, 2009).

In RNAs, genetic information is still encoded by the sequence of four ribonucleosides. However, the huge amount of functions to be performed requires the more complexity in both 3-dimensional structure and properties. Consequently, three

consecutive nucleosides in an mRNA are decoded as a codon to mediate the polymerization of each of 20 natural amino acids, with diverse chemical and physical properties conferred by the side chains of amino acids. Such a translation process is performed on the ribosome, a macromolecule composed of rRNAs and ribosomal proteins, with participation of numerous protein factors. In prokaryotic cells, mRNA is bound to the ribosome for translation before the transcription is complete. In eukaryotic cells, transcription is performed in the nucleus and the transcripts are subject to necessary modification (e.g. splicing, 5'-capping and 3'-poly(A) addition) with the help of small non-coding RNAs before their export to the cytoplasm for translation (Nishikura, 2006; Wahl et al., 2009). Recent studies revealed that co-translational recruitment of different factors to the ribosome helps the folding of proteins into their native states and the transportation of proteins to the places for their function performance (e.g. inner membrane proteins are targeted to the membrane by signal recognition particle)(Luirink et al., 2005).

1.2 Prokaryotic ribosome

In prokaryotic cells, the 70S (S is the unit for sedimentation velocity) ribosome, a macromolecule with a mass of ~ 2.6 MDa, is formed by association of the 30S and the 50S subunits, both of which are composed of rRNA and proteins (Figure 1.2; Table 1.1). The small 30S subunit consists of a 16S rRNA of ~1500 nucleotides and 20 or 21 ribosomal proteins, and the large 50S subunit consists of a 23S rRNA and a 5S

rRNA of ~3000 nucleotides in total, and 31-35 ribosomal proteins (Kaltschmidt and Wittmann, 1970; Yonath, 2010). It is believed that many of the enzymatic and functional sites on the ribosome are primarily constructed by rRNA with exquisitely defined conformation e.g. decoding center (DC), peptidyl transferase center (PTC) and GTPase-associated center (GAC). Ribosomal proteins are located mostly on the periphery of the ribosome and assumed to maintain the ribosome's architecture and facilitate some of the functions of rRNA e.g. L11 in GAC (Qin et al., 2012) and S12 in signal transduction between DC and GAC (Gregory et al., 2009). A series of sites have been defined in the ribosome for tRNA binding within both 30S and 50S subunits: aminoacyl- (A) site, peptidyl- (P) site and exit (E) site (Yonath, 2010; Schmeing et al., 2009a). During the translation process, incoming tRNA needs to bind to each of these sites in turn for a complete elongation cycle.

1.3 Translation cycle

During translation, mRNA binds to the ribosome and its coding sequence directs recruitment of aminoacyl-tRNA (aa-tRNA) and synthesis of nascent polypeptide. Overall the translation cycle can be divided into 4 stages: initiation, elongation, termination and recycling (Figure 1.3).

The formation of 70S initiation complex (70SIC) is facilitated by three initiation factors (IF1–3). mRNA, initiator tRNA (fMet-tRNA^{fMet}) and IF1–3 first bind to the 30S subunit to form a 30S pre-initiation complex (30S PIC) (Laursen et al., 2005).

The IF1 binding site on the 30S subunit partially overlaps with the DC, reflecting its role as preventing the premature binding of any aa-tRNA to the ribosomal A-site (Moazed et al., 1995). IF3 prevents the premature docking of the 50S subunit onto the 30S subunit before 30S IC formation (Grunberg-Manago et al., 1975; Sacerdot et al., 1996). IF2 promotes binding of fMet-tRNA^{fMet}, in the form of IF2.GTP.fMet-tRNA^{fMet}, to the ribosomal P-site, mediated by strict base pairing of three nucleotides on tRNA, denoted anti-codon, with the AUG start codon of mRNA (Gualerzi and Pon, 1990; Boelen and Gualerzi, 2002; Tsai et al., 2012), which is facilitated and monitored also by IF1 and IF3 (Canonaco et al., 1986; Tedin et al., 1999). The specific binding of mRNA on 30S is mediated by the complementary base-pairing between a short segment of RNA in the 5'-untranslated region (5'-UTR) of mRNA, denoted the Shine-Dalgarno sequence, and the anti-Shine-Dalgarno sequence in 16S rRNA, thus precisely place the AUG start codon on mRNA at the P-site of the 30S subunit (Shine and Dalgarno, 1974; Yusupova et al., 2006) (Figure 1.4). The codon-anticodon interaction between mRNA and fMet-tRNA^{fMet} induces the conformational transformation from 30S PIC to 30SIC, followed by the release of IF1–3 and association of the 50S subunit with 30SIC to form 70SIC, in which only ribosomal P-site is occupied by a tRNA (Grigoriadou et al., 2007a, b; Milón et al., 2008; Milón et al., 2012).

Translation elongation can be further dissected in to two stages, peptide bond formation and translocation. Peptide bond formation begins with the delivery of aa-tRNA to the empty ribosomal A-site catalyzed by elongation factor Tu (EF-Tu), in

the form of ternary complex (TC) EF-Tu.GTP.aa-tRNA (Rodnina et al., 1994; Pape et al., 1998) (Figure 1.5A). TC first binds to the highly flexible L7/L12 stalk (Schmeing et al., 2009a; Gao et al., 2009), a common binding site for all translational GTPase, then contacts the body of the ribosome at A/T site, with the anticodon on tRNA interacting with the codon on mRNA in the 30S subunit, and EF-Tu, together with the acceptor arm of tRNA, coming in proximity to GAC in the 50S subunit (Schmeing et al., 2009a). In such a binding status, tRNA displays a distorted conformation compared with what it has in unbound TC, which has been assumed to be functionally significant in tRNA accommodation into the A-site (Schmeing and Ramakrishnan, 2009b; Cochella and Green, 2005). The recognition of cognate codon in the DC triggers both local and global conformational changes in the ribosomal complex and the activation of GTPase activity of EF-Tu bound within the GAC (Voorhees et al., 2010). Rapid and irreversible GTP hydrolysis leads to a series of changes on the ribosome resulting in new peptide bond formation via peptidyl transfer from the P-site peptidyl-tRNA to the newly accommodated A-site aa-RNA, and the formation of pre-translocation (PRE) complex.

Following peptide bond formation, PRE complex spontaneously fluctuates between two states, accompanied by three different kinds of dynamic processes: 1) a ratcheting movement of the 30S subunit relative to the 50S subunit and a swiveling of the head domain of the 30S subunit (Frank and Agrawal, 2000; Zhang et al., 2009); 2) fluctuation of tRNAs between A/A, P/P site (denoted classical state) and A/P, P/E site (denoted hybrid state), respectively (Chen et al., 2011a); 3) a folding-in of L1 stalk,

consisting of ribosomal protein L1 and 23S rRNA, permitting it to interact with the elbow region of P/E tRNA (Valle et al., 2003a). Elongation factor G (EF-G) binds to the ribosome in the form of EF-G.GTP and catalyzes the unidirectional movement of tRNAs, together with mRNA, from A- and P- site to P- and E-site, respectively, leading to the formation of post-translocation (POST) complex, in which peptidyl-tRNA is bound at the ribosomal P-site, and the ribosomal A-site is empty and ready for the next incoming aa-tRNA (Figure 1.5B).

The elongation cycle is repeated to decode the consecutive 3-nucleotide codons until the ribosomal A-site encounters stop codons (UAA, UAG or UGA), a signal of translation termination. Release factor 1 (RF1, reading UAA and UAG) or 2 (RF2, reading UAA and UGA) is recruited to promote the hydrolysis of peptidyl-tRNA and subsequent peptide release from the ribosome (Laurberg et al., 2008; Weixlbaumer et al., 2008). A third release factor 3 (RF3) is also involved to facilitate the dissociation of RF1 and RF2 from the ribosome after peptide hydrolysis in a GTP-dependent manner (Freistroffer, 1997; Zhou et al., 2012). After RF3 dissociation, the remaining ribosomal complex dissociates, assisted by ribosome recycling factor (RRF) and EF-G, into the 50S subunit and the 30S complex carrying mRNA and a deacylated tRNA in the P-site (Hirashima and Kaji, 1973; Franckenberg et al., 2012). Further dissociation of mRNA and tRNA from the 30S subunit requires the action of IF3, thus is coupled to next round of translation initiation (Karimi et al., 1999; Hirokawa et al., 2008).

1.4 Crystallographic studies of the ribosome

Crystallography has long exhibited its power to elucidate the structure and function of biomolecules. An early view of the 70S ribosome by cryo-electron microscopy (cryo-EM) came in 1976 (Lake, 1976), and a reconstruction of the 70S ribosome with three tRNAs at a resolution of 25 Å was obtained in 1995 (Frank et al., 1995). Availability of high-quality crystals and advances in both instrument and data refining method have pushed the resolution down below 10 Å, which permits further understanding of the ribosome and translation. Stark et al. reported the structure of 70S-ribosome bound TC and described the interaction between EF-Tu and the ribosome (Stark et al., 1997). Then the interaction of tRNA in the ribosomal A/T site was also reported to suggest an active role of tRNA in accommodation (Valle et al., 2002). High-resolution reconstruction of TC bound to 70S provided a more clear snapshot of TC interaction with the ribosome, displayed the conformational changes in tRNA, EF-Tu and GAC during codon recognition, and indicated possible mechanisms for EF-Tu catalyzed GTP hydrolysis and codon decoding (Stark et al., 2002; Valle et al., 2003a; Schuette et al., 2009; Villa et al., 2009). Later, the development of time-resolved single particle cryo-EM and unbiased computational sorting of cryo-EM images made possible following a dynamic biological event. Application of these new techniques to tRNA translocation on the ribosome revealed several intermediate states of tRNA, besides the classical and hybrid states reported earlier, and defined the tRNA:70S interactions on the translocation pathway (Fischer et al., 2010). It was indicated that tRNA movements during translocation are coupled

with conformational changes of the ribosome, including the head and body of 30S and the L1 stalk. The ribosome is believed to act as a Brownian machine to direct translocation by coupling spontaneous conformational changes of various regions.

Despite its success in elucidating ribosomal structure and function, the relatively low resolution of cryo-EM makes it hard to rationalize the mechanism of translation at a molecular level. Higher resolution is provided by X-ray crystallography. The structures of the 30S subunit from *T. thermophilus* (Wimberly et al., 2000) and the 50S subunit from *H. marismortui* (Ban et al., 2000) with resolutions of 3.0 and 2.4 Å, respectively, shed light on the organization of rRNA and ribosomal proteins in the ribosome and served as the basis for phasing and molecular-level interpretation of all subsequent ribosomal structures. In 2001, a crystal structure of the complete 70S ribosome bound with mRNA and three tRNAs was reported by Noller and collaborators, into the electron density map of which all of rRNAs, mRNA and tRNAs and most of ribosomal proteins can be fitted (Yusupov et al., 2001). This high-resolution picture of the ribosome complex, with a resolution of 5.5 Å, provided a clear view of the interface between 30S and 50S subunit, especially the intersubunit bridges, and the environments of three tRNA binding sites and the tRNA:ribosome interaction, thus implying the coupling of intersubunit movements with tRNA movements during translocation.

Since then, the X-ray structures have been reported of ribosome complexes engaged in mRNA decoding (Demeshkina et al., 2012; Jenner et al., 2010),

translocation (Gao et al., 2009; Dunkle et al., 2011) and termination (Korostelev et al., 2008). Of particular relevance to the thesis here are two structures of 70S ribosome complexes containing bound TC. In 2009, a structure with TC stabilized in A/T state by kirromycin and paromomycin was published (Schmeing et al., 2009a), showing the details of tRNA distortion in A/T state when it simultaneously interacts with the A-site codon in the DC of the 30S subunit and EF-Tu. Such interactions, together with EF-Tu:70S interactions (at the GAC of the 50S subunit) and with changes of EF-Tu:tRNA interactions, led to the proposal of a possible signal transduction pathway for inducing the GTPase activation of EF-Tu and GTP hydrolysis on EF-Tu upon cognate codon:anticodon interaction (Schmeing and Ramakrishnan, 2009b). Important for the work presented below, the Schmeing's (Schmeing et al., 2009a) structure showed that positions suitable for fluorophore or quencher labeling on i) A/T site bound tRNA, ii) ribosomal protein L11 and iii) EF-Tu form an approximately equilateral triangle, with distances suitable for FRET studies (see Chapter III for details). This serves as the basis for EF-Tu studies presented in Chapter III and IV. A second structure of TC stabilized on the ribosome by paromomycin and GDPCP, a non-hydrolysable GTP analog, was reported later (Voorhees et al., 2010), focusing on the details in GAC region and how EF-Tu is activated for catalyzing GTP hydrolysis.

1.5 Kinetic studies examining ribosome function

Ensemble kinetic studies of the ribosome during translation primarily rely on

site-specific labeling of translation components, including tRNA and translation factors, with organic fluorophores. Monitoring fluorescent signal change during dynamic processes or fluorescence resonance energy transfer (FRET) signal between two fluorophores in proximity, together with some other assays (e.g. GTP hydrolysis, dipeptide formation and puromycin reactivity assays), allow comparison of relative timing of different functional steps, provide evidence for functionally competent intermediates, and provide extensive insights into the mechanism of translation.

The works in our lab, utilizing the FRET signal between labeled 50S subunit and IF2 programmed on 30SIC, demonstrate the interaction of IF2 with GAC and the role of fidelity control played by IF3 in monitoring the initiation codon (Qin et al., 2009). A more recent report (Milón et al., 2012), using labeled IF1–3, fMet-tRNA^{fMet} and mRNA, illustrates a real-time assemble scheme of 30S PIC formation and the checkpoints of mRNA selection. Rodnina and her colleague formulated a quantitative kinetic scheme for tRNA dynamics during its selection, demonstrating how the correct tRNA is differentiated from other tRNAs and how translation has evolved to optimize the speed and accuracy of codon decoding (Pape et al., 1998; Gromadski and Rodnina, 2004a; Wohlgemuth et al., 2010). Pan et. al. (Pan et al., 2007), by using tRNAs with fluorophore labels at the elbow region, successively isolated a kinetically competent intermediate on the translocation pathway, suggesting that the movements of P- and A-site tRNA on conversion from classical to hybrid state could be decoupled. Translation termination was also investigated by using an short mRNA labeled at the 3'-end, showing how stop codon is precisely selected by RF1 against sense codon and

how stop codon decoding is correlated with catalyzed peptide release (Hetrick et al., 2009).

1.6 Monitoring ribosomal translation with smFRET

Biochemical and structural studies have demonstrated the complexity of translation as a multi-step and multi-component process and the highly dynamic nature of the ribosome during translation. Although ensemble kinetic studies have greatly advanced our knowledge of the conformational changes of the ribosome and its communication with translation factors, complete understanding of the mechanism of translation on the molecular level has been confined by the temporal and population averaging nature of current assays. To address these limitations, the capability to characterize the single ribosome molecules was first demonstrated in 2003 (Vanzi et al., 2003). In this report, ribosome elongation complexes programmed with poly(U) were non-specifically adsorbed to the mica surface and connected to a fluorescently labeled polystyrene bead via biotin-neutravidin interaction at the 3'-end of mRNA. Epifluorescence microscopy was used to track the contraction of the diffusion range of the beads because of poly(Phe) synthesis and the slide of the ribosome towards the 3'-end of mRNA.

After a decade of development, labeled ribosomal complexes in different functional states can be specifically immobilized on the surface via various strategies, with their translation functions fully retained, and single molecule FRET (smFRET)

measurement was achieved based on total internal reflection fluorescence (TIRF) (Marshall et al., 2008; Perez and Gonzalez Jr, 2011). An evanescent wave, which is generated when the incident light is totally internally reflected at the interface, is used to illuminate a selected area with a depth of ~100 nm into the sample. Thousands of ribosome molecules could be simultaneously detected with the signal for each single ribosome analyzed separately. Together with data sorting and synchronization, the problem of heterogeneity in ensemble experiments was thus overcome. On the one hand, multiple cycles of translation elongation have been observed by either placing both FRET donor and acceptor on the immobilized ribosome complex to reduce fluorescence background (Aitken and Puglisi, 2010), or introducing zero-mode waveguide technique to limit the regional concentration of labeled components (Uemura et al., 2010). On the other hand, smFRET has been applied to resolve the elementary steps during translation and detect functionally competent intermediates along the reaction coordinate (Chen et al., 2011a, b; Fei et al., 2008; Munro et al., 2007).

smFRET studies by tRNA:tRNA FRET have identified three intermediates during A-site codon decoding, corresponding to i) initial codon recognition, ii) GTPase-activated and iii) fully accommodated states, respectively, and allowed comparisons of different patterns of intermediate state sampling between cognate and near-cognate tRNA binding (Blanchard et al., 2004). It was shown that tRNA thermal fluctuation during codon decoding was utilized for the discrimination between cognate and near-cognate tRNA (Geggier et al., 2010; Lee, 2007; Mishra et al., 2010).

The effects of several antibiotics, including tetracycline, thiostrepton and kirromycin, on tRNA selection were also investigated, with the observations consistent with those observed in ensemble studies (Blanchard et al., 2004; Geggier et al., 2010; Gonzalez et al., 2007).

1.7 EF-Tu in translation elongation

Elongation factor thermally unstable (EF-Tu) is encoded in two genes in *E. coli*, *tufA* and *tufB*, and in this thesis, it's the *tufA* gene and its expression product that are utilized and investigated. EF-Tu, with a cellular concentration ~ 10 fold higher than that of the ribosome (Furano, 1975), consists of 393 amino acids, including three cysteine residues at position 81, 137 and 255. Among these three cysteines, Cys81 has been found to be highly conserved within bacteria and functionally critical for aa-tRNA binding, but not for GTP or GDP binding (Laurentiis et al., 2011).

EF-Tu is organized into three domains. Domain 1 contains the binding site for the nucleotide with an affinity for GDP 100 times higher than for GTP. Before forming a TC, the GDP on EF-Tu is replaced by GTP, catalyzed by elongation factor EF-Ts and driven by high cellular GTP concentration. Such off-the-ribosome nucleotide exchange is accompanied by a conformational change within domain 1 relative to domains 2 and 3 (Kjeldgaard and Nyborg, 1992; Polekhina et al., 1996). Domains 2 and 3 regulate the interaction of EF-Tu with EF-Ts and antibiotics, maintain the bias in favor of GDP binding in domain 1, and mediate EF-Tu interaction with the

ribosome and aa-tRNA (Cetin et al., 1998). To form the TC, EF-Tu binds to an aa-tRNA with the interface of domain 1 and 2 contacting the acceptor stem-loop and amino acid, and domain 3 contacting the T stem (Nissen et al., 1995). The nucleotide sequence in tRNA has evolved to compensate for the diverse thermodynamic contributions of amino acid side chains, making EF-Tu:aa-tRNA affinity similar for all tRNAs in such a way that every aa-tRNA can form a stable TC with EF-Tu-GTP and be easily released from EF-Tu during accommodation (Dale et al., 2004). EF-Tu:aa-tRNA affinity can be modulated by mutating the nucleotides within the T stem of tRNA, which have direct contacts with EF-Tu (Schrader et al., 2011). Although it's now well accepted that EF-Tu binds to aa-tRNA in a 1:1 ratio, several groups have reported that two EF-Tus can simultaneously bind to one aa-tRNA and participate in the decoding process (Bilgin and Ehrenberg, 1995; Ehrenberg, 1990; Rodnina and Wintermyer, 1995a).

Upon recruitment of a TC to the ribosome complex, EF-Tu consumes one GTP molecule and releases the aa-tRNA to the ribosomal A-site (see Section 1.3 for more details), with a dramatic conformational change from the GTP- to GDP-bound form (Kjeldgaard and Nyborg, 1992; Polekhina et al., 1996). The antibiotic kirromycin targets EF-Tu and inhibits elongation by stabilizing EF-Tu on the ribosome in a GTP-like conformation after GTP hydrolysis (Schmeing et al., 2009a). The conformational change of EF-Tu on the ribosome triggers its release from the ribosome and the recruitment of EF-G.

1.8 Fidelity control throughout protein synthesis and antibiotics

When a properly aminoacylated tRNA is delivered to the ribosome in the form of a TC, several mechanisms at different functional stages operate together to ensure the correct selection of cognate tRNA (Zaher and Green, 2009a). tRNA selection in the decoding center of the 30S subunit primarily relies on the exact base pairing between the codon programmed at the ribosomal A-site and the anticodon in tRNA. However, the energetic difference resulting from the incorrect base pairing is not significant enough to account for the observed precision of tRNA incorporation. The high fidelity of tRNA selection is kinetically accomplished by the induced-fit mechanism (Gromadski and Rodnina, 2004a), which consists of two stages, denoted initial selection and proof-reading, separated by the irreversible EF-Tu mediated GTP hydrolysis. In the codon recognition step, the signal of cognate codon:anticodon interaction in the DC of the 30S subunit induces both local and global conformational rearrangements, and is transduced remotely, via an unknown mechanism, to the GAC in the 50S subunit, leading to EF-Tu activation and GTP hydrolysis. In contrast, incorrect base pairing leads to ~ 600-fold slower or no GTP hydrolysis for near-cognate or non-cognate tRNA, respectively. Consequently, most of the near-cognate tRNAs and all of the non-cognate tRNAs are rejected in the initial selection. After GTP hydrolysis, cognate tRNA is accommodated into the A-site, while the improper codon:anticodon interaction of near-cognate tRNA destabilizes the

tRNA binding to the ribosome and leads to tRNA dissociation during the proof-reading step.

When an incorrect amino acid is incorporated into the growing polypeptide chain, the codon:anticodon mismatch error can be amplified in the subsequent aa-tRNA selection steps, ultimately leading to the premature translation termination (Zaher and Green, 2009b). RF3 also exhibits a substantial effect in maintaining the high fidelity of protein synthesis (Zaher and Green, 2011). The ribosome apparatus has evolved to be optimized for speedy and accurate protein synthesis (Johansson et al., 2012; Wohlgemuth et al., 2010), and the cooperation of various quality control mechanisms achieves an overall *in vivo* error rate of 6×10^{-4} to 5×10^{-3} per amino acid incorporated (Bouadloun et al., 1983; Edelman and Gallant, 1977).

Because of its fundamental function in gene expression, the ribosome is a primary target of antibiotics, and some of them have an effect in the quality control of protein synthesis. Streptomycin and paromomycin from aminoglycoside family are two well-documented ones, both of which could induce misreading, but with different mechanisms (Gromadski and Rodnina, 2004b). Streptomycin contacts both S12 and G530 loop of the shoulder and helices 27 and 44 in the central part of the 30S subunit, and holds the 30S subunit in a particular conformation, which, in turn, stabilizes both cognate and near-cognate aa-tRNA on the ribosome and blurs their differences in the rates of EF-Tu-dependent GTP hydrolysis, thus diminishing the selection power of the initial selection step. In contrast, paromomycin stabilizes the ribosome in a

high-activity conformation, which has no effects on the cognate aa-tRNA recognition, but significantly increases the rate of EF-Tu-dependent GTP hydrolysis in the case of near-cognate aa-tRNA to a level comparable to that of cognate aa-tRNA, thereby facilitating the incorporation of near-cognate aa-tRNA (Gromadski and Rodnina, 2004b).

1.9 Emissive nucleoside mimetics

Besides the labeling of biomolecules with organic fluorescent probes, an alternative way to study the conformational change or dynamic processes of biomolecules in a biological event by using fluorescence spectroscopy is to incorporate the emissive analogs of the building blocks into the biomolecules. Emissive nucleoside mimetics have demonstrated their abilities in probing the secondary structure and the structure dynamics of nucleic acids (Sinkeldam et al., 2010). Assays based on such emissive nucleoside analogs have recently been developed to study the ribosome interactions with exogenous proteins and antibiotics by either inserting the emissive nucleoside mimetic into a RNA segment complementary to the rRNA (Srivatsan et al., 2008) or synthesizing a model sequence of rRNA containing the emissive nucleoside analog (Sakakibara et al., 2012; Xie et al., 2009; Xie et al., 2010).

Quite recently, a fluorescent ribonucleoside alphabet derived from thieno[3.4-d]-pyrimidine was reported with structural resemblance to the naturally

occurring ribonucleoside (Figure 1.6) (Shin et al., 2011). These isomorphous analogs result in minimal structural and functional perturbations to the oligonucleotides into which they are incorporated, have desirable photophysical properties suitable for fluorescent spectroscopy studies, and overcome the common drawback of emission quenching of emissive nucleoside analogs upon incorporation into oligonucleotides. These advantages of such thieno-modified emissive nucleoside mimetics offer the potential for systematic real-time studies of the translation apparatus, utilizing both their fluorescent response to the environmental change and energy transfer with other fluorophores.

1.10 Frameshifting in translation

During translation elongation, mRNA repetitively undergoes a movement of three nucleotides relative to the ribosome to place successive codons at the ribosomal A-site for decoding, with the average frequency of spontaneous frameshifting on the order of 10^{-5} to 10^{-4} (Kurland, 1979). A second kind of controlled mRNA displacement relative to the ribosome involves the change of open reading frame, denoted programmed frameshifting, which is utilized for the regulation of gene expression (Dinman, 2012) and replication of numerous viruses (Brierley and Dos Ramos, 2006). The two most common programmed frameshiftings are +1 and -1 shifting, in which the mRNA displacement relative to the ribosome is one nucleotide downstream or upstream, respectively. +1 frameshifting is directed by homopolymeric runs of 3 or 4

nucleotides within mRNA, while the -1 shifting is mediated by a slippery sequence of X_XXY_YYZ (X can be any nucleotide, Y is A or U and Z is not G in the eukaryote) in the original reading frame followed by a downstream secondary structure, usually a pseudoknot. Although genetic and cell biological studies have provided insight into the programmed frameshifting (Dinman, 2012; Giedroc and Cornish, 2009), especially with respect to translation components other than mRNA that are involved in reading frame maintenance, such as the ribosomal E-site (Devaraj et al. 2009) and tRNA modification (Gustilo et al., 2008), real-time observation of programmed frameshifting has not been achieved and its mechanism in the molecular level is still elusive.

Table 1.1. Components of *E. coli* ribosomes.

Ribosome/subunit	70S	50S	30S
Molecular weight (kD)	2520	1590	930
rRNA components	23S, 16S and 5S	23S and 5S	16S
Number of nucleotides in rRNA	4566	2904 for 23S 120 for 5S	1542 for 16S
rRNA molecular weight (kD)	1664	1104	560
Number of ribosomal proteins	55	34	21
Protein molecular weight (kD)	857	487	370

This table is adapted from (Kaltschmidt and Wittmann, 1970; Voet et al., 2006).

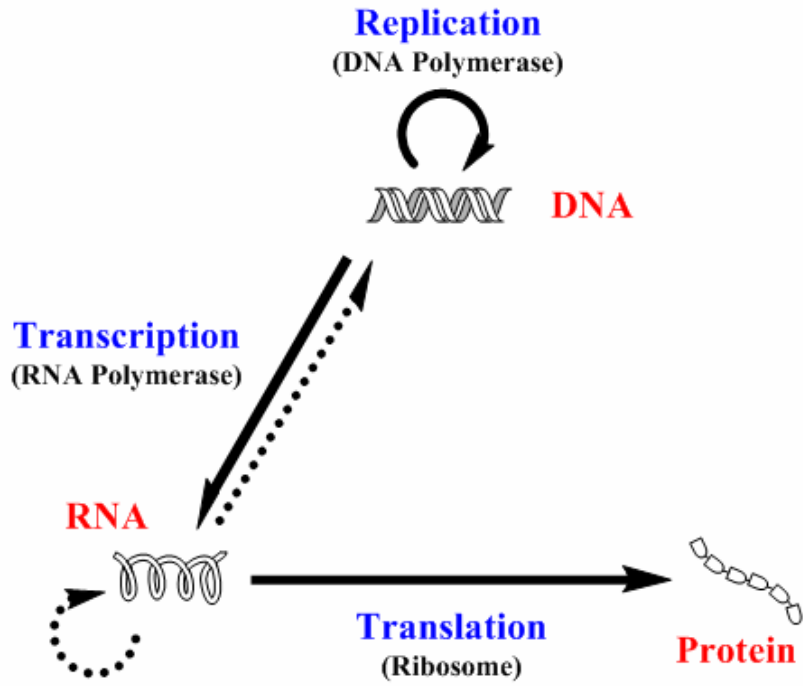


Figure 1.1. Central dogma of molecular biology (Modified from Crick, 1970).

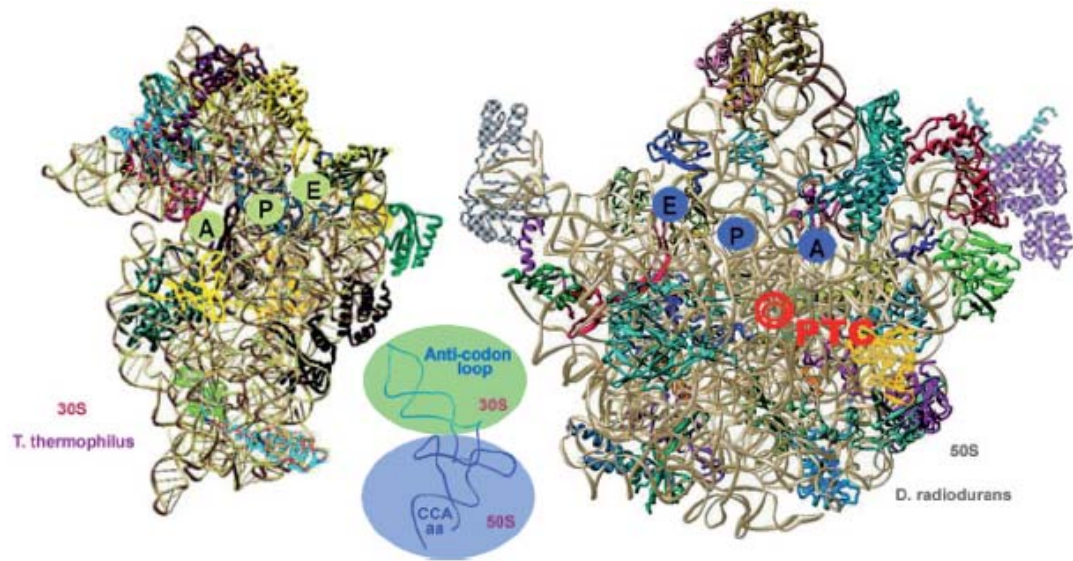


Figure 1.2. Three-dimensional structures of the two ribosomal subunits. Two subunits are from eubacteria with a tRNA molecule placed between them. The rRNA is shown in brownish colors, and each of the ribosomal proteins is shown in a different color. A-, P- and E- sites are for tRNA binding. The approximate site of the peptidyl transferase center is marked in red. Insert: Backbone of a tRNA molecule; circles designate the regions interacting with each of the ribosomal subunits. This figure is taken from (Yonath, 2010).

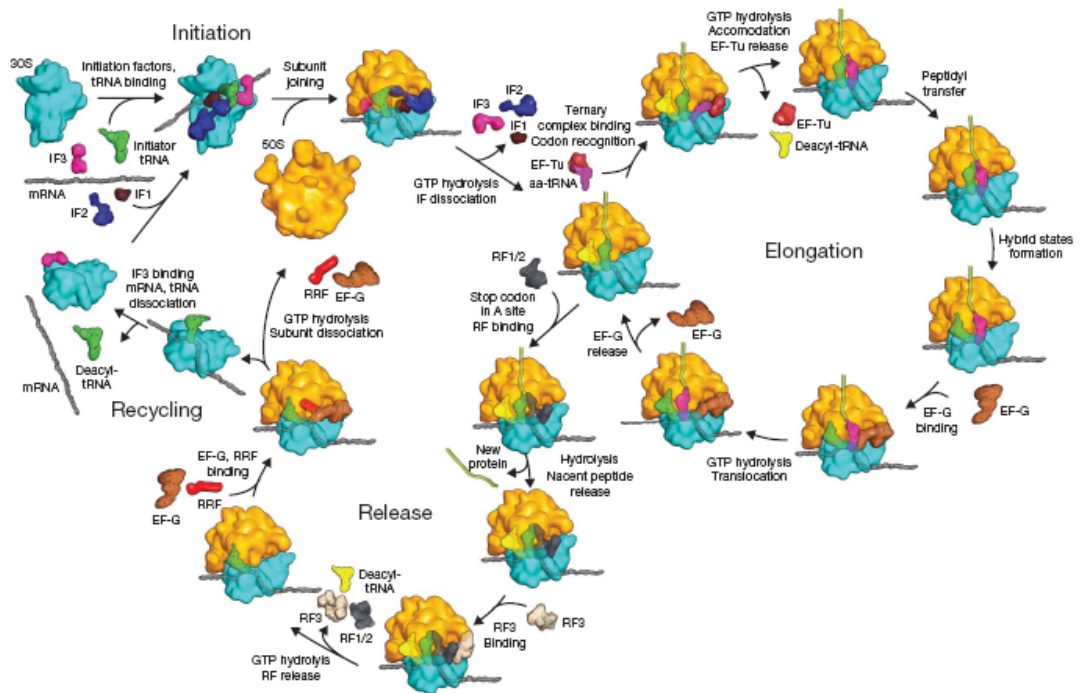


Figure 1.3. Overview of translation cycle. This figure is taken from (Schmeing and Ramakrishnan, 2009b).

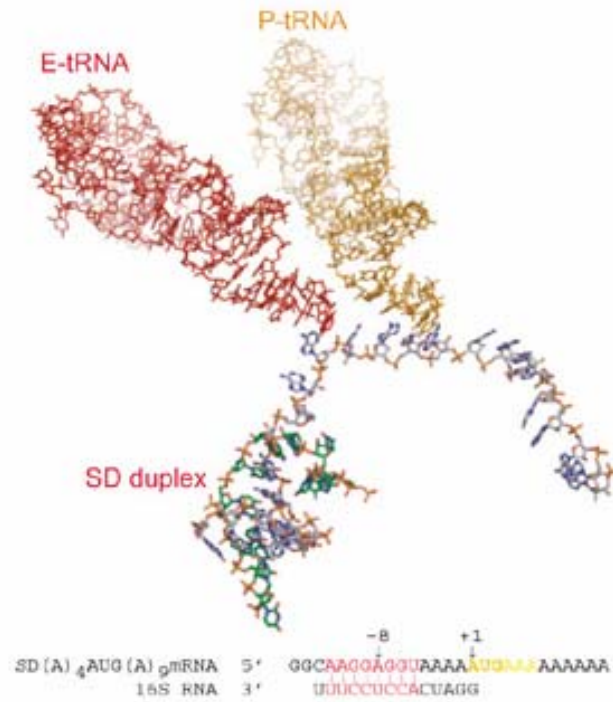
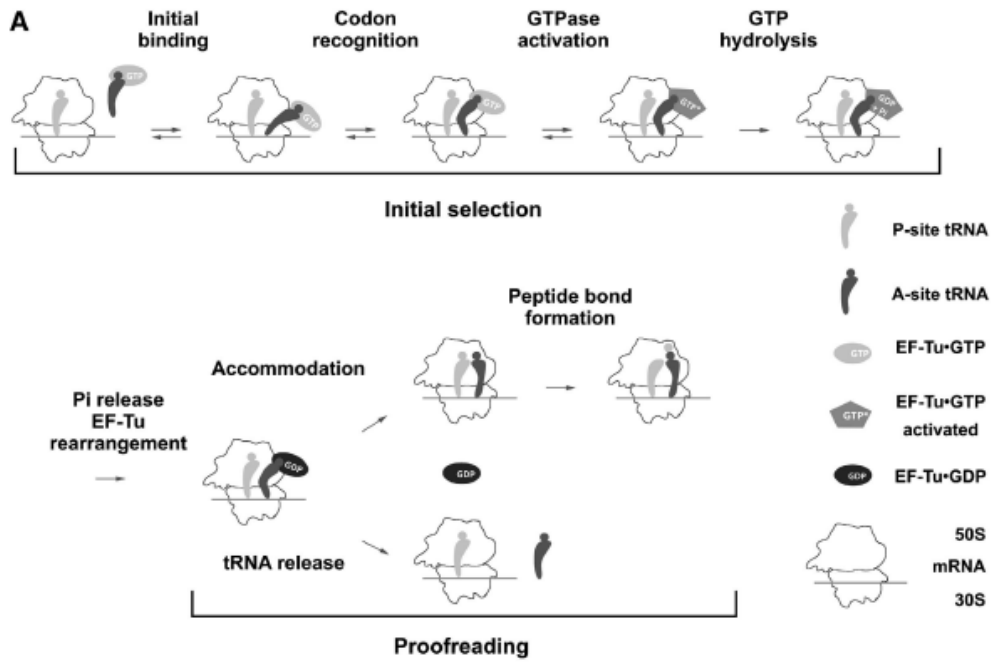


Figure 1.4. mRNA bound to the ribosome initiation complex. SD sequence (red in mRNA sequence) interaction with anti-SD sequence (red in 16S RNA sequence) places the AUG start codon (dark yellow in mRNA sequence) at ribosomal P-site. This figure is taken from (Yusupova et al., 2006).



B

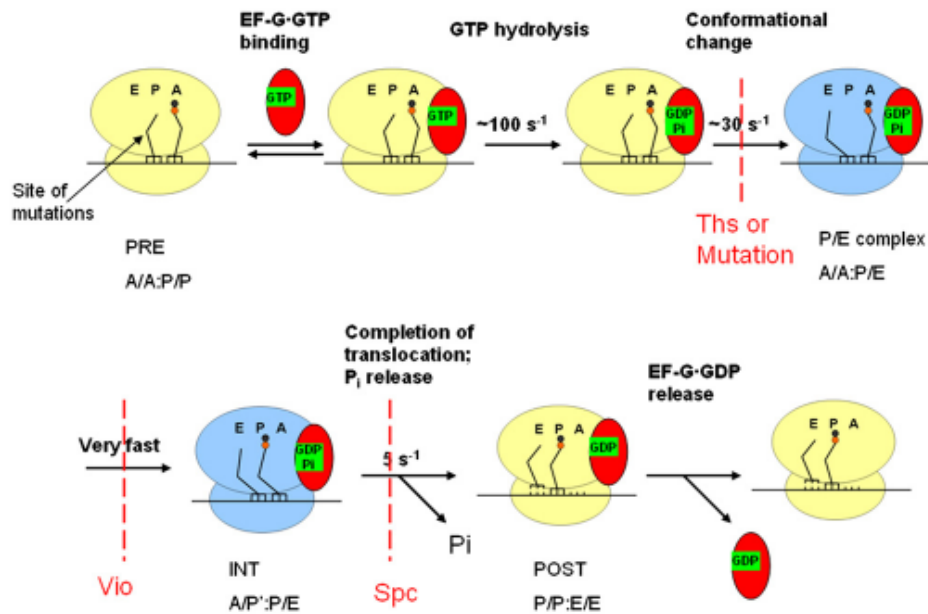


Figure 1.5. Representative schemes of peptide bond formation (A) and translocation (B). Figure A and B are taken from (Wohlgemuth et al., 2010) and (Pan et al., 2007), respectively.

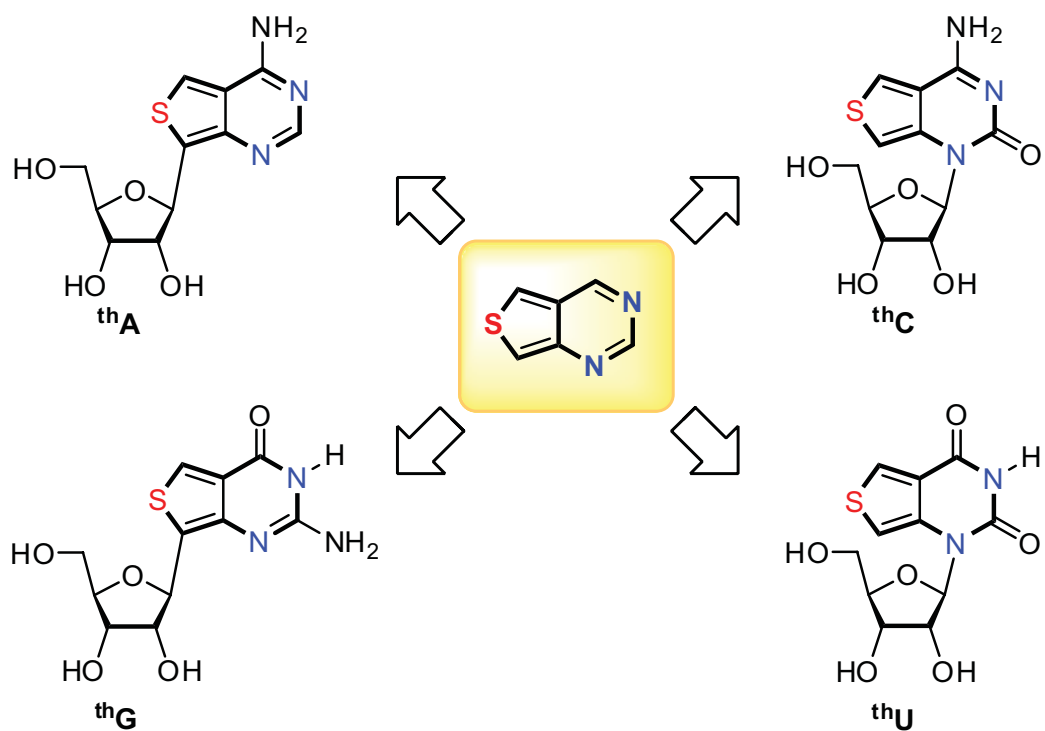


Figure 1.6. Emissive RNA alphabet. This figure is reprinted with permission from (Shin, D., Sinkeldam, R. W., and Tor, Y. (2011). Emissive RNA alphabet. *J Am Chem Soc* 133, 14912–14915.). Copyright (2011) American Chemical Society.

CHAPTER 2

MATERIALS AND METHODS

2.1 Materials

2.1.1 Buffers

All of the following buffers were prepared and the pH was adjusted at 25°C. All of the experiments in this thesis were performed in buffer A unless otherwise specified.

Buffer A: 50 mM Tris-HCl pH 7.5, 70 mM NH₄Cl, 30 mM KCl, 7 mM MgCl₂ and 1 mM DTT.

Buffer B: 50 mM Tris-HCl pH 7.5, 70 mM NH₄Cl, 30 mM KCl, 7 mM MgCl₂ and 1 mM DTT, 100 μM GTP, 2 mM phosphoenolpyruvate, 10 μg/ml pyruvate kinase.

Buffer C: 20 mM Tris-HCl pH 7.6, 200 mM NH₄Cl, 10 mM MgAc₂.

IF3 lysis buffer: 50 mM Tris-HCl pH 8.0, 1 mM EDTA, 10 mM 2-mercaptoethanol, 0.2 mM PMSF.

IF3 purification buffer A: 10 mM Tris-HCl pH 8.0, 200 mM NaCl, 5% glycerol, 1 mM 2-mercaptoethanol.

IF3 purification buffer B: 10 mM Tris-HCl pH 8.0, 500 mM NaCl, 5% glycerol, 1 mM 2-mercaptoethanol.

L11 dialysis buffer: 20 mM Hepes-HCl pH 7.0, 0.5 mM EDTA, 6 M urea, 6 mM 2-mercaptoethanol, 10 mM NaCl.

L11 purification buffer A: 20 mM Hepes-HCl pH 7.0, 0.5 mM EDTA, 6 M urea,

6 mM 2-mercaptoethanol, 10 mM NaCl, 10 mM MgCl₂.

L11 purification buffer B: 20 mM Hepes-HCl pH 7.0, 0.5 mM EDTA, 6 M urea, 6 mM 2-mercaptoethanol, 400 mM NaCl, 10 mM MgCl₂.

L11 labeling buffer: 25 mM Tris-HCl pH 7.0, 100 mM NaCl, 2 mM EDTA.

EF-Tu purification buffer A: 50 mM Tris-HCl pH 7.6, 60 mM NH₄Cl, 7 mM MgCl₂, 7 mM 2-mercaptoethanol, 15 μM GDP, 15% glycerol.

EF-Tu purification buffer B: 50 mM Tris-HCl pH 7.6, 60 mM NH₄Cl, 7 mM MgCl₂, 300 mM KCl, 7 mM 2-mercaptoethanol, 15 μM GDP, 15% glycerol.

EF-Tu purification buffer C: 50 mM Tris-HCl pH 7.6, 60 mM NH₄Cl, 7 mM MgCl₂, 300 mM KCl, 20 mM imidazole, 7 mM 2-mercaptoethanol, 15 μM GDP, 15% glycerol.

EF-Tu elution buffer: 50 mM Tris-HCl pH 7.6, 60 mM NH₄Cl, 7 mM MgCl₂, 300 mM KCl, 300 mM imidazole, 7 mM 2-mercaptoethanol, 15 μM GDP, 15% glycerol.

EF-Tu storage buffer: 50 mM Tris-HCl pH 7.6, 100 mM NaCl, 10 mM MgCl₂, 15 μM GDP.

Hybridization buffer: 100 mM Tris-HCl pH 7.5, 1 M NaCl, 10 mM EDTA.

TMA buffer: 10 mM Tris-HCl pH 7.6, 0.1 mM EDTA pH 8.0, 0.9 M tetramethylammonium chloride.

Aminoacylation buffer A: 100 mM Tris-HCl pH 8.0, 4 mM ATP, 20 mM MgCl₂, 1 mM EDTA pH 8.0, 7 mM 2-mercaptoethanol, 10 mM KCl, 0.01 unit/μl

thermostable inorganic pyrophosphatase, 720 μM formyl donor, 67 μM [^{35}S]fMet mixture, 0.75 mg/ml *E coli*. aminoacyl-tRNA synthetases.

Aminoacylation buffer B: 100 mM Tris-HCl pH 8.0, 10 mM ATP, 50 mM MgCl_2 , 2.5 mM EDTA pH 8.0, 3 mM 2-mercaptoethanol, 200 μM [^3H]Phe mixture, 1.5 mg/ml yeast aminoacyl-tRNA synthetases.

Aminoacylation buffer C: 100 mM Tris-HCl pH 8.0, 4 mM ATP, 5 mM MgAc_2 , 250 μM EDTA pH 8.0, 7 mM 2-mercaptoethanol, 150 μM [^3H]Phe mixture, 1 μM *E coli*. Phe-tRNA synthetases.

Aminoacylation buffer D: 100 mM Tris-HCl pH 8.0, 4 mM ATP, 20 mM MgCl_2 , 1 mM EDTA pH 8.0, 7 mM 2-mercaptoethanol, 0.005 unit/ μl inorganic pyrophosphatase, 100 μM [^3H]Val mixture or 67 μM [^3H]Arg mixture or 100 μM [^3H]Lys mixture, 0.75 mg/ml *E coli*. aminoacyl-tRNA synthetases.

Aminoacylation buffer E: 30 mM Hepes-HCl pH 7.0, 30 mM KCl, 15 mM MgCl_2 , 5 mM DTT, 4 mM ATP, 100 μM [^3H]Val, 0.01 unit/ μl thermostable inorganic pyrophosphatase, 0.75 mg/ml of *E coli*. aminoacyl-tRNA synthetase.

2.1.2 Reagents

All of the aqueous solutions and buffers were prepared using double-deionized water from Milli-A Water System (Millipore) and treated with a BioPak filter (Millipore) to remove the DNase, RNase and protease.

The following materials were purchased from the indicated suppliers: IPTG, GDP, GTP, GDPNP, streptomycin, paromomycin, kirromycin, poly(U), puromycin, glucose, glucose oxidase, phenylmethanesulfonylfluoride (PMSF), streptavidin agarose bead, tris(2-carboxyethyl)phosphine hydrochloride (TCEP), N-hydroxysuccinimide ester, folinic acid, glutathione, 6-hydroxy-2,5,7,8-tetramethyl- chromane-2-carboxylic acid and bovine pancreatic RNase A (Sigma); Talon Superflow Metal Affinity Resin (Clontech); QSY9 maleimide, dNTP, S.O.C. medium and Top 10 competent cells (Invitrogen); Cy3 maleimide, Cy5 maleimide, NAP-5 column and pTZ18R plasmid (GE Healthcare); phosphoenolpyruvate (PEP), pyruvate kinase (PK), RNase T1, catalase and bulk tRNA from *E. coli*. MRE600 cells (Roche); proflavin (MB Biomedicals); Phusion DNA polymerase and DpnI (New England Biolabs); PCR purification kit and Ni-NTA Superflow resin (QIAGEN); BL21(DE3) competent cells (Stratagene); ampicillin, trichloroacetic acid (TCA), saturated phenol pH 4.3 and saturated phenol pH 6.6 (Fischer Scientific); AG 50W-X8 cation exchange resin, Silver Stain Plus kit (Bio-Rad); thermostable inorganic pyrophosphatase (New England BioLabs); Amicon Ultra-4 ultrafiltration units, Ultrafree-MC GV centrifugal filter unit, and nitrocellulose filters (Millipore); LI Silver Stain kit (Nanoprobes); *E. coli* tRNA^{fMet}, *E. coli* tRNA^{Phe}, *E. coli* tRNA^{Val}, *E. coli* tRNA^{Arg}, *E. coli* tRNA^{Lys}, and yeast tRNA^{Phe} (Chemical Block, Moscow).

2.2 Methods

2.2.1 Preparation of proteins

Cloned *E. coli* His-tagged proteins IF1, IF2, EF-G and labeled phosphate binding protein (MDCC-PBP) were prepared and purified as previously reported (Pan et al., 2008). *E. coli* aminoacyl-tRNA synthetases were prepared following an established procedure (Kemkhadze et al., 1981). Yeast aminoacyl-tRNA synthetases were prepared based on the published procedure (Lagerkvist and Waldenstrom, 1964).

2.2.1.1 Purification of IF3

pET21a plasmid carrying His-tagged IF3 is a kind gift from Dr. Ueda, University of Tokyo (Shimizu et al., 2001). All steps below were performed at 4 °C. 10 g of frozen BL21(DE3) pET21a IF3 cells were kept on ice for 10min, and then resuspended in 30 mL of IF3 lysis buffer followed by two passes through a French Press (12,000–14,000 psi). The resulting mixture was subject to centrifugation (10k rpm, 30 min, SS-34 rotor) to pellet the cell debris. The supernatant was loaded onto an 8 ml Ni-NTA column (18 mm in diameter) pre-washed with 60 ml of water and pre-equilibrated with 60 ml of IF3 lysis buffer. The column was washed by 60 ml of IF3 purification buffer A followed by 30 ml of IF3 purification buffer B. IF3 protein was eluted by use of a hyperbolic imidazole gradient in IF3 purification buffer B (5 mM imidazole, 40 ml; 10 mM imidazole, 20 ml; 20 mM imidazole, 10 ml; 300 mM imidazole, 50 ml) and collected in fractions. Fractions with large amounts of IF3 were identified by 18% SDS-PAGE gel and pooled for dialysis against buffer A. IF3 was

concentrated by an Amicon Ultra ultrafiltration units [molecular weight cutoff (MWCO): 10,000] and the concentration was determined by Bradford assay (Bradford, 1976).

2.2.1.2 Purification and labeling of L11(C38S/S87C)

L11(C38S/S87C) double mutant from 12 g of BL21(DE3) pLysS L11(C38S/S87C) cells (Chen et al., 2011a) was first purified using an 8 ml Ni-NTA column (18 mm in diameter), following the procedure used for IF3 and using the same buffers for IF3. All proteins eluted with 300 mM imidazole were dialyzed against L11 dialysis buffer overnight and L11 purification buffer A for 3 hours at 4 °C. After concentrated using Amicon Ultra ultrafiltration units (MWCO: 10,000), crude L11 product was further purified on a SourceS column (4.6 × 100 mm) and pure L11 was eluted using a linear gradient from L11 purification buffer A to L11 purification buffer B. Then an Amicon Ultra ultrafiltration units (MWCO: 10,000) was used to remove the urea and replace the buffer with buffer A (6 times), after each cycle of which L11 sample was kept on ice for at least 30 min to facilitate protein refolding. L11 concentration was determined by Bradford assay (Bradford, 1976), with the concentration multiplied by a correction factor of 0.6 (Wang et al., 2007).

L11 labeling with either Cy3 or Cy5 was performed as described (Chen et al., 2011a). Nap-5 column (bed volume 0.5 ml) was used to exchange the buffer from buffer A to L11 labeling buffer following the manufacture instructions. L11 (100 μM)

was incubated at room temperature for two hours in the presence of TCEP (300 μ M) and Cy5 maleimide (1.1 mM) in 900 μ l of L11 labeling buffer. The reaction was quenched with 3 μ l of 14.3 M 2-mercaptoethanol, and labeled L11 was purified on Source S column as in L11 purification. Fractions were monitored at A_{280} and A_{550} , and pooled for dialysis against buffer A, followed by concentration using an Amicon Ultra ultrafiltration units (MWCO: 10,000). L11 concentration was determined by Bradford assay as above and dye concentration was determined by A_{550} for Cy3 and A_{650} for Cy5 (extinction coefficients: 150,000 and 250,000 $M^{-1} \text{ cm}^{-1}$ for Cy3 and Cy5, respectively). Typical dye/L11 ratio was 0.9.

2.2.2 Preparation of EF-Tu variants and their derivatives

2.2.2.1 Purification of EF-Tu variants

Expression vectors for C-terminal His-tagged *E. coli* EF-Tu variants were based on the pET15b vector. pET15b EF-Tu plasmids (50–80 ng) (Perla-Kajan et al., 2010) were transformed into BL21(DE3) competent cells, and the strains were grown in Super Optimal Broth (S.O.C.) medium at 37 °C for one hour. The cell cultures were plated onto LB-Agar plate with 100 μ g/ml of ampicillin and grown overnight at 37 °C. Single colony on the plate was inoculated into 6 ml of LB medium with 100 μ g/ml of ampicillin for overnight growth at 37 °C. The cell culture was transferred into 1 L of LB medium with 100 μ g/ml of ampicillin for growth until A_{260} reached ~0.6–0.8. Protein expression was started by addition of 1mM IPTG and lasted for 3 hours at 37

°C.

The purification of the expressed proteins was performed as previously described with some changes (Perla-Kajan et al., 2010). BL21(DE3) pET15b EF-Tu cells (6 g) were resuspended in 25 ml of EF-Tu purification buffer A and the mixture was magnetically stirred for 30 min at 4 °C. A second incubation at room temperature for 20 min was performed after addition of lysozyme to 0.75 mg/ml. Cell was broken by French press twice (12,000–14,000 psi) and centrifuged (4 °C, 20k rpm with SS34 rotor, 20 min) to remove the cell debris. The supernatant was mixed with Co(II)-Sepharose (Talon) resin (bed volume 3 ml), pre-washed twice with 30 ml of EF-Tu purification buffer A, and shaken at 4 °C for 1 hour. Resins bound with EF-Tu were pulled down by centrifugation (4 °C, 700 xg, 5 min), washed twice with 30 ml of EF-Tu purification buffer A, and transferred to a small gravity column (18 mm in diameter). The column was washed sequentially with 10 ml of EF-Tu purification buffer A, 10 ml of EF-Tu purification buffer B and 10 ml of EF-Tu purification buffer C. EF-Tu was eluted using EF-Tu elution buffer, and Amicon Ultra ultrafiltration units (MWCO: 10,000) were used to concentrate the samples, remove imidazole and replace the buffer with EF-Tu storage buffer. EF-Tu concentration was determined by Bradford assay.

2.2.2.2 Labeling of EF-Tu with quencher or fluorophore

EF-Tu labeling was carried out in 150 µl EF-Tu storage buffer by incubating

EF-Tu (0.8 mg, 0.1 mM), QSY9, Cy3 maleimide or Cy5 maleimide (1.35 mM) and TCEP (1 mM) at room temperature for 6 hours. The reaction was quenched by addition of 2-mercaptoethanol (final concentration: 300 mM). The mixture was diluted to 0.5 ml with EF-Tu storage buffer and loaded onto a NAP-5 column (bed volume 0.5 ml) at room temperature to remove free QSY9. 1 ml of EF-Tu storage buffer was used to elute the EF-Tu. Three fractions of volumes 200, 400 and 400 μ l were collected, and labeled EF-Tu was eluted in the middle 400 μ l. EF-Tu concentration was determined by Bradford assay. Cy3 or Cy5 concentration was determined by A_{550} or A_{650} as in section 2.2.1.2. QSY9 concentration was determined using a standard curve of free QSY9 measured at A_{562} (extinction coefficient: 88,000 $\text{cm}^{-1} \text{M}^{-1}$).

2.2.2.3 Functional analysis of EF-Tu variants

EF-Tu interaction with aa-tRNA was monitored by the ability of EF-Tu to protect aa-tRNA against RNase degradation as described (Pan et al., 2008). Ternary complexes with 0.10–0.15 μ M of yeast [^3H]Phe-tRNA^{Phe} and different concentrations of EF-Tu were made in 50 μ l buffer B (see Section 2.2.6.2) and chilled on ice for 30 min. 5 μ l of 0.05 mg/ml RNase A was added to ternary complex to digest the tRNA at 4 $^{\circ}\text{C}$ for 15 sec, and then quenched with 200 μ l of 10% TCA. Filter binding with a nitrocellulose filter was used to collect protected [^3H]Phe-tRNA^{Phe} followed by three washes with chilled 5% TCA. Filters were dried, dissolved with 1 ml of ethyl acetate,

and counted in scintillation liquid.

The poly(Phe) assay was carried out in buffer C. All concentrations below are final concentrations after mixing. Initiation complex was made by mixing 70S ribosome (0.3 μ M), poly(U) (0.3 g/L), [3 H]-AcPhe-tRNA^{Phe} (0.36 μ M) at 37 °C for 5 min. 2-Mercaptoethanol (2 mM), PEP (0.4 mM), PK (4 mg/L), GTP (0.5 mM), [3 H]-Phe-tRNA^{Phe} (4.5 μ M) and EF-G (0.5 μ M) were then added, and the mixture was fractionated into 6 μ l aliquots. Reaction was started by adding 0.5 μ M of EF-Tu (2 μ l) to the aliquots. After incubation at 37 °C for 30 min, the reaction mixtures were quenched with 0.3 ml of 5% TCA, heated to 95 °C for 15 min and cooled on ice for 1 hour. Filter binding was performed using a nitrocellulose filter followed by three washes with chilled 5% TCA, and the radioactivity of [3 H]-Phe-tRNA^{Phe} was determined.

Determination of quenching efficiency was performed in buffer B. 0.17 μ M of Phe-tRNA^{Phe} (Cy3) was incubated with different concentrations of free QSY9 or EF-Tu^{QSY} variants at 37 °C for 10 min, and fluorescent emissions of the resulting mixtures were determined at room temperature (see Section 2.2.7.1).

2.2.3 Preparation of mRNAs

All modified mRNAs containing thG, thA, thU or thC are from Prof. Yitzhak Tor and Dr. Dongwon Shin at University of California, San Diego.

2.2.3.1 Preparation of mRNA 022 MFTI and 022 CUC

mRNA 022 and 022CUC were prepared and purified as previously reported (Pan et al., 2008). In 400 µl buffer provided in the T7 transcription kit, plasmid (150 ng/µl) was mixed with NTP (100 mM for each of ATP, CTP, GTP and UTP), DTT (100 mM) and 40 µl of T7 enzyme. The mixture was incubated at 42°C for 2 hours, followed by addition of 20 µl of provided DNase I and 15 min incubation at 37°C. The aqueous layer after one extraction with 1:1 phenol pH 4.3/chloroform mixture and one extraction with chloroform, was mixed with 1 volume of chilled 5 M LiCl, followed by incubation on ice for 1 hour, and the precipitate was collected by centrifugation (Heraeus Instrument D-37520, 15k rpm, 20 min). mRNA pellet was resuspended in DDI H₂O and further purified by addition of 2.5 volumes of EtOH for precipitation, washed with 70% ethanol and subjected to a second resuspension and EtOH precipitation. mRNA purity was confirmed by electrophoretic analysis on a 2% agarose gel (Figure 2.1).

2.2.3.2 Preparation of mRNA MRF and MVF

For mRNA MRF, the corresponding coding sequence with a T7 promoter sequence (GGG AAU UCG AAA UAG AAG UCU UCU UUU UGG A AAA AUU UAA AAG UUA AUA AGG AUA CAU ACU AUG CGU UUC UUC CGU UUC UUC CGU AAA UUC CGU GUG CGU UUU UUC AAA UUU GUG UUC CGU UAA CGC GUC UGC AGG CAU GCA AGC UAA AAA AAA AAA AAA AAA AAA

AAA AAA AAA GCU U; IDT, IA) was ligated into plasmid pTZ18R. Overexpression and purification were performed following the procedures similar to mRNA 022 MFTI. mRNA MVF was prepared the same as mRNA MRF with the corresponding synthesized sequence (GGG AAU UCG AAA UAG AAG UCU UCU UUU UGG A AAA AUU UAA AAG UUA AUA AGG AUA CAU ACU AUG GUG UUC UUC CGU UUC UUC CGU AAA UUC CGU GUG CGU UUU UUC AAA UUU GUG UUC CGU UAA CGC GUC UGC AGG CAU GCA AGC UAA AAA AAA AAA AAA AAA AAA AAA AAA AAA GCU U; IDT, IA).

2.2.3.3 Preparation of mRNA MVYF and MKF

mRNA MVYF was prepared by mutation of the mRNA 022 MFTI sequence via PCR (Chiu et al., 2004), using the following primers: forward, 5'-TTA ACT TTT AAA TTT TTG AAT TCC CTA TAG TGA GTC GTA TTA AAT TC-3'; overreverse, 5'-CAG GTA TAC ATA CTA TGG TCT ACT TTA CTA CGA TCT TCT TCA CTT AAC GCG TCT GCA GGC ATG-3'; reverse, 5'-CTT CAC TTA ACG CGT CTG CAG GCA TG-3'; overforward, 5'-AAG ATC GTA GTA AAG TAG ACC ATA GTA TGT ATA CCT GTT AAC TTT TAA ATT TTT GAA TTC CCT ATA GTG AGT CGT ATT AAA TTC-3'. Two PCR samples were prepared with primer forward and overreverse or primer reverse and overforward, respectively. After PCR, parent plasmid was digested by incubation with DpnI enzyme (0.2 Unit/ μ l) at 37°C for 1 hour and the PCR products were purified using a QIAGEN PCR purification kit. Two

PCR products were combined for hybridization of single strand DNA in hybridization buffer using PCR again, and the resulting plasmids were transformed into TOP 10 competent cells for small scale expression. Plasmid was extracted using QIAGEN Miniprep kit and the target mutation was confirmed by DNA sequencing. Correct plasmid was transformed into TOP 10 competent cells for large scale expression and purification as for mRNA 022 MFTI.

mRNA MKF was prepared following a similar procedure to mRNA MVYF using the following primers: forward, the same as mRNA MVYF; overreverse, 5'-CAG GTA TAC ATA CTA TGA AAT TCC GTA CTA CGA TCT TCT TCA CTT AAC GCG TCT GCA GGC ATG-3'; reverse, the same as mRNA MVYF; overforward, 5'-AAG ATC GTA GTA CGG AAT TTC ATA GTA TGT ATA CCT GTT AAC TTT TAA ATT TTT GAA TTC CCT ATA GTG AGT CGT ATT AAA TTC-3'.

2.2.4 Preparation of tRNAs

2.2.4.1 Preparation of formyl donor

Formyl donor was made as described (Dubnoff and Maitra, 1971). 25 mg of folinic acid was dissolved in 2.0 ml of 50 mM 2-mercaptoethanol. Following addition of 0.22 ml of 1.0 M HCl, the mixture was allowed to react for 3 hours at room temperature. Some precipitation may occur during the reaction, which could be dissolved on gentle heating in a water bath set to 37 °C. Formyl donor concentration was determined by A_{355} (at 355 nm, 1 μ mol/ml = 25 A_{355}). The product was then

aliquoted for storage in the freezer. Before being used for tRNA^{fMet} aminoacylation, the pH of formyl donor was activated by adjusting its pH to neutrality with 1/4 volume of 1 M Tris-HCl, pH 8.0 and incubating at room temperature for 20 minutes.

2.2.4.2 Purification of *E. coli* tRNA^{fMet} from bulk tRNAs

24 nmol (400 μ l) of streptavidin agarose beads was washed twice with 400 μ l of 10 mM Tris-HCl pH 7.6, using Ultrafree-MC GV centrifugal filter units (1 min at 5580 xg). The collected beads were incubated, in the presence of 8 nmol of oligo (5'-ATG AGC CCG ACG AGC TAC CAG GCT GCT C-3'-biotin) in 400 μ l of 10 mM Tris-HCl pH 7.6 buffer, at room temperature for 30 min, shaken by hand every 5 min and washed twice with 400 μ l of 10 mM Tris-HCl pH 7.6 to remove the unbound oligos, as monitored by A_{260} . 200 units of bulk tRNA from *E. coli* MRE600 cells (360 nmol bulk tRNA; ~3.6 nmol tRNA^{fMet}) in 300 μ l of DDI water were heated at 80 °C for 10 min, quickly mixed with 300 μ l of TMA buffer, and immediately added to oligo bound beads. The resulting mixture was heated at 65 °C for 10 min, followed by gradual temperature decrease to 37 °C and 30 min incubation at 37 °C. Unbound tRNAs were removed by 7 washes with 400 μ l of 10 mM Tris-HCl pH 7.6. Bound tRNAs were eluted by a stepwise incubations at 45°C, 55°C and 65°C, respectively. At each temperature, beads were heated for 7 min in the presence of 400 μ l of 10 mM Tris-HCl pH 7.6, centrifuged at 10k rpm for 1 min, and washed twice with 400 μ l of 10 mM Tris-HCl pH 7.6 by centrifugation. Each centrifugation was performed in the

presence of 2 μ l of 1 M MgCl_2 , and the flow-through was collected separately. For those fractions containing $\text{tRNA}^{\text{fMet}}$ as measured by A_{260} , 1/10 volume of 1 M Tris-HCl pH 9.0 was added and the mixtures were incubated at 37°C for 3 hours. tRNAs were obtained by EtOH precipitation with addition of 2.5 volumes of EtOH.

To roughly estimate the aminoacylation efficiency, $\text{tRNA}^{\text{fMet}}$ formylaminoacylation was done in a 10 μ l scale for the tRNA product eluted at each temperature (see section 2.2.4.3), with a negative control performed in the absence of aminoacyl-tRNA synthetases. After incubation, 400 μ l of 5% TCA was added and the samples were left on ice for 1 hour. Filter binding was performed using a nitrocellulose filter followed by three washes with chilled 5% TCA, and the radioactivity of [^{35}S]-fMet-tRNA $^{\text{fMet}}$ was determined. tRNA $^{\text{fMet}}$ was in fractions eluted at 65 °C.

2.2.4.3 Formylaminoacylation of tRNA $^{\text{fMet}}$

Procedures described in Pan et al. (Pan et al., 2007) were used to formylaminoacylate commercial tRNA $^{\text{fMet}}$ from *E. coli*. 36 nmol of tRNA $^{\text{fMet}}$ was incubated in 2000 μ l of aminoacylation buffer A at 37°C for 45 min. The reaction was quenched with 200 μ l of 20% KAc pH 5.0, extracted once with phenol (Tris-saturated, pH 4.3) and once with chloroform, both in 1:1 volume ratio, and, after addition of 1/10 volume of 20% KAc pH 5.0, was precipitated with 2.5 volumes of EtOH. Formylaminoacylated tRNA was further purified on FPLC with a self-packed column

(5×50 mm) using Q-Sepharose resin. tRNAs on the column were washed with 15 ml of 50 mM NaAc pH 5.0, and eluted by a gradient of 0–1 M NaCl in 50 mM NaAc pH 5.0. tRNA concentration was determined by A_{260} and [^{35}S]-fMet-tRNA^{fMet} concentration by radioactivity counting. A typical aminoacylation efficiency of 850–1200 pmol/ A_{260} was normally obtained. tRNA^{fMet} purified from bulk tRNA was formylaminoacylated in a similar procedure except that 4 nmol of tRNA^{fMet} was used in every 2000 μl of aminoacylation mixture, to a level of 1250–1800 pmol/ A_{260} . Commercial tRNA^{fMet} was used in all of the experiment in Chapter III and IV. Purified tRNA^{fMet} was used for most of the experiments in Chapter V and commercial tRNA^{fMet} was used for some of the experiments. In control experiments, no difference was observed between using commercial and purified tRNA^{fMet} within the experimental error.

2.2.4.4 Aminoacylation of tRNA^{Phe}

Commercial tRNA^{Phe} from yeast was aminoacylated using a procedure similar to commercial tRNA^{fMet} except for in the aminoacylation buffer B and the use of yeast PheRS (Pan et al., 2007). A typical aminoacylation stoichiometry was 550–700 pmol/ A_{260} .

Commercial *E. coli*. tRNA^{Phe} was aminoacylated similar to yeast tRNA^{fMet} except that: 1) aminoacylation buffer C was used; 2) incubation was 20 min at 37°C (Pan et al., 2007). *E. coli*. tRNA^{Phe} could be aminoacylated to a level of 550–700 pmol/ A_{260} .

2.2.4.5 Preparation of yeast AcPhe-tRNA^{Phe}

1.2 nmol yeast [³H]-Phe-tRNA^{Phe} was lyophilized and re-dissolved in 50 µl 0.1 M NaAc pH 5.0. 0.0484 g N-hydroxysuccinimide ester was dissolved in 480 µl of dry DMSO, 400 µl of which was added to the [³H]-Phe-tRNA^{Phe} solution. After incubation on ice for 2 hours, the sample was mixed with 50 µl of 20% KAc pH 6.5, EtOH precipitated, and centrifuged at 15k rpm for 20 min (Heraeus Instrument D-37520). Precipitation was repeated twice and the tRNA was resuspended in 150 µl of H₂O. A fraction of 10 µl was aliquoted out and added into 1 M NH₄OH as a control for overall [³H]-Phe-tRNA^{Phe} radioactivity counting, and the remaining sample was diluted 25-fold in H₂O. To pack a small column, 200 µl of cation exchange resin AG 50W-X8 resuspended in 0.01 M HCl was loaded onto small spin column and washed 5 times with 500 µl of H₂O. Diluted sample in 500 µl portions was loaded onto a packed column, and washed 5 times with 500 µl of H₂O and 5 times with 1 M NH₄OH, all of the flow-through being collected separately. 50 µl aliquot from each fraction and the control were incubated at 75°C for 5 hours, mixed with 500 µl of H₂O to dissolve everything, and counted in scintillation liquid to identify the fractions containing the product. Ac-[³H]-Phe-tRNA^{Phe} was eluted with H₂O, and EtOH precipitated with addition of 2.5 volumes of EtOH and dissolved in H₂O at a final concentration of ~ 5 µM.

2.2.4.6 Aminoacylation of *E. coli* tRNA^{Val}, tRNA^{Arg} and tRNA^{Lys}

E. coli tRNA^{Val}, tRNA^{Arg} and tRNA^{Lys} were aminoacylated by using a similar procedure to tRNA^{fMet}, except that 1) aminoacylation buffer D was used; 2) the incubation time for tRNA^{Lys} was 10 min. Typical aminoacylation stoichiometries were 500–700 pmol/A₂₆₀ for tRNA^{Val}, 1000–1200 pmol/A₂₆₀ for tRNA^{Arg}, 500–650 pmol/A₂₆₀ for tRNA^{Lys}.

2.2.4.7 Aminoacylation of tRNA^{Val2B} variants

tRNA^{Val2B} variants were kind gifts from Dr. Olke C. Uhlenbeck (Northwestern University). tRNA^{Val2B} was aminoacylated following reported procedures (Dale et al., 2004) with some modifications. 1.2 nmol tRNA was incubated in 600 µl of aminoacylation buffer E at 37°C for 15 min. The reaction was quenched by 60 µl of 20% KAc pH 5.0, and extracted once with phenol (Tris-saturated, pH 4.3) and once with chloroform, both in 1:1 volume ratio. tRNA was EtOH precipitated with addition of 2.5 volumes of EtOH and used with no further purification. [³H]-Val-tRNA^{Val2B} concentration was determined by radioactivity counting.

2.2.4.8 tRNA labeling with proflavin

A modified procedure for the preparation of fMet-tRNA^{fMet}(prf) (Pan et al., 2007) was utilized to perform tRNA labeling with proflavin. To reduce the dihydrouridine

residues in the tRNA D-loop, 36 nmol of tRNA in 324 μ l of 40 mM Tris-HCl pH 7.5 was rapidly mixed with 36 μ l of 100 mg/ml NaBH₄ in 0.01 M KOH, followed by 1 hour incubation on ice and H₂ release every 10 min. The reduction reaction was terminated by drop-wise addition of 60 μ l of 6 N HAc, and the product was purified by EtOH precipitation for three times in the presence of 1/10 volume of 20% KAc pH 5.0 and 2.5 volumes of EtOH. Reduced tRNA was aminoacylated and purified by FPLC as described above, resuspended in 100 μ l of H₂O, and mixed with 1 ml of 0.52 mg/ml proflavin in 0.1 M HCOONa pH 3.7 for 45 min incubation at 37°C. After incubation, the solution was adjusted to about pH 7.5 by addition of 1/10 volume of 1 M Tris, and extracted twice with phenol (Tris-saturated, pH 6.5). Labeled tRNA was EtOH precipitated twice after addition of 1/10 volume of 20% KAc pH 6.5 and 2.5 volumes of EtOH. Aminoacylation and labeling efficiencies were generally obtained as following: 700–900 pmol/A₂₆₀ and 0.9–1.1 prf/tRNA for tRNA^{fMet}; 250–400 pmol/A₂₆₀ and 0.8–1.0 prf for *E. coli*. tRNA^{Phe}; 250–400 pmol/A₂₆₀ and 1.0–1.2 prf/tRNA for tRNA^{Val}; 800–1000 pmol/A₂₆₀ and 0.9–1.1 prf/tRNA for tRNA^{Arg}; 200–350 pmol/A₂₆₀ and 1.0–1.2 prf/tRNA for tRNA^{Lys}.

2.2.4.9 tRNA^{Phe} labeling with Cy3

Yeast tRNA^{Phe} was labeled with Cy3 (Pan et al., 2009) or Cy5 (Kaur et al., 2011) as previously reported. tRNA^{Phe} was reduced and aminoacylated as above described, then purified using phenyl RP-HPLC (RP-C18 column, 4.6 \times 250 mm, Alltech) with a

gradient of 0% to 30% ethanol in 20 mM NH₄Ac pH 5.0, 10 mM Mg(Ac)₂ and 400 mM NaCl. Pooled fractions were EtOH precipitated with 20% KAc pH 5.0 and 2.5 volumes of EtOH, and resuspended in 10 µl of 0.1 M HCOONa pH 3.7. Labeling was performed by mixing reduced and aminoacylated tRNA with 2 µl of 270 mM of Cy3 or Cy5 hydrazide in DMSO, followed by a incubation at 37°C for 2 hours. Then the sample was lyophilized, EtOH precipitated as above for three times with 1/10 volume of 20% KAc pH 5.0. Phe-tRNA^{Phe}(Cy3 or Cy5) was obtained with an aminoacylation efficiency of ~900 pmol/A₂₆₀ and ~0.5 Cy3/tRNA.

2.2.4.10 Preparation of highly labeled tRNA^{Phe} with Cy5

Yeast tRNA^{Phe} was highly labeled with Cy5 as above described except that: 1) reduced and aminoacylated tRNA^{Phe} was purified on FPLC; 2) 20% KAc pH 6.5 was used all the times. Phe-tRNA^{Phe}(Cy5) was obtained with an aminoacylation efficiency of ~500 pmol/A₂₆₀ and a labeling efficiency of ~0.8 Cy5/tRNA.

2.2.5 Preparation of the 70S ribosomal complex and ternary complex

Tightly-coupled wild-type 70S ribosomes from *E.coli* MRE600 cells and mutant 70S ribosomes lacking L11 from *E.coli* AM77 cells were prepared and purified as previously reported (Pan et al., 2008).

2.2.5.1 Preparation of the 70S ribosome labeled with Cy3 or Cy5

The reconstitution of 70S ribosomes containing L11^{Cy3} (70S^{Cy3}) or L11^{Cy5} (70S^{Cy5}) was performed as described (Chen et al., 2011a). 100 μ l of 30 μ M labeled L11 and 40 μ l of 50 μ M 70S lacking L11 were first incubated at 37°C for 5 min separately, then combined for a further incubation at 37°C for 15 min. After an increase of magnesium concentration to 20 mM, the mixture was subject to centrifugation through a sucrose cushion in buffer A with 1.1 M sucrose and magnesium concentration increased to 20 mM (SORVALL S120-AT2 rotor, 110K rpm, 40 min, 4 °C) to pull down the labeled 70S. The pellet was suspended in buffer A. 70S concentration was determined by A_{260} and dye concentration was determined by A_{550} for Cy3 or A_{650} for Cy5, respectively. A typical labeling efficiency is 0.8–1.0 dye/70S.

2.2.5.2 Preparation of ribosomal complexes and ternary complex

All ribosome complexes were prepared in buffer A at 37 °C. 70SIC was made by incubating 70S ribosome (0.8–4 μ M) with mRNA (4-fold excess over 70S for all experiments in Chapter III and IV; half of 70S for experiments presented in Chapter V, Figure 5.2–5.3; 2-fold excess over 70S for all other experiments in Chapter V), IF1–3 (1.5-fold excess over 70S), GTP (1 mM) and [³⁵S]-fMet-tRNA^{fMet} (1.5-fold excess over 70S) for 25 min. For experiments using fMet-tRNA^{fMet}(prf), MDCC-PBP or GDPNP in Chapter III and IV and all experiments in Chapter V except for experiments presented in Figure 5.2C,D and 5.3B, 70SIC was purified by

centrifugation through a 1.1 M sucrose cushion in buffer A (SORVALL S120-AT2 rotor, 110K rpm, 40 min, 4 °C). In all other experiments, the ultracentrifugation step was omitted. Purified 70SIC was quantified (Figures 5.2A,B and 5.3A) as co-sedimenting [³⁵S]-fMet-tRNA^{fMet} per mRNA, where mRNA stoichiometry was assumed to be half of 70S.

TC was formed by incubating aminoacyl-tRNA (0.8–8 μM) with EF-Tu (4-fold excess over aa-tRNA), GTP (1 mM), phosphoenolpyruvate (1.5 mM) and pyruvate kinase (10 μg/mL) for 10 min. No PEP and PK were added when GDPNP was used. For P_i release experiments, GTP concentration was 50 μM, and no PEP and PK were added. TC solution was premixed with MDCC-PBP (2.5 μM), 7-methylguanosine (200 μM) and nucleoside phosphorylase (0.2 Unit/ml) before kinetic experiments.

PRE complex was formed by incubating 70SIC (0.5–2 μM, as measured by A₂₆₀ of 70S) with TC (2-fold ratio to 70S) for 1 min. Purified PRE complex was prepared by centrifugation through a 1.1 M sucrose cushion in buffer A with 20 mM MgCl₂, performed as 70SIC, and quantified (Figures 5.2C,D and 5.3B) as co-sedimenting [³H]-Val (thG4- or thG6-programmed ribosomes), [³H]-Arg (thG5-programmed ribosomes) or [³H]-Lys (thA1-, thA4-, thA5- or thA6-programmed ribosomes). All experiments reported in this thesis used purified PRE complexes, except for those shown in Figure 5.2E, for which the ultracentrifugation step was omitted.

POST complex was prepared and quantified (Figures 5.2E,F and 5.3C) using two different procedures. PRE complexes programmed with thG4, thG6 or MVF (0.8 μM,

as measured by A_{260} of 70S) were incubated with EF-G.GTP (2 μ M) and puromycin (2.5 mM) at 37 °C for 30 s, the reaction was quenched with 1 volume of 0.3 M NaAc, pH 5.0, fMet-[3 H]-Val-puromycin was quantitatively extracted with ethyl acetate and the radioactivity in the extract was determined. A different procedure was required for PRE complexes programmed with $^{th}G5$, MRF, $^{th}A1$, $^{th}A4$, $^{th}A5$, $^{th}A6$ or MKF, because of the insolubility of fMet-[3 H]-Arg-puromycin and fMet-[3 H]-Lys-puromycin in ethyl acetate. Here PRE complex (5 μ M, as measured by A_{260} of 70S) was incubated with EF-G.GTP (10 μ M) and puromycin (15 μ M) at 20 °C for 30 s, and the reaction was quenched by adding 5 volumes of buffer A adjusted to pH 5. These conditions were sufficient for full puromycin reaction with translocated fMet-[3 H]-Arg-tRNA^{Arg} or fMet-[3 H]-Lys-tRNA^{Lys}, resulting in fMet-Arg-puromycin or fMet-Lys-puromycin formation. The resulting mixture was subject to ultracentrifugation through a 1.1 M sucrose cushion in buffer A with 20 mM MgCl₂, performed as above. fMet-Arg-puromycin or fMet-Lys-puromycin remained in the supernatant during centrifugation. Unreactive fMet-Arg-tRNA^{Arg} or fMet-Lys-tRNA^{Lys} co-sedimented with the ribosome. Radioactivity in the pellet was determined.

The relative amount (RA) of EF-G- and mRNA-dependent POST complex formation was obtained by correcting the results obtained for differences in the efficiencies of formation of the 70SIC (Figure 5.2E) and PRE (Figures 5.2E–F and 5.3C) complexes and normalizing to the value found for unmodified mRNA. This was accomplished by measuring the amounts of [3 H]-Val, [3 H]-Arg, [3 H]-Lys or found in either the ethyl acetate extract ($^{th}G4$, $^{th}G6$, or MVF) or sucrose cushion pellet ($^{th}G5$,

MRF, thA1, thA4, thA5, thA6 or MKF) in four different samples formed in the presence (a) or absence (c) of EF-G in the presence of mRNA, or in the presence (b) or absence (d) of EF-G, in the absence of mRNA, and calculating the efficiencies using Equation 2.1A (thG4, thG6 or MVF) or 2.1B (thG5, MRF, thA1, thA4, thA5, thA6 or MKF).

$$RA = 1-[(c-d)/(a-b)] \text{ (2.1A); } RA = 1-[(a-b)/(c-d)] \text{ (2.1B)}$$

Data for thG4, thG6 and thG5 were used for sample calculation of relative translocation. The relative amounts of [³H]-Val per ribosome in the ethyl acetate extract were: (a) 0.057, 0.030 and 0.052 for MVF, thG4 and thG6, respectively; (c) 0.009, 0.006 and 0.012 for MVF, thG4 and thG6, respectively. The values of [³H]-Val per ribosome for (b) and (d) were 0.002 and 0.001, respectively. From Equation 2.1A, the translocation efficiencies were 0.85, 0.82 and 0.78 for MVF, thG4 and thG6, respectively, which were all normalized to the efficiency of MVF. Therefore, the relative POST complex formation efficiencies, as shown in Figure 5.2E, were 1.0, 0.96 and 0.92 for MVF, thG4 and thG6, respectively. The relative amounts of [³H]-Arg per ribosome in sucrose cushion pellet were: (a) 0.032 and 0.040 for MRF and thG5, respectively; (c) 0.100 and 0.084 for MRF and thG5, respectively. The values of [³H]-Arg per ribosome for (b) and (d) were 0.010 and 0.015, respectively. From Equation 2.1B, the translocation efficiencies were 0.75 and 0.57 for MRF and thG5, respectively, which were both normalized to the efficiency of MRF. Therefore, the relative POST complex formation efficiencies, as shown in Figure 5.2F, were 1.0 and 0.76 for MRF and thG5, respectively.

2.2.5.3 Purification of ternary complex

To evaluate the quenching efficiency between E348C-EF-Tu^{QSY9} and Phe-tRNA^{Phe}(Cy3), TC [formed by combining 2 nmol of E348C-EF-Tu^{QSY9} and 0.7 nmol of Phe-tRNA^{Phe} (Cy3)] was purified on Co(II)-Sepharose (Talon) resin (bed volume 0.5 ml). TC and resin pre-washed with buffer A with no DTT were mixed and shaken at 4 °C for 30 min, pulled down by centrifugation (Heraeus Instrument D-37520, 8000 rpm, 2 min), and transferred to a small spin column. The resin was washed sequentially with 4 ml of buffer A with no DTT, 2 ml of buffer A with no DTT but 300 mM KCl and 10 mM imidazole. TC was eluted with 2 ml of buffer A with no DTT but 300 mM KCl and 300 mM imidazole. All of the washes and elutions were collected in 500 µl fractions. TC was normally in the first fraction of the elution and its concentration was determined by scintillation counting.

2.2.6 Fluorescence experiments

2.2.6.1 Static fluorescence experiments

Steady-state fluorescence was measured on a Fluorolog-3 spectrofluorometer (Horiba Jobin Yvon). The emission spectrums were recorded with an excitation at 530 nm for Cy3, 360 nm for thA and thG. Excitation spectrums of modified nucleosides were performed by monitoring the emission at 410 nm for thA and 450 nm thG. Distances between FRET donor and acceptor were calculated using the equation

shown as below:

$$\text{Distance} = R_0 \cdot (1/E - 1)^{1/6}$$

where R_0 is the Förster distance (Medintz et al., 2003) and E is measured FRET efficiency.

2.2.6.2 Stopped-slow experiments

Kinetic experiments were performed in buffer A at 25 °C on KinTek SF-300X stopped-flow spectrofluorometer. Cy3 was excited at 530 nm and monitored using either a 570-nm long-pass filter for experiments employing QSY9 or a 570 ± 10 -nm band-pass filter for all other experiments. Cy5 fluorescence was monitored using a 680 ± 10 -nm band-pass filter. Proflavin was excited at 462 nm and monitored using a 515 ± 15 -nm band-pass filter. MDCC-PBP was excited at 436 nm and monitored using a 455 nm long-pass filter. thG was excited at 360 nm and monitored using a 450 ± 10 -nm band-pass filter. thA was excited at 360 nm and monitored using a 410 ± 10 -nm band-pass filter. In each independent kinetic experiment, traces of fluorescence intensity changes were obtained as an average of at least 4 shots. Each experiment was performed twice. Apparent rate constants (k_{app} s) were obtained by either single (Equation 2.2) or double (Equation 2.3) exponential fitting of each independent experiment using Origin (OriginLab), respectively. Global fittings of selected data sets were carried out using Scientist (MicroMath Research).

$$F = F_0 + F_1 e^{-k_{1app} t} \quad (\text{Equation 2.2})$$

$$F = F_0 + F_1 e^{-k_{1app} t} + F_2 e^{-k_{2app} t} \quad (\text{Equation 2.3})$$

2.2.6.3 Single-molecule experiments

smFRET studies were carried out at 23 °C. 70S ICs formed using a 5'-biotinylated mRNA (Dharmacon RNAi Tech.) were immobilized on a biotin/PEG-streptavidin coated glass surface (Roy et al., 2008). After washing away unbound complexes, collection of real-time fluorescence traces began 5 s prior to injecting 10 nM ternary complexes, which were preformed from EF-Tu, GTP and charged tRNAs. Recording continued for 60 s without further washing. An enzymatic deoxygenation system of 3 mg/ml glucose, 100 µg/ml glucose oxidase, 40 µg/ml catalase, and 1.5 mM 6-hydroxy-2,5,7,8-tetramethyl-chromane-2-carboxylic acid (by dilution from a DMSO solution) was present in the final single-molecule imaging solutions to diminish fluorophore photobleaching and blinking. A custom-built objective-type total internal reflection fluorescence (TIRF) microscope was used to collect Cy3 and Cy5 (due to FRET from Cy3) fluorescence intensities on excitation by a 532 nm laser (Chen et al., 2011a). The 11 ms integration time was achieved by cutting the exposure area down to 128 pixels × 512 pixels without further binning. Other details of materials preparation, experimental setup, and data analysis were as previously described (Chen et al., 2011a).

FRET probability density plots were two-dimensional contour maps plotted from

time-resolved FRET histograms. For each plot, FRET traces were synchronized at the same specific event, such as the first or the last time points of FRET events. The FRET value was set to 0 when there are no Cy3 and Cy5 fluorescence signals.

Synchronized FRET traces were averaged traces from FRET traces synchronized at the same specific event, such as the first or the last time points of FRET events (Veigel et al., 2002; Stevens et al., 2012). Before averaging, for the pre-synchronization process, FRET traces were synchronized at the time points of FRET appearance and were extended after FRET disappearance using the FRET value of the last time point of FRET event. Similarly, for the post-synchronization process, FRET traces were synchronized at the time points of FRET disappearance and were back-extended before FRET appearance using the FRET value of the first time point of the FRET event.

2.2.7 Quenched-flow experiments

Kinetics of fMetPhe dipeptide formation were measured following previous procedures (Pan et al., 2008) by mixing IC (1.2 μM) and TC (0.3 μM) containing [^3H]-Phe-tRNA^{Phe} at 25°C on quench-flow machine (KinTek Chemical Quench-Flow Model RQF-3). Reaction was quenched with 5 M NH_4OH at different time points (e.g. 0.01, 0.02, 0.05, 0.1, 0.2, 0.4, 0.5, 0.7, 3, 5, 7, 10, 15, 30, 45, 60 sec). Quenched samples were lyophilized and resuspended in 500 μl of H_2O . 50 μl aliquot from each sample was scintillation counted as positive control to measure total radioactivity. The

remaining samples were loaded onto cation exchange resin AG 50W-X8 (bed volume 400 μ l) pre-washed with 5 \times 400 ul of 0.01 M HCl and 5 \times 400 ul of H₂O. Dipeptide was eluted with 2 ml of H₂O. Dipeptide was in both flow-through of sample loading and elution, and they are combined for scintillation counting determination of dipeptide. .

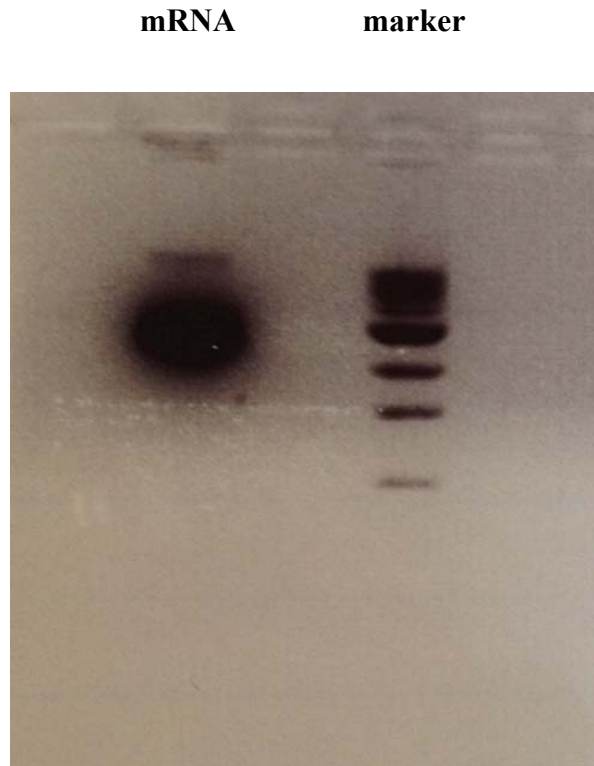


Figure 2.1. Electrophoretic analysis of purified mRNA. The gel contains 2% agarose.

022 MFTI:

GGG AAU UCA AAA AUU UAA AAG UUA ACA GGU AUA CAU ACU AUG
UUU ACG AUU ACU ACG AUC UUC UUC ACU UAA CGC GUC UGC AGG
CAU GCA AGC UAA AAA AAA AAA AAA AAA AAA AAA AAA AAA GCU U

022 CUC:

GGG AAU UCA AAA AUU UAA AAG UUA ACA GGU AUA CAU ACU AUG
CUC ACG AUU ACU ACG AUC UUC UUC ACU UAA CGC GUC UGC AGG
CAU GCA AGC UAA AAA AAA AAA AAA AAA AAA AAA AAA AAA GCU U

MRF:

GGG AAU UCA AAA AUU UAA AAG UUA AUA AGG AUA CAU ACU AUG
CGU UUC UUC CGU UUC UAU CGU UUC

MVYF:

GGG AAU UCA AAA AUU UAA AAG UUA ACA GGU AUA CAU ACU AUG
GUC UAC UUU ACU ACG AUC UUC UUC ACU UAA CGC GUC UGC AGG
CAU GCA AGC UAA AAA AAA AAA AAA AAA AAA AAA AAA AAA GCU U

MVF:

A GGU AUA CAU ACU AUG GUG UUC CGU AAA UAU UUG CCC GGG CCC
GGG AAAA CCC GGG CCC GGG CCC TT TTT TCT GCA

MKF:

GGG AAU UCA AAA AUU UAA AAG UUA ACA GGU AUA CAU ACU AUG
AAA UUC CGU ACU ACG AUC UUC UUC ACU UAA CGC GUC UGC AGG
CAU GCA AGC UAA AAA AAA AAA AAA AAA AAA AAA AAA AAA GCU U

Figure 2.2. Unmodified mRNA sequence. AUG initiation codons are underlined.

CHAPTER 3

LABELED EF-TUS FOR RAPID KINETIC STUDIES OF PRE-TRANSLOCATION COMPLEX FORMATION

3.1 Abstract

As one of the two universally conserved translation elongation factors, EF-Tu delivers aminoacyl (aa)-tRNA in the form of a ternary complex (TC) to the ribosome to decode the codon programmed at the ribosomal A-site. Here, a QSY9 derivative of E348C-EF-Tu was prepared and shown to be fully functional in translation elongation. Together with fluorophore derivatives of aa-tRNA and L11, labeled EF-Tu was utilized for the development of two new assays to study the relative dynamics within the EF-Tu:L11:tRNA triangle. Our results showed that EF-Tu comes into proximity to L11 when delivering aa-tRNA to the ribosome, and leaves L11 and releases aa-tRNA after EF-Tu mediated GTP hydrolysis. These assays were used to examine the effects of two misreading antibiotics, streptomycin (Str) and paromomycin (Par), on tRNA selection at the ribosomal A-site in both initial selection and proof-reading stages. It was also shown that the contacts between T stem-loop of aa-tRNA and EF-Tu have crucial effects in tRNA release from EF-Tu and accommodation into the A-site.

3.2 Introduction

EF-Tu is, along with EF-G, one of two G-protein factors that are required for nascent polypeptide elongation by the prokaryotic 70S ribosome (Kavaliauskas et al., 2012). These factors are crucial for controlling the speed and accuracy of the polymerization of amino acids into polypeptides encoded by mRNA. 70S ribosomes are formed by the association of the 30S and the 50S subunits, within which the mRNA codon : tRNA anticodon interaction and peptide bond formation occur, respectively. During an elongation cycle, a tRNA binds sequentially to several sites in the 70S ribosome. These sites are named according to several major defined locations within the 30S and the 50S subunits, as follows: A/T, A/A (or just A), A/P, P/P (or just P), P/E, and E/E (or just E) (Schmeing et al., 2009). In the first elongation cycle, EF-Tu acts as a chaperone in accelerating the binding of a cognate aa-tRNA, in the form of a EF-Tu.GTP.aa-tRNA ternary complex (TC), to the ribosomal A/T-site of a 70S initiation complex (70SIC), which contains initiator fMet-tRNA^{fMet} bound in the P-site. TC binding to the ribosome brings EF-Tu into proximity with ribosomal protein L11 within the GTPase associated center (GAC) of the 50S subunit, to which all ribosomal G-proteins bind (Allen et al., 2005). Formation of Watson-Crick base pairs between the anticodon loop of cognate aa-tRNA and the three-nucleotide codon sequence in mRNA at the decoding center of the 30S subunit leads to changes in ribosome conformation and an activation of the EF-Tu GTPase activity. GTP hydrolysis is followed by P_i release, movement of aa-tRNA from the A/T to the A/A site, a process also known as “accommodation” into the A-site, peptide bond

formation between fMet-tRNA^{fMet} and aa-tRNA, and EF-Tu.GDP release from both peptidyl-tRNA and the ribosome, resulting in pretranslocation (PRE) complex formation. Structural studies show a dramatic conformational difference between the GTP- and GDP-bound forms of EF-Tu (Kjeldgaard and Nyborg, 1992; Polekhina et al., 1996). The antibiotic kirromycin inhibits elongation by "freezing" EF-Tu.GDP on the ribosome in a GTP-like conformation (Schmeing et al., 2009a).

Selection of the correct isoacceptor tRNA takes place in two steps, one preceding and one following GTP hydrolysis. During initial selection, all non-cognate and the major fraction of near-cognate TCs dissociate. After GTP hydrolysis, almost all remaining near-cognate tRNAs are rejected in the so-called proofreading step; a small fraction goes forward and participates in peptide bond formation. The selectivity of the decoding process for cognate tRNA is reduced by aminoglycosides (Vicens and Westhof, 2003).

Although the movement of tRNA through the ribosome during PRE complex formation has been extensively studied by kinetic, structural and modeling studies (Pape et al., 1998; Pan et al., 2007; Schmeing and Ramakrishnan, 2009b), tools allowing description of the dynamic properties of EF-Tu as it interacts with both the ribosome and aa-tRNA have heretofore been unavailable. Here we describe the preparation and utilization of functionally active fluorescent and fluorescence quencher derivatives of EF-Tu that address this deficiency. In conjunction with either ribosomes containing fluorescent-labeled L11, or with fluorescent-labeled forms of

aa-tRNA, these derivatives allow the development of real-time fluorescence resonance energy transfer (FRET) assays that monitor EF-Tu proximity to L11 (FRET assay 1) and contact with aa-tRNA (FRET assay 2). These assays, along with a previously described assay measuring aa-tRNA movement from the A/T-site to the A-site (Pan et al., 2008) permit us to measure the rates of several key substeps of PRE complex formation, including i) initial TC interaction with the A/T site, ii) movement of EF-Tu.GDP away from its initial binding site during accommodation, and iii) release of EF-Tu.GDP from aa-tRNA. In addition, they allow us to determine how the rates of these processes are influenced by mechanistically important variables, such as substitution of near-cognate for cognate mRNA in the presence or absence of aminoglycoside antibiotics, and the strength of EF-Tu interaction with aa-tRNA.

3.3 Results

3.3.1 Nomenclature

The labeled protein synthesis components employed in this work are named and described in Table 3.1. QSY9 is an efficient quencher of Cy3 fluorescence.

3.3.2 Probe-labeled EF-Tu variants and their formation of TCs with Phe-tRNA^{Phe}

We chose positions for probe introduction into *E. coli* EF-Tu based on the structure of a kirromycin- and paromomycin-stabilized ribosome complex containing

bound EF-Tu.GDP and aa-tRNA (Protein Data Bank accession codes 2WRN, 2WRO, 2WRQ, and 2WRR) (Figure 3.1). Three EF-Tu residues, K324, G325, and E348 (using *E. coli* EF-Tu numbering), met the criteria of i) falling within $<50 \text{ \AA}$ of residue 87 in L11 (Chen et al., 2011b) and of residues 16/17 of A/T-bound tRNA (Kaur et al., 2011); ii) pointing toward solvent, and iii) not being highly conserved (Perla-Kajan et al., 2010). They were thus suitable for probe introduction via replacement by a Cys residue and reaction with a QSY9 or Cy3 maleimide derivative.

EF-Tu contains three endogenous Cys residues (C81, C137 and C255), which can potentially be labeled, possibly leading to decreased EF-Tu functional activity and/or interference with interpretation of FRET signals. As expected based on lack of conservation, Cys 137 and Cys 255 could be replaced by Ala or Val, respectively, without affecting aa-tRNA binding (unpublished from Dr. Darius Kavaliauskas and Prof. Charlotte R. Knudsen). Efforts to replace Cys 81 consistently led to loss of EF-Tu activity (unpublished from Dr. Darius Kavaliauskas and Prof. Charlotte R. Knudsen; also in Figure 3.2B), consistent with a previous study of the functional role of Cys 81 (Anborgh et al., 1992). In contrast, a more recent study claimed that aa-tRNA binding to EF-Tu was retained when Cys 81 is replaced by Ala (Laurentiis et al., 2011). However, in this latter work concentrations of both aa-tRNA and EF-Tu were in great excess over the dissociation constant, so that even comparatively large decreases in affinity would not have been detected.

In view of our results, EF-Tu variants containing cysteines at positions K324,

G325, and E348 were prepared by single mutation of wt-EF-Tu. The Cys at position 324, 325, or 348 was much more reactive toward derivatization than the endogenous Cys residues. As a result, stoichiometric labeling at these positions could be obtained with only minor labeling of the endogenous residues (Table 3.2) that was inconsequential for subsequent EF-Tu:tRNA or EF-Tu:L11 FRET measurements (see Figures 3.2A and 3.5B).

Two QSY9-labeled derivatives of single EF-Tu variants, E348C-EF-Tu^{QSY9} and K324C-EF-Tu^{QSY9}, showed similar high affinities for Phe-tRNA^{Phe}(Cy3) as measured by the quenching of Phe-tRNA^{Phe}(Cy3) fluorescence (Figure 3.2A) or protection of Phe-tRNA^{Phe}(Cy3) from hydrolysis (Figure 3.2B), and both supported poly(U)-dependent poly(Phe) synthesis by ribosomes to equal extents (Figure 3.2C). A third QSY9-labeled derivative, G325C-EF-Tu^{QSY9}, showed clearly weaker affinity for Phe-tRNA^{Phe}(Cy3) in the fluorescence quenching assay (Figure 3.3A) and in this same assay the apparent quenching by E348C-EF-Tu^{QSY9} was greater than by K324C-EF-Tu^{QSY9}. On the basis of these results, E348C-EF-Tu^{QSY9} was selected for subsequent studies.

Phe-tRNA^{Phe}(Cy3) fluorescence is decreased 82% within the TCs it forms with E348C-EF-Tu^{QSY9} (Fig. 3.3A). Based on the FRET R_0 values for the pairs Cy3/QSY9 (55 Å) (Medintz et al., 2003), this decrease corresponds to dye-dye distances of ~ 43 Å for the TC formed by E348C-EF-Tu^{QSY9}, assuming that the dye rotates freely. This distance is in reasonable accord with an expected distance of 34 Å ($C_{\alpha,348}$, EF-Tu; to

16 N¹, tRNA) measured in ternary complexes (Nissen et al., 1999), allowing for some increase due to the dye dimensions. Measuring the rate of Phe-tRNA^{Phe}(Cy3) quenching as a function of E348C-EF-Tu^{QSY9} concentration allowed estimation of $k_{\text{on}} = 1.3 \pm 0.1 \mu\text{M}^{-1}\text{s}^{-1}$ and $k_{\text{off}} = 0.17 \pm 0.07 \text{ s}^{-1}$ for TC formation (Figure 3.3B), consistent with previous estimates of the K_d value using unlabeled EF-Tu (Pan et al., 2008).

3.3.3 Interaction of TCs containing labeled EF-Tu with 70SICs

Rapid mixing in a quenched-flow apparatus of the TC formed from E348C-EF-Tu^{QSY9}.GTP and Phe-tRNA^{Phe}, denoted TC^{QSY9}, with a 70SIC programmed with mRNA022 MFTI, which has a UUU codon following the AUG initiation codon, led to an apparent rate constant for fMetPhe-tRNA^{Phe} formation, 4.5 s^{-1} , similar to the values reported earlier using unlabeled TC and unlabeled 70SIC (Figure 3.4) (Gromadski and Rodnina, 2004a; Pan et al., 2008). This result demonstrates the functionality of E348C-labeled EF-Tu in catalyzing dipeptide formation during PRE complex formation.

We developed two new stopped-flow FRET assays for monitoring TC interaction with 70SIC in real time. The FRET-1 assay involves rapid mixing of 70SIC containing Cy3-labeled L11, denoted 70SIC^{Cy3}, with TC^{QSY9} (Figure 3.5). Such mixing results in a biphasic change in Cy3 fluorescence, with an initial decrease corresponding to TC binding to the ribosome that places EF-Tu position 348 in

proximity to L11 position 87, followed by a restoration of fluorescence intensity as these two positions move apart (Figure 3.5B). These changes are completely dependent on the presence of mRNA, with barely any change observed when mRNA is omitted.

The FRET-2 assay involves rapid mixing of unlabeled 70SIC with the TCs formed from Phe-tRNA^{Phe}(Cy3), GTP and E348C-EF-Tu^{QSY9}, denoted TC^{QSY9/Cy3}, which resulted an increase in Cy3 fluorescence (Figure 3.6B), ultimately leading to a complete loss of FRET interaction between labeled tRNA and labeled EF-Tu (Figure 3.6C). This corresponds most probably to EF-Tu-GDP release from the ribosome. Although the curves obtained could be adequately fit with single exponentials, in both cases superior fits were obtained using double exponentials, giving the k_{app1} and k_{app2} values provided in Table 3.3.

3.3.4 Kirromycin and GTP hydrolysis effects on TC interaction with 70SIC

Perturbing the interaction of TC with 70SIC by adding kirromycin or replacing GTP with a non-hydrolyzable analogue in both cases has the effect of holding EF-Tu in proximity to L11, in each case resulting in a stalled ribosome. High resolution structures of both stalled complexes show similar placements of EF-Tu, although some differences are seen in the switch 1 and G-domain regions (Schmeing et al., 2009a; Voorhees et al., 2010). Not unexpectedly, these perturbations display similar effects in eliminating the second phase of the FRET-1 assay that corresponds to

moving EF-Tu away from L11 and in forming stalled ribosome complexes having virtually identical EF-Tu:L11 FRET efficiencies (Figure 3.5B). Other studies measuring aa-tRNA(A/T site):L11 and tRNA(A/T site):tRNA^{fMet}(P site) FRET efficiencies have also provided evidence for the structural similarity of stalled ribosomes formed in the presence of kirromycin- or of a non-hydrolyzable GTP analogue (Geggier et al., 2010; Lee et al., 2007).

However, the results presented in Figures 3.5 and 3.6 also show some interesting differences in the two types of stalled complexes: 1) the first phase of the FRET-1 assay proceeds more rapidly when kirromycin is added than when GDPNP replaces GTP (Figure 3.5B; Table 3.3); 2) more strikingly, while substitution of GDPNP for GTP completely blocked the increase in Cy3 fluorescence in the FRET-2 assay, a partial increase of this fluorescence is seen in the presence of added kirromycin, indicative of a partial separation of EF-Tu from tRNA, monitored at the D-loop of tRNA, in the absence of EF-Tu separation from L11.

3.3.5 tRNA misreading

The FRET-1 and FRET-2 assays provide convenient measures of the selectivity of TC binding to 70SIC programmed at the decoding center with cognate (UUU), near-cognate (CUC), and non-cognate (CGU) codons, and of the ability of aminoglycoside antibiotics to modulate such selectivity.

As measured in the FRET-1 assay, reaction of TC^{QSY9} with 70SIC^{Cy3} programmed

with near-cognate CUC leads to a monophasic decrease in Cy3 fluorescence intensity, which proceeds with a rate constant similar to that found for the first phase of TC^{QSY9} binding to 70SIC^{Cy3} programmed with cognate UUU (Figure 3.7A; Table 3.3). The magnitude of the intensity drop is somewhat lower than in the cognate case, but it can be increased by raising the TC^{QSY9} concentration. However, the second phase of reaction is strongly inhibited, mimicking the results obtained in the binding of a cognate TC either in the presence of kirromycin or on substitution of GDPNP for GTP (Figure 3.5B). These results indicate that near-cognate TC binding closely mirrors that of cognate TC binding to the A/T site, albeit with somewhat lower affinity, but that subsequent movement away from the A/T site must be at best very slow, consistent with conclusions reached in earlier studies (Gromadski et al., 2006). Almost no change in Cy3 fluorescence is observed with either non-cognate mRNA or when mRNA is omitted.

TC^{QSY9/Cy3} reacts more slowly with near-cognate mRNA than with cognate mRNA programmed 70SICs (FRET-2 assay, Figure 3.7B; Table 3.3), with substantial decreases in the apparent rate constants for both phases of Cy3 fluorescence increase (~ 3- and 8-fold, respectively). In addition, although the overall fluorescence change is similar in both reactions, for the near-cognate programmed 70SIC the amplitudes of the first and second phases show a large decrease and a large increase, respectively, with respect to the cognate-programmed 70SIC. The magnitude of the decrease in the overall rate of fluorescence increase is similar to that seen for the rate of GTPase hydrolysis measured under comparable conditions (Gromadski et al., 2006). For

ribosomes programmed with near-cognate mRNA, there is a relatively rapid rise in Cy3 fluorescence intensity in the FRET-2 assay (Figure 3.7B) in a time period, 0.2 – 3 s, over which there is no change in Cy3 fluorescence in the FRET-1 assay (Figure 3.7A). This indicates that partial movement of aa-tRNA away from EF-Tu can take place in the absence of any movement of EF-Tu away from L11, paralleling what was found for cognate-programmed ribosomes in the presence of kirromycin (Figures 3.5 and 3.6).

Addition of the antibiotics streptomycin (Str) or paromomycin (Par), each of which is known to induce misreading, albeit by different mechanisms (Gromadski and Rodnina, 2004b), decreases the differences in TC interactions with cognate or near-cognate programmed 70SIC, as measured in both FRET assays. In the FRET-1 assay, the presence of either antibiotic gives rise to similar biphasic changes in Cy3 fluorescence for ribosomes programmed with either mRNA (Figure 3.7C). Relative to what is observed for cognate mRNA and near-cognate mRNA in the absence of antibiotic, the decrease of fluorescence in the first phase is much less pronounced, an indication that the binding of either antibiotic has the effect of increasing the L11 to EF-Tu distance within the initial complex formed on TC binding. k_{app1} is little affected by either antibiotic. For cognate-programmed 70SICs, both antibiotics slow k_{app2} by ~2-fold (Table 3.3). For near-cognate-programmed 70SICs, both antibiotics restore the second phase reaction by which EF-Tu moves away from L11, with k_{app2} values ~5-fold lower than for cognate-programmed 70SICs in the absence of antibiotic. In the FRET-2 assay (Figure 3.7D), added Str leads to almost identical Cy3 fluorescence

increases for near-cognate and cognate programmed 70SICs, reflecting, relative to cognate programmed 70SICs in the absence of Str, ~2-fold decreases in both apparent rate constants and a large shift in the relative amplitudes of phases 1 and 2 in favor of phase 2 (Table 3.3). Added Par has a less effect on the results obtained with cognate programmed 70SICs, decreasing both k_{app1} and k_{app2} by ~ 35% without altering the relative amplitudes of phases 1 and 2, but gives results with near-cognate programmed 70SICs similar to those obtained with added Str.

3.3.6 Altering EF-Tu:aa-tRNA interaction

Schrader et al. have recently presented results leading to the conclusion that the affinities of aa-tRNAs for EF-Tu are constrained to be uniform by their need to bind tightly enough to form the ternary complex but weakly enough to release from EF-Tu during decoding (Schrader et al., 2011). In this work the affinity of variant tRNA^{Val2B_S} for EF-Tu was varied by manipulating a portion of the aa-tRNA stem that binds directly to EF-Tu. Their principal finding was that overall activity, as measured by the rate of dipeptide formation with a 70SIC, was conserved for variants binding to EF-Tu.GTP up to 100 times more weakly than wt, but that such activity fell off very quickly for variants binding to EF-Tu more tightly than wt. Here we re-examine this question at higher kinetic resolution by examining the influence of aa-tRNA affinity for EF-Tu on the L11-tRNA interactions measured by the FRET-1 assay, and on movement of aa-tRNA from the A/T site into the A/A site, as measured by a third assay. In this work

we compare measurements on TCs formed by wt Val-tRNA^{Val2B} and two variants, denoted T1 and Ψ , which bind to EF-Tu.GTP with much higher or slightly lower affinities compared to wt, respectively (Table 3.4).

We first examined TC formation. The fluorescence intensity of E348C-EF-Tu^{Cy3}.GTP increases on forming a TC with each of the Val-tRNA^{Val2B} transcripts examined. The second-order association rate constant for the wt-transcript, determined by measuring the apparent association rate constant as a function of E348C-EF-Tu^{Cy3} concentration, is $0.74 \pm 0.06 \mu\text{M}^{-1}\text{s}^{-1}$ (Figure 3.8A). A measure of the dissociation rate constant, equal to $0.039 \pm 0.001 \text{ s}^{-1}$, is provided by the rate of decrease in Cy3 fluorescence when the labeled complex is mixed with a large excess of unlabeled EF-Tu, under conditions where dissociation of the labeled complex is rate limiting for formation of unlabeled TC (Figure 3.8B). Similar measurements were made for the Ψ and T1 variants, giving relative values comparable to those measured by Schrader et al (Schrader et al., 2009) using a different approach (Table 3.4).

Carrying out the FRET-1 assay with the TC formed by combining E348C-EF-Tu^{QSY9}.GTP with wt-Val-tRNA^{Val2B} transcript with a 70SIC^{Cy3} programmed with mRNA MVYF gave biphasic changes in Cy3 fluorescence (Figure 3.8C) similar to those displayed in Fig. 3.5B for the TC containing native Phe-tRNA^{Phe}, with somewhat lower values of k_{app1} (14.7 s^{-1} vs. 26 s^{-1} , respectively) and k_{app2} (4.3 s^{-1} vs. 6.2 s^{-1} , respectively). The corresponding results for the Ψ variant, with respect to both fluorescence changes and rates are comparable to those for wt,

although both rate constants have slightly larger values (Table 3.4). For the T1 variant, however, both reaction phases are considerably slower, with a significant reduction in k_{app1} (2.7-fold) and a very large reduction in k_{app2} (22-fold). The much more pronounced decrease in Cy3 fluorescence in phase 1 for the T1 variant as compared with the wt and Ψ variant is due, at least in part, to more complete formation of the intermediate formed in phase 1 as a result of k_{app2} being so much less than k_{app1} . For this variant, measurement of k_{app1} and k_{app2} as a function of TC concentration provides clear evidence that they approximate actual rate constants for a 2nd order binding step and a first-order conformational change step, respectively (Figure 3.9). Thus, tightening aa-tRNA binding to EF-Tu markedly decreases the rate of EF-Tu movement away from L11 that follows initial TC binding (Table 3.4, k_{app2}).

Proflavin-labeled fMet-tRNA^{fMet} [denoted fMet-tRNA^{fMet}(prf)] bound in the P-site of a 70SIC displays a decrease in fluorescence when aa-tRNA bound in the A/T-site is accommodated into the A-site, providing a convenient tool for measuring the rate of the accommodation process (Pan et al., 2008). Applying this assay to the reaction of the TCs formed by the three Val-tRNA^{Val2B} variants with a 70SIC programmed with mRNA MVYF gave the results shown in Figure 3.8D. Interestingly, allowing for some differences in experimental conditions, there is fairly close agreement for the wt and Ψ variants with respect to both the absolute and relative values of the rate constants for accommodation measured in this work (k_{accom}) and those for dipeptide formation (k_{dipep}) measured by Schrader et al. (Schrader et al., 2011) (Table 3.4), consistent with the prevailing view that peptide bond formation

proceeds rapidly after accommodation.

However, it is worth noting that whereas the values of k_{app2} , k_{accom} and k_{dipep} are all fairly similar to one another for both the wt and Ψ variants, indicating that for these variants movement of EF-Tu away from L11, aa-tRNA accommodation and peptide bond formation occur roughly simultaneously, for the T1 variant accommodation clearly proceeds significantly faster (3-fold) than the movement of EF-Tu away from L11. Thus, for this variant, some movement of aa-tRNA toward the P-site, as measured by the change in fMet-tRNA^{fMet}(prf) fluorescence, precedes the full accommodation that allows rapid peptide formation, in accord with previous results demonstrating that movements of the elbow and 3'-end regions of tRNA during both forward (Whitford, 2010) and reverse (Liu et al., 2010) translocation can be decoupled from one another.

3.4 Discussion

EF-Tu.GTP acts as a chaperone in accelerating the binding of a cognate aa-tRNA to the ribosomal A-site during PRE complex formation, and, following GTP hydrolysis, is released from the ribosome as EF-Tu.GDP. Such release requires the breaking of strong contacts that EF-Tu makes both with aa-tRNA and with the ribosomal GAC. Here we demonstrate that EF-Tu variants labeled at position 348 with a fluorescent quencher form functional labeled TCs with wild-type or fluorescent-labeled wild-type Phe-tRNA^{Phe} and with several unlabeled Val-tRNA^{Val2B}

variants. We use such labeled TCs to develop two new FRET assays that provide tools for determining the dynamics, during PRE complex formation, of distance changes between EF-Tu and both ribosomal protein L11, located within the GAC (FRET-1 assay), and aa-tRNA (FRET-2 assay). Application of these assays, in conjunction with related measurements, has led to several new mechanistic insights concerning the details of PRE complex formation, as well as demonstrating the potential that such assays have for high throughput screens of protein synthesis inhibitors.

The first insight concerns the order in which EF-Tu breaks its contacts to the GAC and to aa-tRNA. Our results, as summarized in Table 3.3, indicate that, following cognate TC binding to the 70SIC leading to PRE complex formation, movement of EF-Tu away from L11, and presumably therefore from the GAC, as measured by k_{app2} in FRET-1 assay, consistently proceeds somewhat faster (1.5 – 3-fold) than movement of EF-Tu away from aa-tRNA, as measured by k_{app1} in FRET-2 assay. This inequality is found in the absence or presence of the antibiotics Str or Par. It is also seen for near-cognate TC in the presence of Par, although for near-cognate TC in the presence of Str, the two apparent rate constants are equal. These results indicate that movement of EF-Tu away from the GAC generally precedes movement of EF-Tu away from aa-tRNA, and that, given the relatively small differences in the values of the two rate constants, the second step follows rapidly after the first. However, it is also possible for EF-Tu to move away from aa-tRNA when EF-Tu is constrained to remain in close proximity to L11, as when 70SIC is combined with either cognate TC in the presence of kirromycin (Figures 3.5

and 3.6) or with near-cognate TC in the absence of antibiotic (Figures 3.7A–B). Such movement may require GTP hydrolysis, since it is not observed when EF-Tu is constrained to remain in close proximity to L11 by replacing GTP with GDPNP (Figures 3.5 and 3.6). Thus, under certain circumstances, GTPase-dependent movement of EF-Tu away from aa-tRNA could precede movement of EF-Tu away from the GAC during PRE complex formation.

The second insight concerns the effects of strengthening the binding of aa-tRNA to EF-Tu via mutation of the T-stem (Table 3.4). Comparing the wt and Ψ variants of Val-tRNA^{Val2B}, which have comparable binding affinities for EF-Tu, the values of each of the rate constants k_{app2} (FRET-1 assay), k_{accom} and k_{dipep} are quite similar to one another. Furthermore, for each of these variants, all three of these rate constants have similar values, indicating that for both variants, the movements of EF-Tu away from L11 and of aa-tRNA from the A/T site to the A/A site, and peptide bond formation occur roughly simultaneously. The situation is quite different for the T1 variant of Val-tRNA^{Val2B}, which binds to EF-Tu considerably more tightly than the other two variants. This variant was previously shown to also have a markedly decreased rate of dipeptide formation (Table 3.4, k_{dipep}). Here we show that this decreased rate is likely a consequence of decreases in the rates of two distinct processes that precede dipeptide formation, the movement of aa-tRNA from the A/T site to the A/A site (k_{accom}), and the movement of EF-Tu away from L11 (k_{app2}). Based on the similarities in the values of k_{app2} and k_{dipep} (Table 3.4), this latter movement may be rate limiting for dipeptide formation. The >20-fold reduction of k_{app2} for the

T1 variant (Table 3.4) likely reflects an allosteric effect transmitted through the EF-Tu structure, since the region of EF-Tu that interacts with the GAC is far removed from the region of EF-Tu that interacts with the tRNA T-stem (Schmeing et al., 2009a; Voorhees et al., 2010). The T1 variant also differs from wt and Ψ variants in having a k_{accom} that is substantially (3-fold) greater than k_{app2} , indicating that movement of aa-tRNA toward the P-site precedes the full accommodation of aa-tRNA into the A/A site that allows rapid peptide bond formation. This is in accord with previous results demonstrating that movement of the flexible 3'-end region of ribosome-bound tRNA can be kinetically decoupled from movement of the rest of the tRNA molecule (Liu et al., 2010; Liu et al., 2011).

The third insight concerns the function of ribosomal protein L11. L11 is encompassed by L7/L12 stalk consisting of L7/L12 protein and 23S rRNA, and together with a 58-nucleotide stretch of 23S rRNA, forms GAC for the GTPase activation of all translational GTPase, including EF-Tu. The 70S ribosome lacking L11 maintains considerable activity in protein synthesis (Rosenblum et al., 2012), but the specific function of L11 remains elusive. Previous studies indicated that TC initially binds to the ribosome at L7/L12 stalk and then at A/T site with EF-Tu contacting both aa-tRNA and GAC on the 50S subunit (Sheiming et al., 2009a). Very recently, Wang et al. showed that TC binding to the ribosome brings EF-Tu in close proximity to L11 N-terminal region, and some residues from domain I and domain III of EF-Tu (Arg117, Lys121, Tyr310 and Lys312), functioning together as a peptidyl-prolyl *cis-trans* isomerase, catalyze the configuration change at Pro22 of L11,

which then bring the L11 N-terminal region into a conformation contacting L12 C-terminal region (Wang et al., 2013). Our results confirm the EF-Tu:L11 proximity upon TC binding and implicate that EF-Tu movement away from L11 has close correlation with tRNA selection and accommodation, possibly through proper L11 configuration and L11:L12 contacts. During cognate tRNA binding, EF-Tu:L11 separation may occur in a time scale prior to EF-Tu:tRNA separation, whereas, near-cognate tRNA binding leads to EF-Tu:tRNA separation before observable EF-Tu movement away from L11. Binding of antibiotics that promote near-cognate tRNA accommodation alters the patterns of EF-Tu:L11 proximity upon both cognate and near-cognate tRNA binding and blurs their differences in the absence of antibiotic. Moreover, a tighter EF-Tu:tRNA binding slows down tRNA accommodation, as well as EF-Tu:L11 separation. A possible explanation for all these observations is that cognate mRNA:tRNA base pairing in the DC of the 30S subunit put EF-Tu in a proper position that triggers L11 configuration change and L11:L12 interaction, which subsequently induces relatively fast GTPase activation and GTP hydrolysis on EF-Tu, and tRNA accommodation and EF-Tu release from the ribosome reverse the L11 configuration change and break L11:L12 contacts. In contrast, near-cognate tRNA binding places EF-Tu only in proximity to L11 but not in a position required for L11 configuration change and GTPase hydrolysis, therefore EF-Tu mediated GTP hydrolysis is significantly slowed down.

The fourth insight concerns step-wise tRNA accommodation. The tertiary structure of tRNA in L shape consists of four regions: acceptor stem-arm, D stem-loop,

T stem-loop and anticodon stem-loop. On binding at the A/T site of the ribosome in the form of TC, tRNA interacts with EF-Tu through its 3'-end and T-stem and mRNA with its anticodon; thus D stem-loop is the only region that has no contacts with the surroundings at all. During accommodation, tRNA relieves its distortion in the A/T state with the anticodon maintaining its base pairing with mRNA codon and the acceptor end, together with D and T stem-loop, fully entering the A-site on the 50S subunit. Whitford et al. suggested that tRNA accommodation is a step-wise process, with D stem-loop accommodated prior to 3'-end by using theoretical calculations (Whitford et al., 2010). Previous results from our lab also indicated that, during EF4 catalyzed back-translocation, the movement of different tRNA regions was decoupled. The results reported here provide further clues for the step-wise tRNA movement on the ribosome. The presence of antibiotic kirromycin allows GTPase activation and GTP hydrolysis but freezes EF-Tu in a GTP-bound form on the ribosome. Our results show that, although full tRNA release from EF-Tu is inhibited, tRNA D-stem, where a fluorophore was placed in our experimental setup, can still step into its accommodation site, which is reflected by the Cy3 fluorescence release in the EF-Tu:tRNA FRET experiment (Figure 3.6B). Additional evidence comes from the fact that D-stem movement to the A-site could be probed with fMet-tRNA^{fMet} (prf) programmed at the ribosomal P-site faster than EF-Tu:L11 separation and dipeptide formation (Table 3.4), which were all slowed down by the nucleotide mutation at tRNA T-stem. It is unclear whether this decoupled movement of tRNA has any functional implications.

The FRET-1 and FRET-2 assays provide convenient measures of the selectivity of TC binding to 70SIC programmed at the decoding center with cognate (UUU), near-cognate (CUC), and non-cognate (CGU) codons, and of the ability of aminoglycoside antibiotics to modulate such selectivity. The effects of substituting near-cognate- for cognate-programmed 70SIC on reaction with TC, and the Str and Par modulation of these effects, as measured using the FRET-1 and FRET-2 assays, are, with one caveat, in generally good agreement with those derived from earlier studies using different assays (binding of fluorescent-labeled tRNA, ribosome-dependent EF-Tu GTPase, dipeptide formation) in showing similar but weaker binding of the near-cognate vs. cognate TC to the 70SIC, and in the lower overall rate of aa-tRNA separation from EF-Tu that parallels the lower rate of ribosome-dependent EF-Tu GTPase (Gromadski and Rodnina, 2004a; Gromadski et al., 2006). Str and Par have previously been characterized as misreading-inducing antibiotics that act either by slowing cognate 70SIC reaction and speeding up near-cognate 70SIC reaction, such that the kinetic behavior of both complexes becomes quite similar (Str) (Gromadski and Rodnina, 2004b; Cochella et al., 2007), or by selectively speeding near-cognate reaction while having only a minor effect on cognate reaction (Par) (Pape et al., 2000; Cochella et al., 2007). The Str effects measured in the FRET-1 and FRET-2 assays and the Par effects measured in the FRET-2 assay support such characterization. The caveat concerns the Par effect in the FRET-1 assay in significantly slowing cognate reaction (phase 2). Based on the lower FRET efficiency of cognate complexes formed in the presence of either antibiotic

(Figure 3.7A), we speculate that this result may be due to propagation of Str- and Par-induced structural changes at the decoding center in the 30S subunit (Demirci et al., 2013) through the ribosome structure that results in a distancing of the labeled positions in EF-Tu and L11 when TC binds to the ribosome. Such structural changes need not necessarily affect either GTPase or dipeptide formation activities. Notwithstanding this caveat, it is clear that the fluorescence changes seen in the FRET-1 and FRET-2 assays make them desirable candidates as high throughput assays for screening new misreading-inducing antibiotics. The FRET-2 assay is likely to be superior for this purpose for two reasons. First, fluorescence increases monotonically as a function of time, eliminating the need for millisecond time resolution, and second, it is less subject to potential complications arising from antibiotic-induced changes in ribosome conformation.

3.5 Conclusions

Functional EF-Tu variants labeled with a fluorescent quencher were prepared and found capable of forming TCs with wild-type or labeled Phe-tRNA^{Phe} with stabilities equivalent to that of the wild-type ternary complex. Subsequently, the labeled EF-Tu variant was utilized for studying the EF-Tu dynamics relative to ribosomal protein L11 and aa-tRNA during PRE complex formation. In addition, the effects on PRE complex formation of antibiotics, of substituting near-cognate for cognate tRNA, and of manipulating the EF-Tu:tRNA interface were investigated.

Kirromycin and GDPNP fix EF-Tu relative to L11, as expected. In contrast, a partial rearrangement of aa-tRNA relative to EF-Tu is observed in the presence of kirromycin. The binding of a near-cognate TC to the A/T site resembles that of cognate TC binding, while the subsequent movement away from the A/T site is very slow for the near-cognate TC. The antibiotics streptomycin and paromomycin blur the distinction between cognate and near-cognate codon:anticodon interactions. This appears to be the case during both initial binding and proofreading. Altering of the EF-Tu·tRNA interface via mutation within the tRNA T-stem shows that an increase in the strength of this interaction decreases the rate of EF-Tu movement away from L11. This movement occurs after at least partial aa-tRNA accommodation, and may be rate-limiting for subsequent dipeptide formation.

Table 3.1. Labeled protein synthesis components.

Labeled Component	Description
E348C-EF-Tu ^{QSY9}	E348C variant of wt-EF-Tu labeled with QSY9
E348C-EF-Tu ^{Cy3}	E348C variant of wt-EF-Tu labeled with Cy3
K324C-EF-Tu ^{QSY9}	K324C variant of wt-EF-Tu labeled with QSY9
G325C-EF-Tu ^{QSY9}	G325C variant of wt-EF-Tu labeled with QSY9
Phe-tRNA ^{Phe} (Cy3)	Yeast Phe-tRNA ^{Phe} labeled at positions 16/17 with Cy3
fMet-tRNA ^{fMet} (prf)	<i>E. coli</i> fMet-tRNA ^{fMet} labeled at position 20 with proflavin
TC ^{QSY9}	TC containing E348C-EF-Tu ^{QSY9} .GTP and Phe-tRNA ^{Phe}
TC ^{QSY9/Cy3}	TC containing E348C-EF-Tu ^{QSY9} .GTP and Phe-tRNA ^{Phe} (Cy3)
TC ^{Cy3}	TC containing EF-Tu.GTP and Phe-tRNA ^{Phe} (Cy3)
70SIC ^{Cy3}	70S initiation complex made with ribosomes containing C38S/S87C-L11 labeled with Cy3

Table 3.2. Labeling stoichiometries of EF-Tu variants^a.

EF-Tu variant	Label/EF-Tu
wt	0.5 QSY9 0.4 Cy5
K324C	1.6 QSY9
G325C	1.8 QSY9
E348C	1.5 QSY9 1.4 Cy3

^a Labeling conditions as described in Chapter II.

Table 3.3. Kinetic parameters for EF-Tu:L11 or EF-Tu:tRNA FRET experiments.

Figure and Samples ^a	conditions	k_{app1} , s ⁻¹	k_{app2} , s ⁻¹	Relative A ₁	Relative A ₂
70SIC ^{Cy3} (0.1) +TC ^{QSY9} (0.4)	Standard	26 ± 4	6.2 ± 0.3	(-1.0 ± 0.2) ^d	1.0 ± 0.2
	+kirro ^b	35 ± 1	3.0 ± 0.7	-0.8 ± 0.1	-0.8 ± 0.2
	GDPNP ^c	5.1 ± 0.2	—	-0.7 ± 0.1	—
70SIC (0.4) + TC ^{QSY9/Cy3} (0.1)	Standard	2.1 ± 0.3	0.31 ± 0.05	(1.0 ± 0.2)	0.7 ± 0.1
	+kirro	5.1 ± 0.8	1.1 ± 0.2	0.3 ± 0.1	0.5 ± 0.1
70SIC ^{Cy3} (0.1) + TC ^{QSY9} (0.4)	Cog ^e	26 ± 4	6.2 ± 0.3	(-1.0 ± 0.2)	1.0 ± 0.2
	NCog	24 ± 6	—	-0.4 ± 0.1	—
	NCog (1.0) ^f	22 ± 6	—	-1.0 ± 0.3	—
	Cog + Str	22 ± 2	3.0 ± 0.2	-0.3 ± 0.1	0.2 ± 0.1
	Cog + Par	17 ± 3	2.5 ± 0.1	-0.4 ± 0.1	0.3 ± 0.1
	NCog + Str	32 ± 1	1.0 ± 0.3	-0.2 ± 0.1	0.2 ± 0.1
	NCog + Par	23 ± 2	1.6 ± 0.4	-0.3 ± 0.1	0.2 ± 0.1
70SIC (0.4) + TC ^{QSY9/Cy3} (0.1)	Cog	2.1 ± 0.3	0.31 ± 0.05	(1.0 ± 0.2)	0.7 ± 0.1
	NCog	0.74 ± 0.02	0.04 ± 0.01	0.3 ± 0.1	1.6 ± 0.1
	Cog + Str	0.94 ± 0.04	0.13 ± 0.02	0.4 ± 0.2	1.0 ± 0.3
	Cog + Par	1.4 ± 0.1	0.22 ± 0.01	1.0 ± 0.1	0.8 ± 0.1
	NCog + Str	1.1 ± 0.3	0.15 ± 0.04	0.4 ± 0.2	1.0 ± 0.2
	NCog + Par	0.89 ± 0.10	0.15 ± 0.06	0.4 ± 0.2	0.8 ± 0.2

^a Numbers in parentheses are final concentrations in μM . All antibiotics had final concentrations of 100 μM . Average \pm average deviation, 2–4 independent determinations, except as otherwise indicated

^b Antibiotic abbreviations: kirro, kirromycin; Str, streptomycin; Par, paromomycin

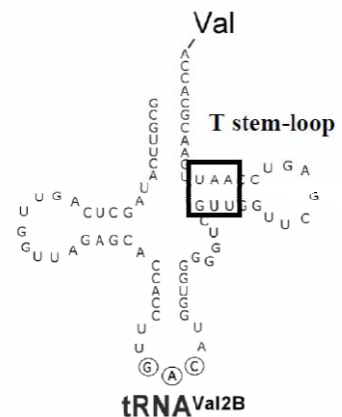
^c GDPNP substituted for GTP in TC

^d Normalized value. All amplitudes are normalized to A_1 of standard (cognate) experiment

^e mRNA abbreviations: Cog, cognate; NCog, near cognate

^f 1 μM TC was used in this experiment. The lack of dependence of $k_{\text{app}1}$ on TC concentration suggests that phase 1 includes a reversible step following binding, in agreement with Pape et al. (1998).

Table 3.4. Thermodynamic and kinetic parameters for tRNA^{Val2B} variants.

	tRNA ^{Val2B} variant ^a	wt	T1	Ψ
	constant ^b	UAA GUU	UGC GCG	UUC GGG
	TC, rel. K_d ^c	1.0 ± 0.8	0.16 ± 0.12	1.8 ± 0.7
	TC, rel. k_d ^c	1.00 ± 0.31	0.15 ± 0.04	1.7 ± 0.4
	TC, rel. k_d ^d	1.00 ± 0.05	0.085 ± 0.003	1.4 ± 0.1
	70SIC ^{Cy3e} + TC ^{QSY9} , k_{app1} , s ⁻¹	14.7 ± 0.7	5.8 ± 0.4	19.0 ± 0.7
	70SIC ^{Cy3} + TC ^{QSY9} , k_{app2} , s ⁻¹	4.3 ± 0.5	0.20 ± 0.01	5.1 ± 1.1
k_{accom} , s ⁻¹	7.2 ± 0.1	0.6 ± 0.2	5.5 ± 1.1	
k_{dipep} ^f , s ⁻¹	4.5 ± 0.7	0.32 ± 0.02	4.5 ± 0.8	

^a Sequences show portion of T-loop stem: top line: nts 65–63; bottom line: nts 49–51

^b Values are from this work, measured at 25 °C, unless otherwise specified. Measurements were generally performed in duplicate, with average deviations indicated.

^c K_d and k_d , equilibrium and dissociation rate constants, 4 °C. Values for wt are 1.2×10^{-8} M and 0.0013 s⁻¹, respectively (Schrader et al., 2011).

^d This work. Value for wt is 0.039 s⁻¹. The increase of ~30-fold from the value measured at 4 °C is consistent with the high ΔH^\ddagger for this reaction reported in Schrader et al. 2011 (Schrader et al., 2011).

^e This 70SIC has the cognate codon for tRNA^{Val2B}, GUC, in the A-site.

^f 20 °C, Schrader et al. 2011.

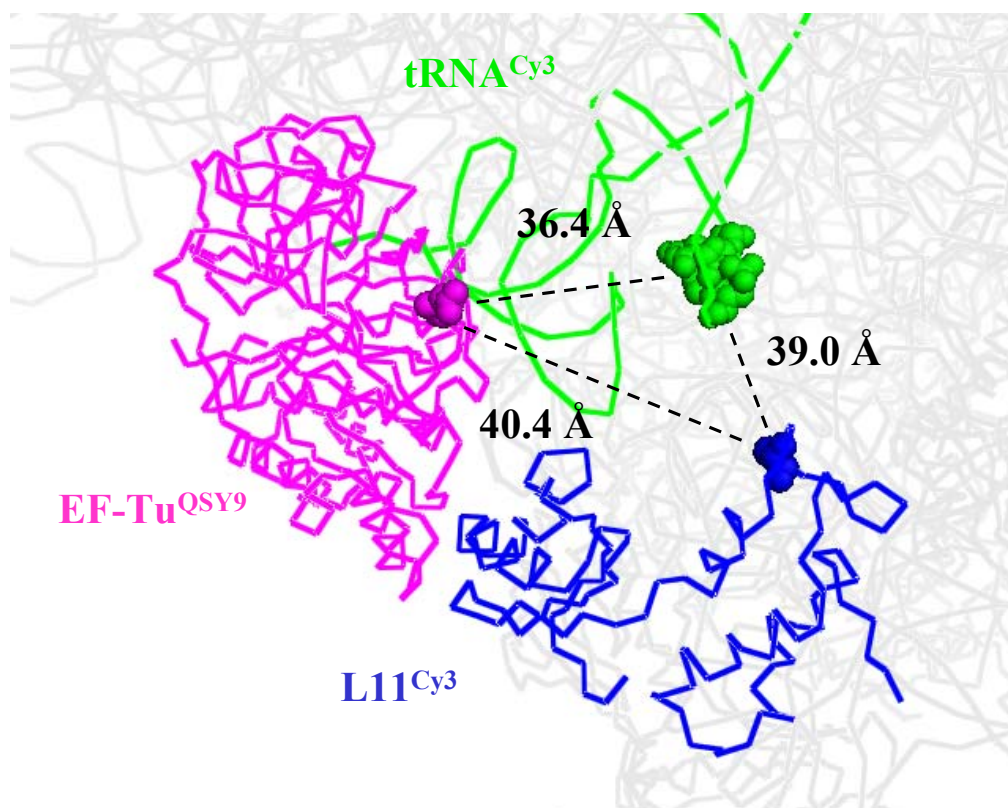


Figure 3.1. Distances within EF-Tu:L11:aa-tRNA triangle. These distances are between residue numbers 348 (C_{α} , EF-Tu), 87 (C_{α} , L11) and 16 (N-1, aminoacyl-tRNA) in a kirromycin- and paromomycin- stabilized ribosome complex with Thr-tRNA^{Thr} bound in the A/T site. In this chapter, EF-Tu at position 348, L11 at position 87 and aa-tRNA at positions 16/17 are labeled with QSY9, Cy3 and Cy3, respectively. Protein Data Bank accession codes 2WRN, 2WRO, 2WRQ, and 2WRR. This figure is adapted from (Cooperman et al., 2011).

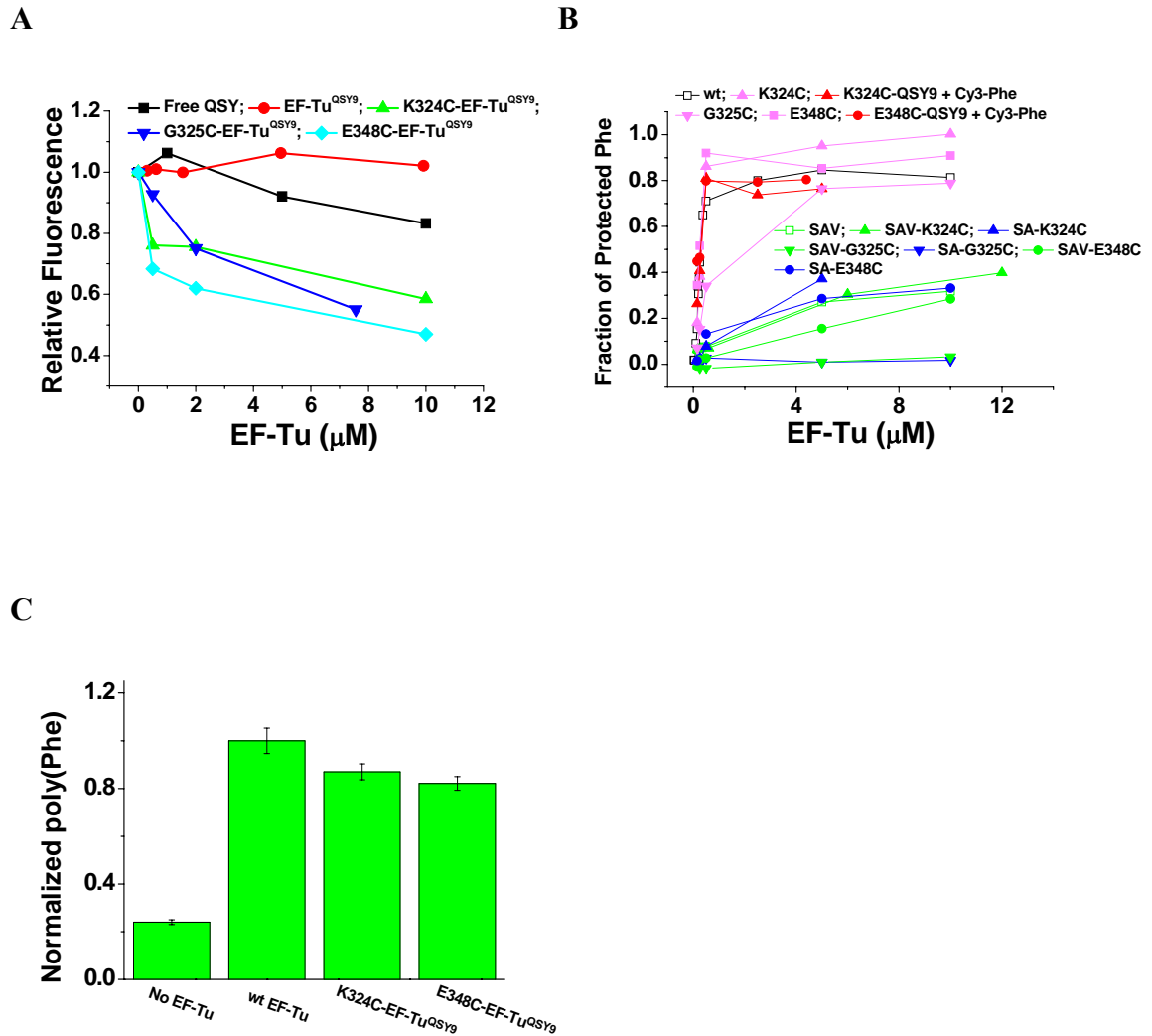


Figure 3.2. Characterization of ternary complexes (TCs) formed by labeled EF-Tus. **A.** Quenching of the fluorescence of Phe-tRNA^{Phe} (Cy3), 0.17 μ M, by QSY9 derivatives of K324C-EF-Tu, G325C-EF-Tu, or E348C-EF-Tu or by free QSY9. No quenching is seen with wt-EF-Tu labeled at a background level with QSY9. **B.** Protection of [³H]-Phe-tRNA^{Phe} or [³H]-Phe-tRNA^{Phe} (Cy3) (0.10 – 0.15 μ M) from RNase A hydrolysis by variant EF-Tus and as well as QSY9 derivatives of K324C-EF-Tu and E348C-EF-Tu. EF-Tu variants containing cysteines at possible positions K324, G325 and E348 were prepared by 1) single mutation of wt-EF-Tu; 2) two further mutations at position C81 and C137 (denoted K324C-EF-Tu^{SA}, G325C-EF-Tu^{SA} and E348C-EF-Tu^{SA}); 3) three further mutations at position C81, C137 and C255 (denoted K324C-EF-Tu^{SAV}, G325C-EF-Tu^{SAV} and E348C-EF-Tu^{SAV}, respectively). **C.** Relative poly(U)-dependent polyPhe activity using different EF-Tus.

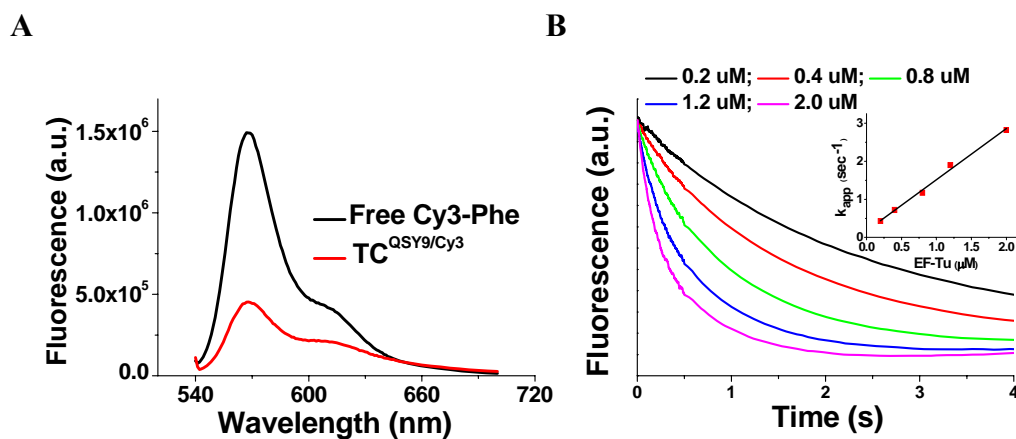


Figure 3.3. FRET in TCs formed from E348C-EF-Tu^{QSY9} variants and Phe-tRNA^{Phe}(Cy3). *A.* Quenching of the fluorescence of [³H]-Phe-tRNA^{Phe} (Cy3) by E348C-EF-Tu^{QSY9} in a purified TC (0.05 μM). *B.* Kinetics of quenching of Phe-tRNA^{Phe}(Cy3) (0.1 μM) fluorescence following rapid mixing with various concentrations of E348C-EF-Tu^{QSY9}. A plot of k_{app} vs. EF-Tu gives a k_{on} value of $1.3 \pm 0.1 \mu\text{M}^{-1}\text{s}^{-1}$ and k_{off} value of $0.17 \pm 0.07 \text{ s}^{-1}$.

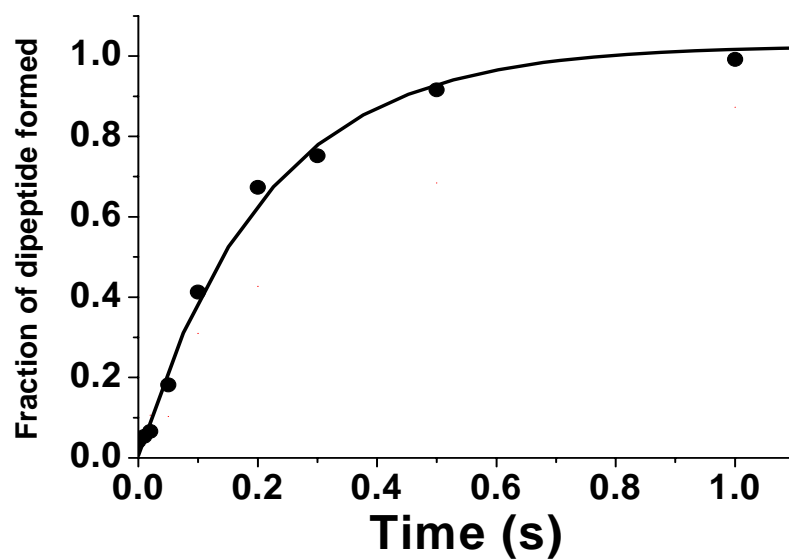
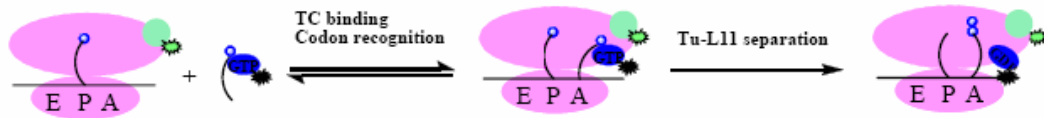


Figure 3.4. Dipeptide formation of E348C-EF-Tu^{QSY9}. Dipeptide is formed by mixing TC formed from E348C-EF-Tu^{QSY9}.GTP and Phe-tRNA^{Phe}, denoted TC^{QSY9} (0.3 μ M final concentration), with a 70SIC (1.2 μ M final concentration). Solid lines are single exponential results.

A



B

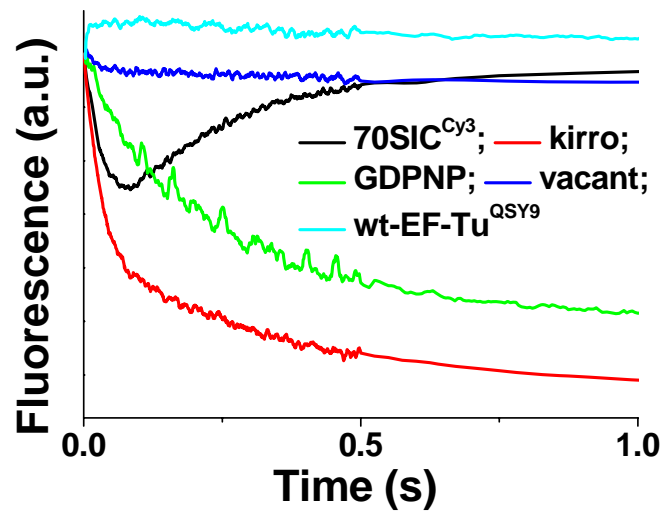


Figure 3.5. Labeled TC interaction with 70SIC^{Cy3}. *A.* Cartoon showing placement of labels. Cy3 fluorescence intensity decreases on TC^{QSY9} binding to the A/T-site and increases on accommodation of tRNA into the A-site. *B.* Changes of 70SIC^{Cy3} fluorescence on rapid mixing with TC^{QSY9} (black); in the presence of kirromycin (precombined with 70SIC^{Cy3}, red); with GDPNP in place of GTP (green). Very little change in fluorescence is seen with wt-EF-Tu labeled at a background level with QSY9 (light blue) or when mRNA is omitted (dark blue). Final concentrations were: 70SIC^{Cy3}, 0.1 μ M; TCs, 0.4 μ M; kirromycin, 100 μ M; GDPNP, 250 μ M.

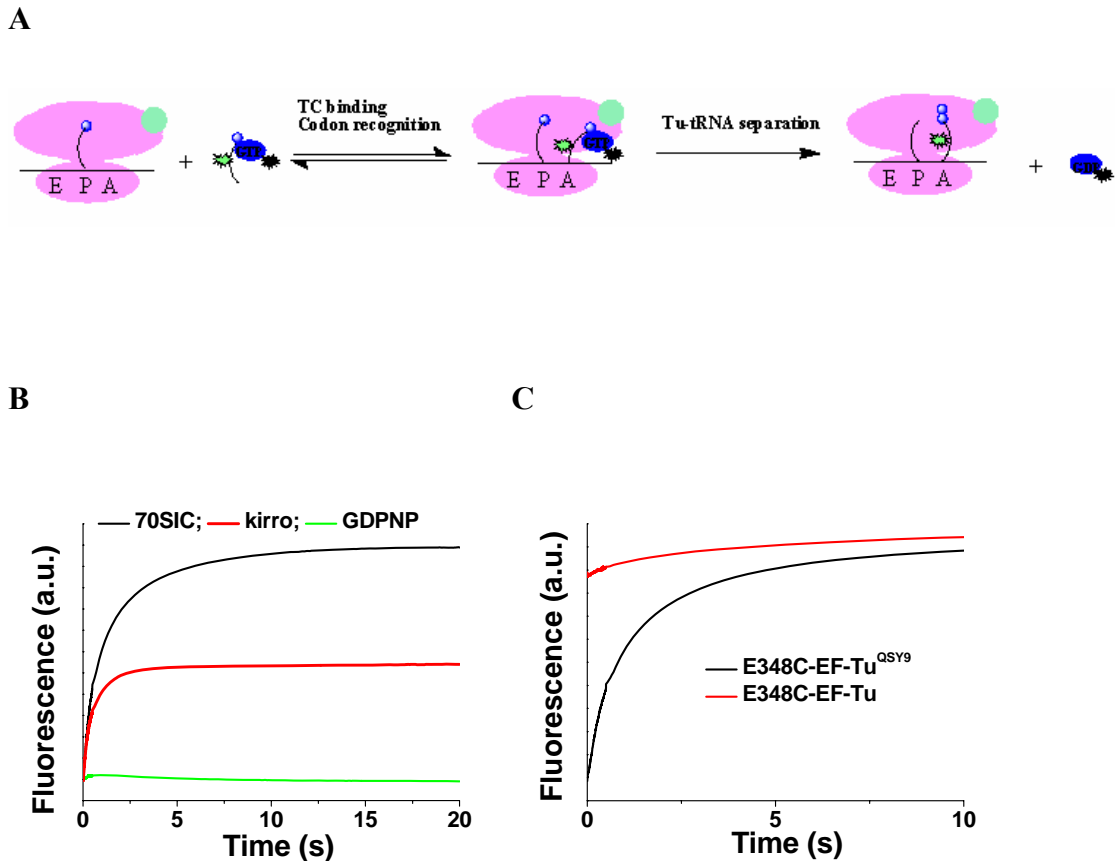


Figure 3.6. Interaction of double-labeled TC with 70SIC. **A.** Cartoon showing placement of labels. A Cy3 fluorescence intensity increase occurs on EF-Tu dissociation from the ribosome. **B.** TC^{QSY9/Cy3} (0.1 μ M) was rapidly mixed with 70SIC (0.4 μ M) and Cy3 fluorescence was monitored (black); in the presence of kirromycin (precombined with 70SIC, red); with GDPNP in place of GTP (green). When GDPNP replaced GTP, adding kirromycin had no effect (data not shown). **C.** Complete loss of fluorescence quenching due to FRET on rapid mixing of TC^{QSY9/Cy3} (0.1 μ M) and 70SIC (0.4 μ M) in a stopped-flow spectrofluorometer, as shown by an increase in Cy3 fluorescence (black) on EF-Tu release from the ribosome. The red trace is a control showing that rapid mixing of TC^{Cy3} (0.1 μ M) and 70SIC (0.4 μ M), for which there is no FRET, gives a nearly constant fluorescence equal to the final fluorescence seen in the black trace.

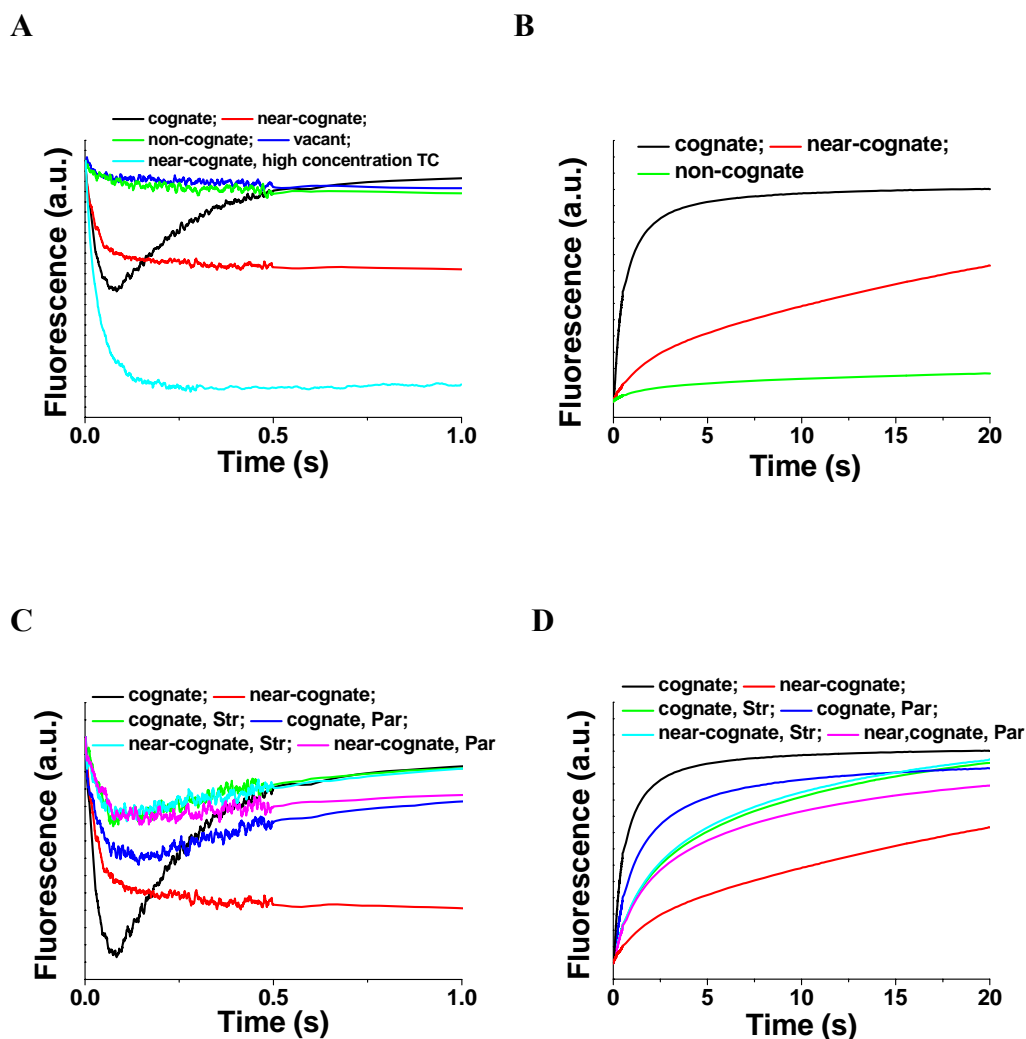


Figure 3.7. Transfer RNA selection and antibiotic effects. tRNA selectivity demonstrated by A. TC^{QSY9} effects on the fluorescence of $70SIC^{Cy3}$ or B. by $70SIC$ effects on the fluorescence of $TC^{QSY9/Cy3}$. Cognate mRNA (UUU, black); near-cognate mRNA (CUC, red); near-cognate mRNA, high TC concentration (CUC, cyan); non-cognate mRNA (CGU, green); -mRNA (blue). Parts C and D repeat the assays shown in A and B, respectively in the presence of aminoglycoside antibiotics. Cognate mRNA, no antibiotic (black); cognate mRNA, Str (green); cognate mRNA, Par (blue); near-cognate mRNA, no antibiotic (red); near-cognate mRNA, Str (cyan); near-cognate mRNA, Par (lavender). Final concentrations: $70SIC^{Cy3}$ in A, $0.1 \mu M$; $70SIC$ in B, $0.4 \mu M$; TC^{QSY9} in A, $0.4 \mu M$, high concentration, $1.0 \mu M$; $TC^{QSY9/Cy3}$ in B, $0.1 \mu M$; Str, $100 \mu M$; Par, $100 \mu M$.

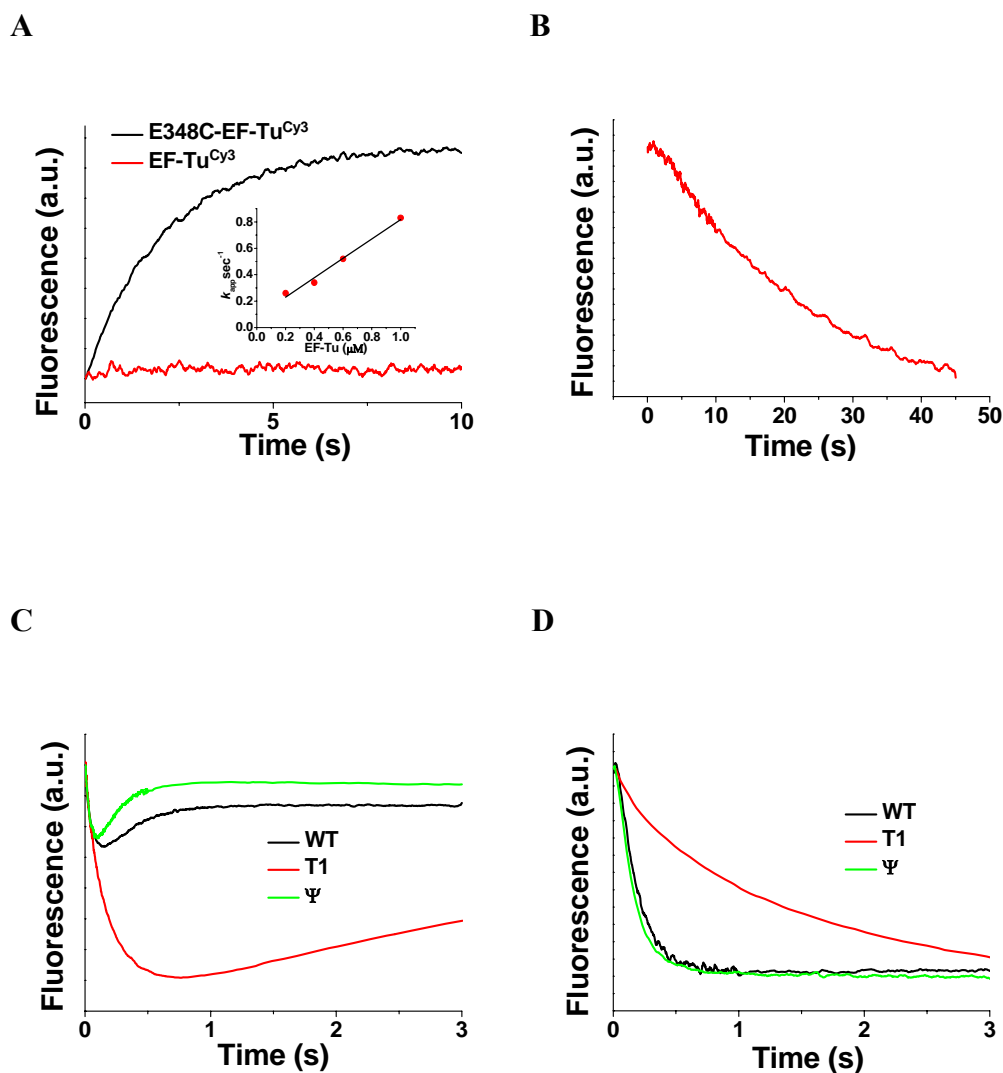


Figure 3.8. Effects of tRNA^{Val2B} mutation. **A.** TC formation. Increase in E348C-EF-Tu^{Cy3}.GTP (0.4 μM) fluorescence intensity on rapid mixing with wt-Val-tRNA^{Val2B} (0.1 μM) (Black line). Inset shows k_{app} dependence on E348C-EF-Tu^{Cy3}.GTP concentration. Wt-EF-Tu labeled to background levels showed no fluorescence change (red line). **B.** TC dissociation. The dissociation of E348C-EF-Tu^{Cy3}.GTP.Val-tRNA^{Val2B} (formed by premixing of 0.4 μM of labeled EF-Tu and 0.1 μM of Val-tRNA^{Val2B}), observed as a decrease in Cy3 fluorescence intensity on rapid mixing with excess (8 μM) unlabeled EF-Tu. **C.** FRET with L11. Changes of 70SIC^{Cy3} (0.1 μM) fluorescence on rapid mixing with TCs formed by combination E348C-EF-Tu^{QSY9}.GTP (1.6 μM) with various Val-tRNA^{Val2B} variants (0.4 μM). **D.** Movement of Val-tRNA^{Val2B} from the A/T position. Monitored as a change in proflavin fluorescence intensity on rapid mixing of unlabeled Val TCs (0.4 μM) with 70SIC (0.1 μM) containing fMet-tRNA^{fMet}(prf). All concentrations are final after rapid mixing.

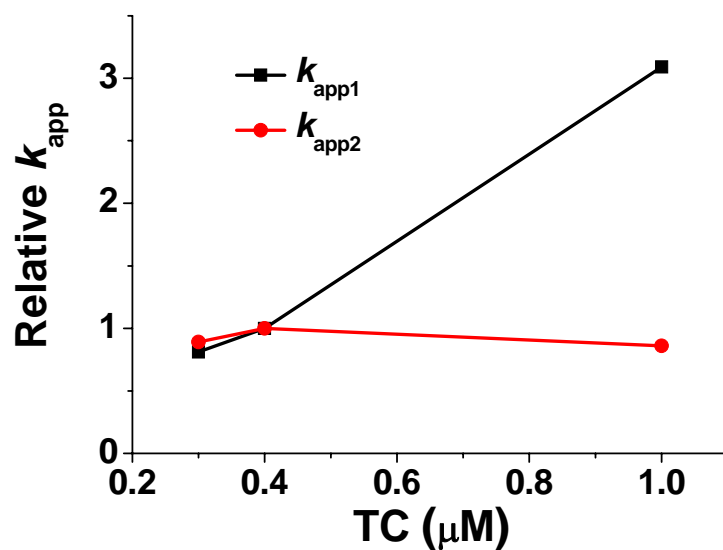


Figure 3.9. Concentration dependent EF-Tu:L11 FRET of tightly coupled ternary complex. Dependence of the apparent rate constants, k_{app1} and k_{app2} , measuring changes in 70SIC^{Cy3} (0.1 μM) fluorescence, on rapid mixing with varying concentrations of the TC formed from E348C-EF-Tu^{QSY9}.GTP and the Val-tRNA^{Val2B} T1 variant. Values are normalized to those found at 0.4 μM TC.

CHAPTER 4

EF-TU DYNAMICS DURING PRE-TRANSLOCATION

COMPLEX FORMATION: EF-TU.GDP DISSOCIATES VIA TWO DIFFERENT PATHWAYS

4.1 Abstract

During the first elongation cycle of protein synthesis, aa-tRNA having an anticodon cognate to the codon programmed at the ribosomal A-site binds to the 70SIC via a TC, resulting in PRE complex formation. Fluorophore or fluorescence quencher labels placed on L11, EF-Tu and aa-tRNA form an approximately equilateral triangle within the ribosomal complex prior to accommodation, with their distances appropriate for FRET studies. Here we combine time-dependent ensemble and single-molecule FRET (smFRET) measurements of this triangle during PRE complex formation with parallel ensemble assays measuring the rates of P_i release and of accommodation. Our results suggest that P_i release, EF-Tu separation from L11 and aa-tRNA accommodation occur in concert and all proceed prior to EF-Tu release from aa-tRNA and the ribosome. Moreover, EF-Tu release can occur prior to the EF-Tu conformational change, possibly from GTP to GDP bound form after GTP hydrolysis, or either concomitant with or following such conformational change. Our results provide direct real-time insights into the dynamics of EF-Tu during tRNA selection and accommodation and the timing and possible pathways of EF-Tu release from aa-tRNA and the ribosome.

4.2 Introduction

Protein biosynthesis on the ribosome, also called translation, requires the participation of various translational factors during each of its three stages: IF1–3 for initiation, EF-Tu and EF-G for elongation, and RF1–3 and RRF for termination and ribosome recycling. After the formation of 70SIC with fMet-tRNA^{fMet} programmed at the P-site and an empty A-site, aa-tRNA is delivered to the ribosome in the form of TC formed with EF-Tu.GTP (Pape et al., 1998). The signal of cognate mRNA:tRNA base pairing at the DC of the 30S subunit is transduced to the GAC of the 50S subunit and activates EF-Tu GTPase activity (Voorhees et al., 2010). GTP hydrolysis on EF-Tu is followed by P_i release, aa-tRNA accommodation into the A-site, EF-Tu conformational change as a result of GTP hydrolysis to form GDP, peptide bond formation, and, finally, EF-Tu.GDP dissociation from the ribosome, resulting in PRE complex formation (Rodnina and Wintermyer, 1995b; Pape et al., 1998). Translocation of fMet-aa-tRNA from the A-site to the P-site, along with the mRNA codon to which it is bound, a reaction catalyzed by EF-G.GTP, completes the first elongation cycle (Valle et al., 2003b; Frank and Gonzalez, 2010; Chen et al., 2011a). This opens up the A-site for the binding of the next cognate TC, which initiates the next elongation cycle.

Although the movement of tRNA through the ribosome during PRE complex formation has been extensively studied by kinetic, structural and modeling studies (Pape et al., 1998; Pan et al., 2007; Schmeing and Ramakrishnan, 2009b), very little is

known about the dynamics of EF-Tu interaction with either the ribosome or aa-tRNA during this process, including the timing of the major conformational change in EF-Tu that accompanies conversion of EF-Tu.GTP to EF-Tu.GDP (Kjeldgaard and Nyborg, 1992; Polekhina et al., 1996), and the interplay between EF-Tu and EF-G during their repetitive recruitments to the ribosome in the elongation stage. In Chapter III, two assays, based on functional derivatives of EF-Tu, were developed to investigate relative movements in the EF-Tu:L11:tRNA triangle during tRNA selection at the ribosomal A-site. Here we use these assays, in both ensemble and single molecule format, together with other assays measuring TC interaction with 70SIC, to formulate a quantitative kinetic scheme describing EF-Tu dynamics during PRE complex formation. Our results indicate that EF-Tu moves away from L11 in concert with Pi release and tRNA accommodation, but prior to releasing its hold on aa-tRNA, and that EF-Tu.GDP can dissociate from the ribosome by two different pathways, one more rapid but readily reversible, while the slower pathway proceeds essentially irreversibly. They also lead to the suggestion that the rapid and slower pathways correspond to EF-Tu.GDP dissociation from the ribosome occurring prior to or accompanying the major conformational change in EF-Tu, respectively.

4.3 Results

4.3.1 Labeled component nomenclature

Labeled initiation complexes, denoted 70SIC^{Cy3} or 70SIC^{Cy5}, contained protein

L11 labeled at position 87 with Cy3 or Cy5, respectively. EF-Tu derivatives, denoted E348C-EF-Tu^{QSY9} and E348C-EF-Tu^{Cy3}, were labeled at a Cys residue introduced by site-directed mutagenesis at position 348 by reaction of E348C-EF-Tu with the maleimide derivatives of the quencher QSY9 and the fluorophore Cy3, respectively. tRNAs labeled at dihydrouridine positions are denoted Phe-tRNA^{Phe}(Cy3) and fMet-tRNA^{fMet}(prf), where prf is an abbreviation for proflavin. Labeled TCs were prepared from labeled EF-Tu derivatives and either unlabeled Phe-tRNA^{Phe} or Phe-tRNA^{Phe}(Cy3), and named as indicated in Table 4.1.

4.3.2 Ensemble experiments

Rapid mixing in a stopped-flow spectrofluorometer of TC^{QSY9} with a 70SIC^{Cy3} programmed with mRNA022 MFTI, which has a UUU codon following the AUG initiation codon, leads to a biphasic change in Cy3 fluorescence, with an initial decrease corresponding to TC binding to the ribosome that places EF-Tu position 348 in proximity to L11 position 87, followed by a restoration of fluorescence intensity as these two positions move apart. In Figure 4.1, we compare, all as a function of TC^{QSY9} concentration, rates of fluorescence change on rapid mixing of TC^{QSY9} and 70SIC^{Cy3} as measured by: biphasic changes in Cy3 fluorescence (Figure 4.1A), increases in MDCC-labeled phosphate binding protein (MDCC-PBP) fluorescence on binding of released P_i (Figure 4.1B) (Pan et al., 2006), and decreases in P-site bound fMet-tRNA^{fMet}(prf) fluorescence (Figure 4.1C), which measures accommodation of

aa-tRNA into the A-site (Pan et al., 2007). Fitting of the Cy3 fluorescence change to Equation 2.2 demonstrates that k_{app1} increases linearly with TC^{QSY9} concentration whereas k_{app2} is largely independent of TC^{QSY9} concentration (Figure 4.1D), corresponding to a binding step and a following conformational rearrangement step, respectively. The results in Figure 4.1A were obtained using 70SIC^{Cy3} containing fMet-tRNA^{fMet}(prf) in the absence of MDCC-PBP. Quantitatively similar results were obtained using unlabeled fMet-tRNA^{fMet} or in the presence of MDCC-PBP (Figure 4.2).

Both of the signal traces of fluorescent PBP and fMet-tRNA^{fMet}(prf) show essentially monophasic changes, giving k_{app} values at various TC^{QSY9} concentrations, when fitted with Equation 2.1, that are in close agreement with each other and are approximately equal to the values of the overall rates of EF-Tu separation from L11 [given by $k_{app1}k_{app2} / (k_{app1} + k_{app2})$] measured in the reaction of TC^{QSY9} with 70SIC^{Cy3} (Figure 4.1D). These results indicate that EF-Tu separation from L11, Pi release and aa-tRNA accommodation occur approximately in concert under the conditions employed in our experiments.

In parallel experiments, the rate of increase in Cy3 fluorescence as a function of 70SIC concentration on rapid mixing of $TC^{QSY9/Cy3}$ with 70SIC made with fMet-tRNA^{fMet}(prf) (Figure 4.3A), measuring EF-Tu release from aa-tRNA, was compared directly with the rate of aa-tRNA accommodation (Figure 4.3B) measured as above by fitting each set of results to Equation 2.1 (Figure 4.3C). The values of k_{app}

for accommodation measured in this experiment are quite similar to those measured in Figures 4.1C–D but are ~1.7-fold greater than the values of k_{app} measured for EF-Tu release from aa-tRNA (Figure 4.3C). Since accommodation occurs in concert with EF-Tu separation from L11 (Figure 4.1D), the difference in the rate constants presented in Figure 4.3C provides strong evidence that, as measured by ensemble reactions, ribosome-bound EF-Tu separates from L11 prior to its release from aa-tRNA. Importantly, simultaneous rapid mixing of both EF-G.GTP and TC^{QSY9/Cy3} with 70SIC, while having no effect on k_{app} for accommodation, increases the value of k_{app} for EF-Tu:tRNA separation (Figure 4.3D), nearly abolishing the gap between the two k_{app} values. Direct comparison in the presence and absence of a saturating concentration of EF-G.GTP (4 μM) of the rates of EF-Tu:tRNA separation and tRNA accommodation as a function of 70SIC shows that added EF-G consistently increased the rate of EF-Tu:tRNA separation while having only a negligible effect on the rate of tRNA accommodation (Fig. 4.3E; Table 4.2).

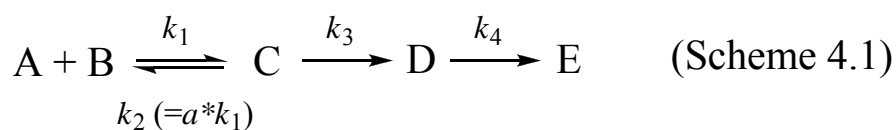
4.3.3 Single molecule FRET studies of PRE complex formation

PRE complex formation using labeled TCs was further examined by smFRET, using a total internal reflection fluorescence (TIRF) microscope as described earlier (Chen et al., 2011a, b). PRE complex formation was monitored by addition of either TC^{Cy3} or TC^{Cy3/Cy5} to immobilized 70SIC^{Cy5} (Figure 4.4A) or unlabeled 70SIC (Figure 4.4B), respectively. The results in both cases are very similar to one another, both

showing single FRET states over the entire duration of the FRET signal, as demonstrated by analysis of both FRET probability density plots (Figures 4.4C–D) and synchronized FRET traces (Figures 4.5A–B, and D–E) (Chen et al., 2012), with efficiencies equal to 0.90 ± 0.01 and 0.69 ± 0.01 , respectively. Further, for both experiments essentially identical values were obtained for the 2nd order rate constant, k_{assoc} , for TC binding to the ribosome (Figures 4.6A–B) and k_{dissoc} of EF-Tu from the ribosome (Figures 4.6D–E). For the reaction of TC^{Cy3} and immobilized 70SIC^{Cy5}, neither of these rate constants changed significantly (Figures 4.6C and F) in the presence of a near-saturating value of EF-G.GTP (4 μM , Figure 4.3D) which catalyzes PRE complex conversion to POST complex. Here again, only a single FRET state for ribosome-bound EF-Tu is observed (Figures 4.5C and F).

4.3.4 A simplified quantitative model for TC interaction with 70SIC leading to PRE complex formation

The ensemble and smFRET measurements presented in Figs. 4.1–4.6 allow formulation of a quantitative kinetic model for PRE complex formation (Scheme 4.1; Figure 4.7)



that, while building on the more complete model formulated by Pape et al (Pape et al., 1998), stresses changes in the interactions of EF-Tu with both the ribosome and aa-tRNA that occur during the process. The main features of this model are:

1. The identification of two distinct complexes, C_1 and C_2 , prior to PRE complex formation.
2. C_1 corresponds to what Rodnina et al. (Rodnina et al., 1994) identify as the codon recognition complex that forms prior to GTP hydrolysis, and thus is stabilized when GDPNP is substituted for GTP, as shown in Chapter III. In this complex, position 87 in L11 and the D-loop in aminoacyl-tRNA are each close enough to position 348 in EF-Tu to give rise to strong FRET signals (Figure 3.1), as measured by quenching of either Cy3 fluorescence (Figures 4.1A and 4.3A) or increase in Cy5 fluorescence (Figures 4.4A–B; see also Chapter III).
3. C_2 is formed from C_1 by a multistep process, grouped as Step 2, that is initiated by GTP hydrolysis and is followed by four processes occurring approximately concurrently: P_i release, aa-tRNA accommodation into the A-site, dipeptide formation and EF-Tu separation from L11 (Figure 4.1A). Two of these processes, tRNA accommodation and EF-Tu separation from L11, are likely to be reversible (Agirrezabala et al., 2012; Fischer et al., 2010). As a consequence, the overall rate constant for step 2 could reflect sums of forward and reverse rate constants. This, along with differences in experimental conditions and dye labeling [$TC^{QSY9} + 70SIC^{Cy3}$ (Fig. 4.1) vs. $TC^{Cy3} + 70SIC^{Cy5}$ (Figure 4.4)], might account for a somewhat

higher apparent rate constant for step 2 ($k_2 = 18 \pm 3 \text{ s}^{-1}$, Table 4.3) as compared with k_{dissoc} ($6.3 \pm 0.4 \text{ s}^{-1}$, Figure 4.6D) determined from ensemble and single molecule studies, respectively.

4. EF-Tu.GDP separation from L11 in Step 2 occurs prior to EF-Tu.GDP separation from Phe-tRNA^{Phe} and dissociation from the ribosome by either Step 3 or Step 3A. Here it should be noted that, conversely, EF-Tu can separate from aa-tRNA without separating from L11 either in the presence of kirromycin, an antibiotic that stabilizes EF-Tu.GDP binding to the ribosome (Rodnina et al., 1994), or when EF-Tu GTPase activity is strongly inhibited by replacement of cognate TC, as used in this paper, with near-cognate TC (Gromadski et al., 2006; also see Chapter III).

5. Step 3A proceeds more rapidly than Step 3 (i.e., $k_{3A} > k_3$). Under ensemble conditions, in which relatively high concentrations of ribosomes and TC are employed, Step 3A is rapidly reversible and, in the absence of EF-G, C₂ accumulates transiently. Under single molecule conditions, performed at very low concentrations of ribosomes and TC, Step 3A is essentially irreversible, C₂ does not accumulate, and virtually all EF-Tu dissociation proceeds via step 3A. The failure to detect C₂ in the smFRET experiment indicates that its lifetime must be $\leq 20 \text{ ms}$, given the 11 ms integration time per frame used in the experiment. Step 3 is an essentially irreversible step under both ensemble and single molecule conditions.

6. Addition of EF-G.GTP has no effect on the residence time of EF-Tu on the ribosome, as determined by smFRET (Figures 4.6D, F). However, it does accelerate

EF-Tu separation from tRNA in the ensemble experiment, such that its rate constant approaches that seen for accommodation (Figure 4.3D). This acceleration results from EF-G.GTP sequestration of the PRE complex that is the product of step 3A, which converts step 3A into an essentially irreversible step, even under ensemble conditions.

7. Dye incorporation into Phe-tRNA^{Phe} can significantly alter rate constants for C₁ formation and dissociation, but has little effect on the rate of C₁ conversion to C₂. Rate constants for two dye combinations, derived from results presented in Figures 4.1 and 4.3, are compared in Table 4.3. Replacement of TC^{QSY9} with TC^{QSY9/Cy3} leads to a ~10-fold increase in the equilibrium dissociation constant for TC binding, largely due to an increase in k_{-1} , indicating that Cy3 labeling of Phe-tRNA^{Phe} reduces TC affinity for the ribosome. This is consistent with other studies of ours showing reduced activity in protein synthesis of Cy3-labeled vs. unlabeled Phe-tRNA^{Phe} under conditions of limiting Phe-tRNA^{Phe} concentration (Rosenblum et al., 2012).

4.3.5 The timing of EF-Tu conformational change

While it is clear from the differences between the structures of the GTP- and GDP-bound forms of EF-Tu (Kjeldgaard and Nyborg, 1992; Polekhina et al., 1996) that dissociation from EF-Tu of the P_i produced on GTP hydrolysis must ultimately lead to a major conformational change within EF-Tu, the timing of such change, and whether it occurs on or off the ribosome, is unclear. Our scheme posits two pathways for EF-Tu.GDP dissociation from the ribosome. Our results are consistent with the

assumption that the rapid, reversible dissociation step, 3A, corresponds to dissociation of EF-Tu.GDP*, which retains the “EF-Tu.GTP” conformation, while the slower, essentially irreversible step corresponds to dissociation of EF-Tu.GDP, having the altered “EF-Tu.GDP” conformation. Experiments testing this assumption more directly, and reaching the same conclusion, are described elsewhere (unpublished data from Dr. Darius Kavaliauskas and Prof. Charlotte R. Knudsen). The suggestion that EF-Tu.GDP* has an at least transient existence both on and off the ribosome is supported by considerable evidence, summarized recently (Hauryliuk et al., 2008), that GTPases like EF-Tu fluctuate in a dynamic equilibrium between different conformational states, independently of which nucleotide, GTP or GDP, is bound. A particularly striking example of this phenomenon is provided by the X-ray crystal structure of a Rab6A' mutant containing bound GDP, which shows the protein to be in a GTP-like conformation (Shin et al., 2012). As we have demonstrated (Figure 4.3D), addition of EF-G.GTP accelerates overall EF-Tu.GDP dissociation, which we attribute to its binding to the PRE complex produced via reaction 3A. Given the high cellular concentration of EF-G (~20 μ M, stoichiometrically equivalent to ribosomes), it seems probable that reaction 3A is the major route for EF-Tu dissociation *in vivo*.

4.4 Discussion

A quantitative kinetic model has been proposed more than a decade ago to describe the elementary steps during PRE complex formation (Pape et al., 1998).

Herein, we add more details to this model by ensemble multi-color experiments combining FRET assays based on a labeled EF-Tu derivative (see Chapter III) and assays measuring fluorescence changes of Pi release and aa-tRNA accommodation, as well as smFRET experiments utilizing fluorophore labeled EF-Tu. Our results indicate that EF-Tu gets into proximity to L11 upon TC binding to the 70SIC, and moves away from L11 in concert with Pi release after GTP hydrolysis and tRNA accommodation. After tRNA release, EF-Tu can dissociate from the ribosome via two different pathways depending on the timing of EF-Tu conformational change.

Previous studies using labeled tRNA showed that TC binding to the ribosome proceeded through an initial mRNA-independent binding, presumably to the L7/L12 stalk (Schmeing et al., 2009a), followed by a mRNA-dependent binding to the ribosome body, with roughly equal forward rates for these two steps (Rodnina et al., 1994). Our EF-Tu:L11 FRET experiments show that the step by which EF-Tu achieves proximity to L11 is second order, with an apparent rate constant that increases linearly as a function of TC concentration, but is much slower than what has previously been measured for initial TC binding (Pape et al., 1998). This result suggests the possibility that initial TC binding to the L7/L12 stalk is immediately followed by repositioning of EF-Tu to bring it to the proximity to L11, consistent with recent results showing that part of EF-Tu interacts with L11 to induce L11 conformational change and construct L11:L12 contacts (Wang et al., 2012). However, we can not exclude the possibility that TC initial binding to L7/L12 stalk directly put EF-Tu at a position interacting with L11 or binding to L7/L12 stalk is not a

pre-requisite for TC to reside at the A/T site of the ribosome.

After GTP hydrolysis, EF-Tu moves away from L11 approximately at the same time as Pi release and tRNA accommodation, which is evidenced by their similar apparent rate constants in concentration dependence experiments and successfully fitting to a global kinetic scheme with all of these three processes occurring in one step. Concurrent EF-Tu:L11 separation and tRNA accommodation confirms their correlation as revealed in experiments using tight tRNA^{Val2B} mutant, in which delayed tRNA release from EF-Tu slowed down EF-Tu:L11 separation and tRNA accommodation to the same level (see Chapter III).

In multi-color experiments simultaneously measuring tRNA accommodation by fMet-tRNA^{fMet}(prf) programmed at ribosomal P-site and EF-Tu:tRNA separation by TC^{QSY9/Cy3}, the rates of EF-Tu:tRNA separation were apparently slower than those of tRNA accommodation (Figure 4.3C), presumably also slower than those of Pi release and EF-Tu:L11 separation, indicating a delayed EF-Tu dissociation from the ribosome. Global fitting results suggest that EF-Tu:tRNA separation can be treated as a separate step after EF-Tu:L11 separation, Pi release and tRNA accommodation, with the latter three steps proceeding with the same rate constant. In our scheme (Figure 4.7), it is proposed that, EF-Tu undergoes a conformational change after GTP hydrolysis, which occurs after EF-Tu:L11 separation, Pi release, and tRNA accommodation. This proposal is consistent with what was previously reported that Pi release after GTP hydrolysis is much slower than GTP hydrolysis, leading to slow EF-Tu

conformational rearrangement from GTP to GDP bound form after GTP hydrolysis (Kothe and Rodnina, 2006), in which the rate of conformational change was indirectly obtained from the difference between the lag phase of Pi release and tRNA accommodation experiments.

This dissociation occurs via two possible pathways: 1) rapid but reversible dissociation from the ribosome in the high-affinity state followed by the conformational change off the ribosome (Step 3A in Figure 4.7); or 2) conformational change on the ribosome followed by slow but irreversible dissociation from the ribosome in the low affinity state (Step 3 in Figure 4.7). Under ensemble condition, because of the relatively high concentration components used, backward re-association in Step 3A becomes significant and intermediate C_2 is accumulated, making Step 3 dominantly observable. Thus, presence of EF-G has no effect on the rates of tRNA accommodation but increase the rates of EF-Tu:tRNA separation to a level similar to tRNA accommodation by trapping the ribosome complex after EF-Tu.GDP* dissociation, pushing the reaction mostly through Step 3A. In contrast, under single molecule conditions, highly diluted components make the rapid TC dissociation in the high affinity state essentially irreversible and C_2 mostly proceeds through Step 3A. EF-Tu and EF-G share the same binding site on the ribosome both as translational GTPase and are recruited to the ribosome regulated by the ribosome states. Our observations raise the question of, if EF-Tu conformational rearrangement changes its affinity with the ribosome and facilitates its dissociation from the ribosome, why a second pathway exists with this rearrangement occurring off the

ribosome, and whether the EF-Tu:EF-G interplay has any functional significance during translation elongation.

4.5 Conclusions

Here we describe the dynamics of EF-Tu interaction with tRNA and with the ribosome during PRE complex formation by combining the results of multi-color ensemble stopped-flow and single-molecule FRET measurements. We demonstrate that EF-Tu separation from L11 within the GTPase associated center of the ribosome occurs prior to EF-Tu separation from Phe-tRNA^{Phe} and that EF-Tu.GDP dissociates from the ribosome via two different pathways, one more rapid and reversible and one slower and essentially irreversible, that are likely to correspond to two different EF-Tu.GDP conformations on the ribosome.

Table 4.1. Labeled ternary complexes (TCs).

TC name	Labeled EF-Tu variant	Phe-tRNA^{Phe}
TC ^{QSY9}	E348C-EF-Tu ^{QSY9}	Phe-tRNA ^{Phe}
TC ^{QSY9/Cy3}	E348C-EF-Tu ^{QSY9}	Phe-tRNA ^{Phe} (Cy3)
TC ^{Cy3}	E348C-EF-Tu ^{Cy3}	Phe-tRNA ^{Phe}
TC ^{Cy3/Cy5}	E348C-EF-Tu ^{Cy3}	Phe-tRNA ^{Phe} (Cy5)

Table 4.2. Comparison of apparent rate constants between TC^{QSY9/Cy3} and fMet-tRNA^{fMet}(prf)^a.

70SIC (μM)	No EF-G ^b		EF-G (4 μM) ^c	
	$k_{\text{app}}(\text{Cy3})$ (s^{-1})	$k_{\text{app}}(\text{prf})$ (s^{-1})	$k_{\text{app}}(\text{Cy3})$ (s^{-1})	$k_{\text{app}}(\text{prf})$ (s^{-1})
0.4	3.2 ± 0.8	4.9 ± 0.5	4.9	4.9
0.8	3.9 ± 0.5	6.1 ± 0.4	6.9	8.0
1.2	5.2 ± 0.8	8.7 ± 0.9	8.0	10.2
2.4	6.5 ± 1.1	8.8 ± 0.8	11.0	13.5

^aTC^{QSY9/Cy3} (0.1 μM) was rapidly titrated with 70SIC programmed with fMet-tRNA^{fMet}(prf) at indicated concentrations, in absence or presence of EF-G (4 μM).

^bAverage \pm error of two determinations.

^cSingle determination.

Table 4.3. Fitted rate constants for scheme^a.

Reaction Components	$k_1, \text{s}^{-1} \mu\text{M}^{-1}$	$k_{-1}/k_1, \mu\text{M}$	k_2, s^{-1}	k_3, s^{-1}
TC ^{QSY9} + 70SIC ^{Cy3} Fig. 4.1	39.3 ± 1.3	0.12 ± 0.03	17.7 ± 2.5	(19.6)
Tu ^{QSY9/Cy3} + 70SIC	100 ± 39	1.2 ± 0.1	19.9 ± 0.5	19.6 ± 1.1

^a Rate constants in parentheses are fixed during fitting using Scientist.

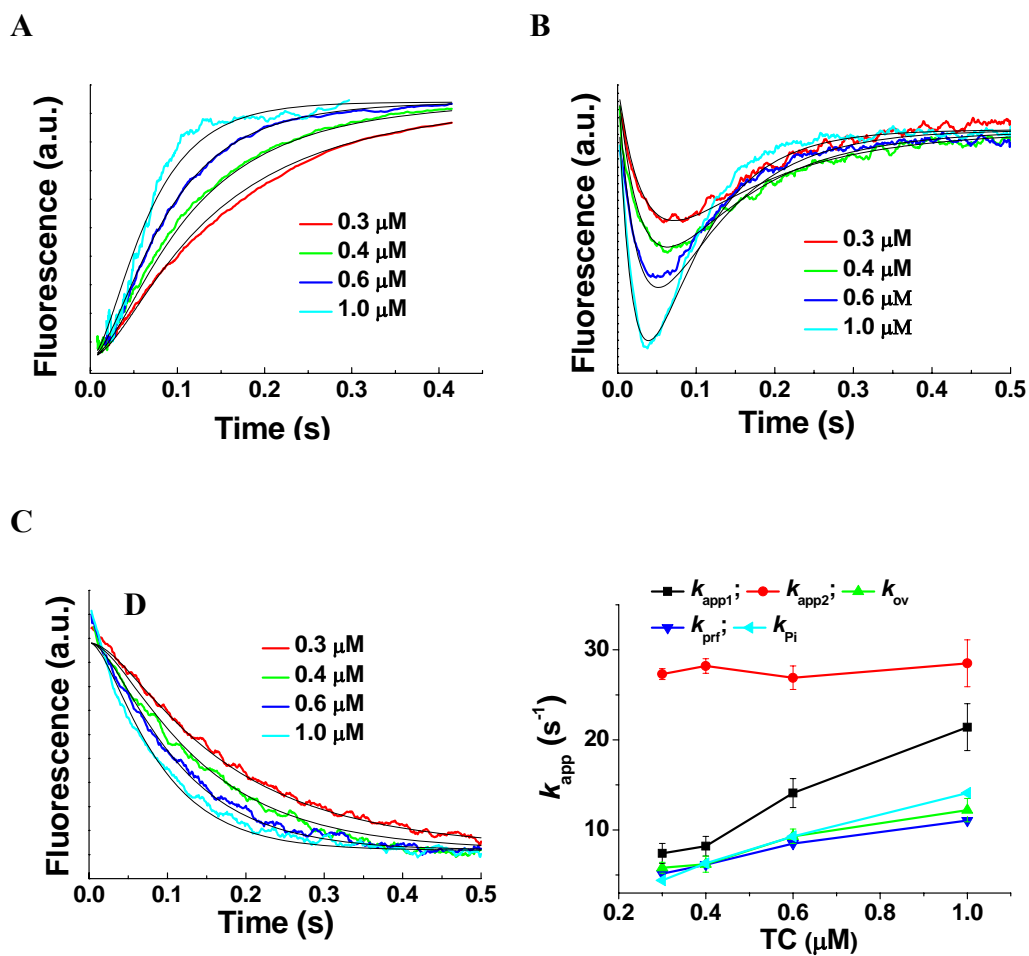


Figure 4.1. Ensemble studies of TC^{QSY9} reaction with $70\text{SIC}^{\text{Cy3}}$. A – C. Changes of fluorescence on rapid mixing of $70\text{SIC}^{\text{Cy3}}$ ($0.1 \mu\text{M}$) with TC^{QSY9} as a function of TC^{QSY9} concentration. Lines through the traces are fit to Scheme 4.1 (Table 4.3). A. Cy3 fluorescence. B. MDCC-PBP fluorescence. C. $\text{fMet-tRNA}^{\text{fMet}}(\text{prf})$ fluorescence. In parts A and C, 70SIC contained $\text{fMet-tRNA}^{\text{fMet}}(\text{prf})$. Unlabeled $\text{fMet-tRNA}^{\text{fMet}}$ was used in part B. D. k_{app} values derived from measurements of changes in the fluorescence: Cy3, k_{app1} (black); Cy3, k_{app2} (red); Cy3, k_{ov} (green); prf (blue); MDCC-PBP (cyan). Rate constants for Cy3 are averaged values obtained in the presence of MDCC-PBP or $\text{fMet-tRNA}^{\text{fMet}}(\text{prf})$.

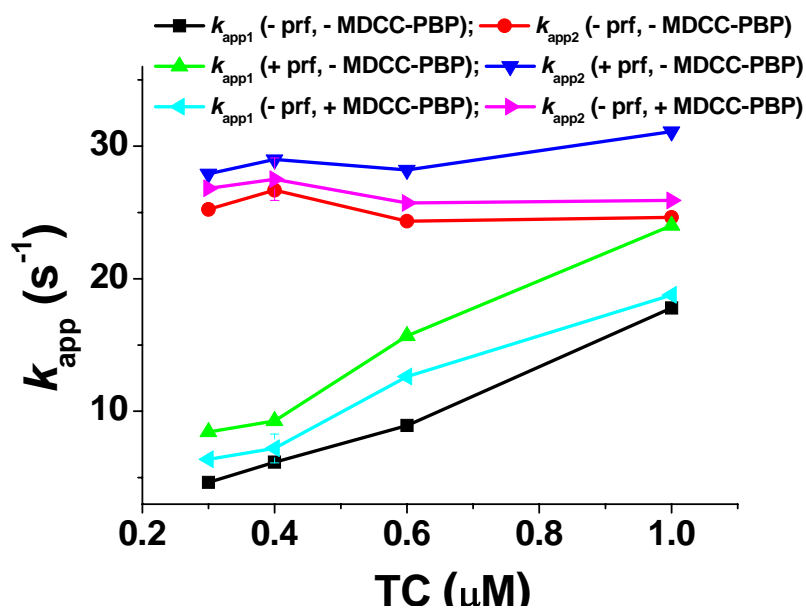


Figure 4.2. Concentration dependence of EF-Tu:L11 FRET. k_{app1} and k_{app2} are as a function of TC^{QSY9} concentration for the reaction with $70SIC^{Cy3}$ ($0.1 \mu M$). These experiments were carried out with $70SIC^{Cy3}$ containing either fMet-tRNA^{fMet}(prf) or fMet-tRNA^{fMet} (indicated as +prf and -prf, respectively) and in the presence or absence of MDCC-PBP (indicated as +MDCC-PBP and -MDCC-PBP, respectively). The values at $0.4 \mu M$ are mean \pm standard deviation of four determinations.

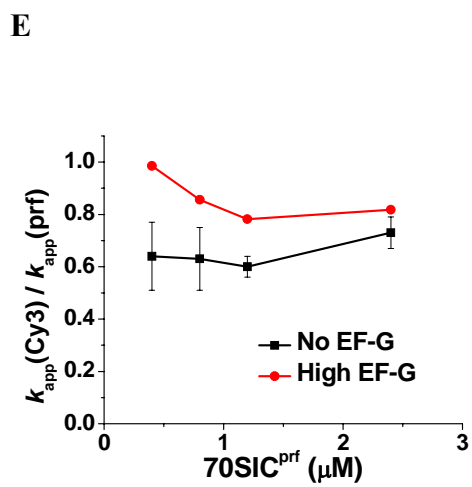
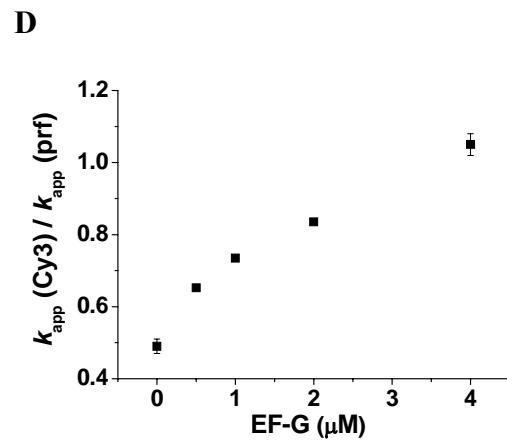
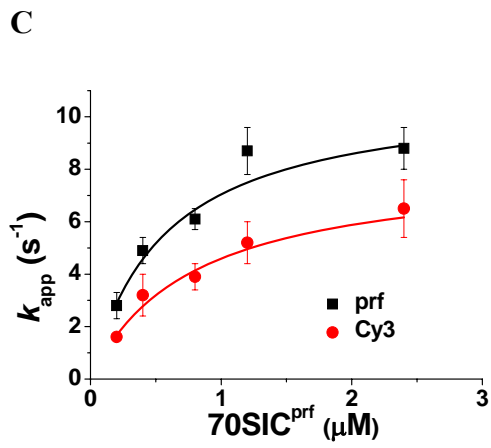
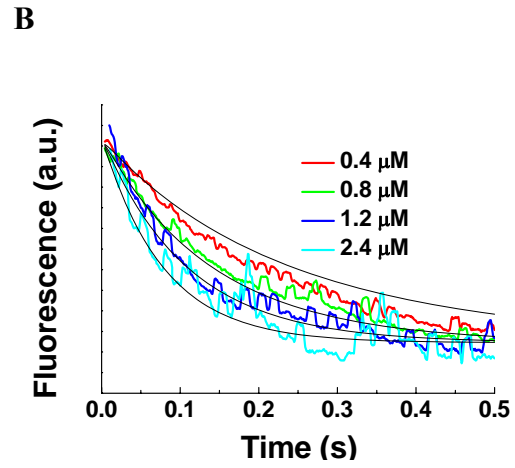
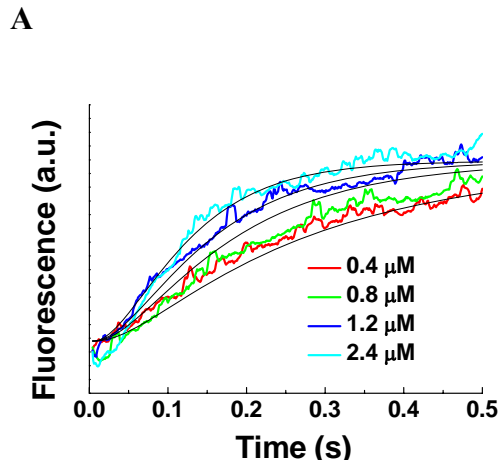


Figure 4.3. Ensemble studies of TC^{QSY9/Cy3} reaction with 70SIC. Changes of fluorescence on rapid mixing of 70SIC with TC^{QSY9/Cy3} (0.1 μ M) as a function of 70SIC concentration. 70SIC was made up with fMet-tRNA^{fMet}(prf). *A.* Cy3 fluorescence. *B.* fMet-tRNA^{fMet}(prf) fluorescence. In *A* and *B* lines through the traces are fit to Scheme 4.1 (Table 4.3). *C.* k_{app} values for parts A and B. Data shown are average \pm error of two determinations. *D.* $k_{app}(\text{Cy3})/k_{app}(\text{prf})$ as a function of EF-G.GTP concentration. Data shown in the absence or in the presence of EF-G (4 μ M) are average \pm error of two determinations. 70SIC, 0.4 μ M. *E.* Relative rates of EF-Tu:tRNA separation and tRNA accommodation in the presence of EF-G (4 μ M) at different 70SIC concentrations. Data in the absence of EF-G come from part C.

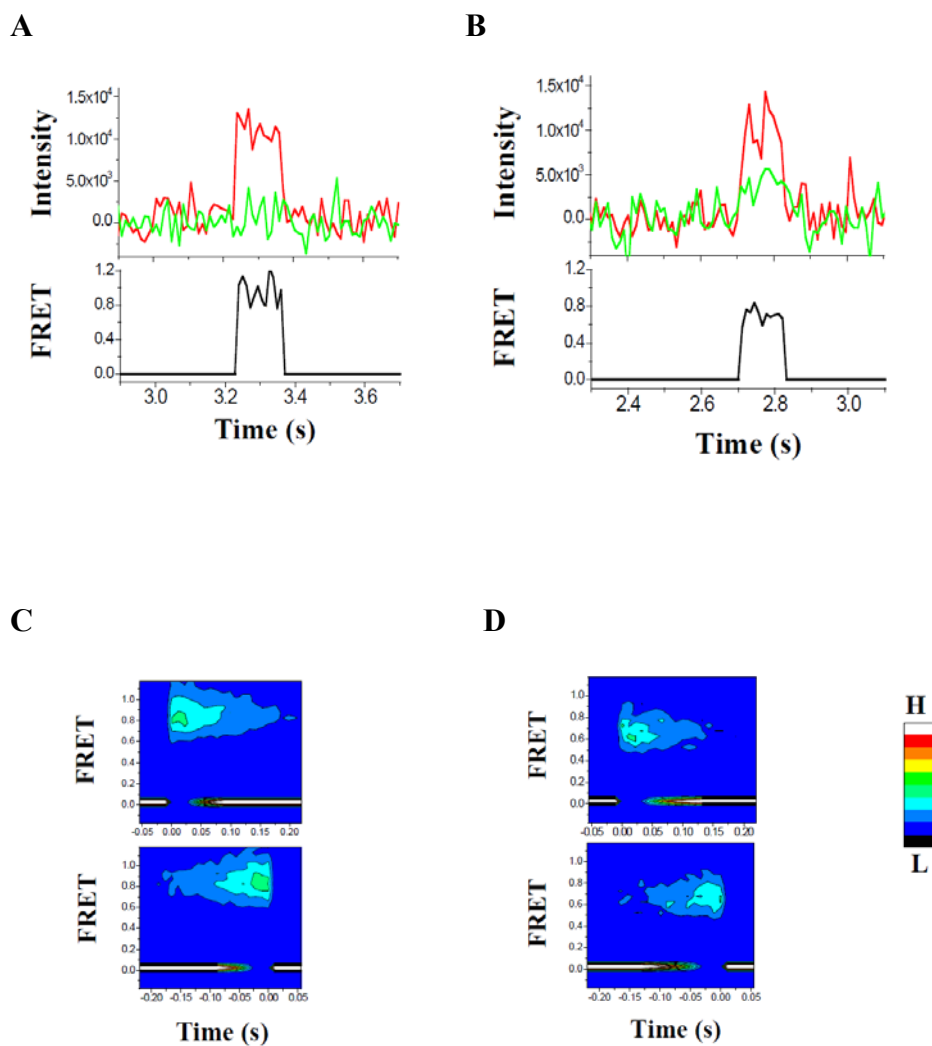


Figure 4.4. Real-time courses of single molecule fluorescence intensities and FRET. EF-Tu.GTP assisted tRNA delivery was measured between *A.* TC^{Cy3} and 70SIC^{Cy5} and *B.* TC^{Cy3/Cy5} and 70SIC. TC (10 nM) was injected at time zero into the imaging chamber with immobilized 70SIC. Cy3 (green) and Cy5 (red) fluorescence intensity traces were under excitation of 532 nm TIRF illumination at 11 ms integration time per frame. The FRET ratio was calculated as $I_{Cy5}/(I_{Cy5} + I_{Cy3})$ *C.* and *D.* FRET probability density plots for the reactions described in *A* and *B*, respectively. Upper and lower traces are aligned to the first or last time points, respectively, of the FRET events as $t = 0$. Besides the 0 FRET state, which corresponds to no fluorescence signal, only one FRET state is observed in each reaction. The same conclusion is reached from consideration of the synchronized FRET traces shown in Fig. 4.5.

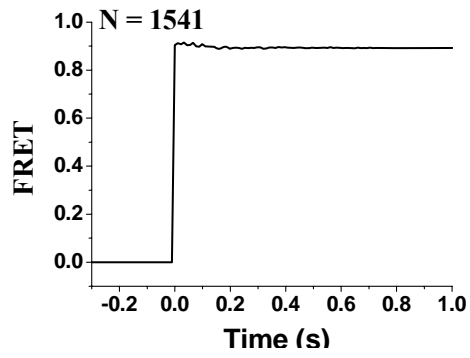
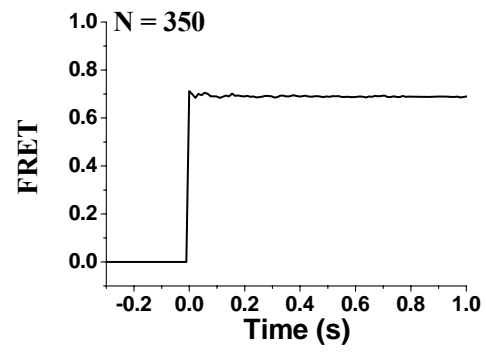
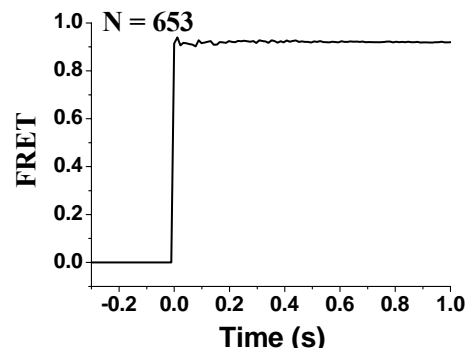
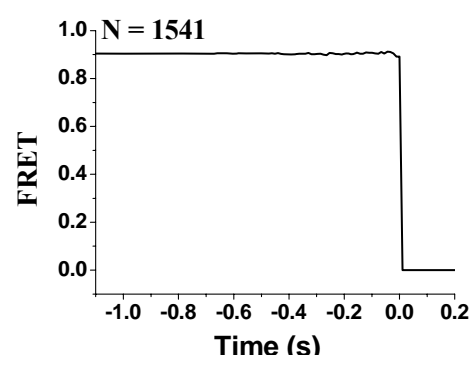
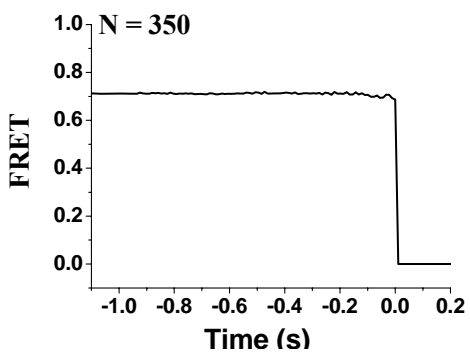
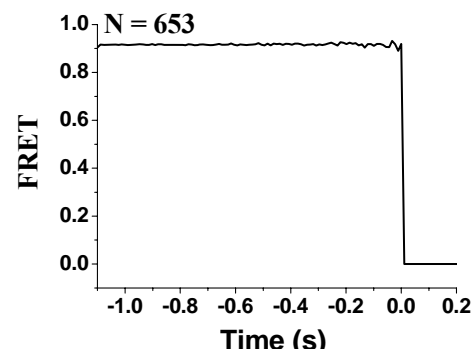
A**B****C****D****E****F**

Figure 4.5. Synchronized smFRET values. *A.* and *D.* Synchronized to FRET appearance and disappearance, respectively, for TC^{Cy3} added to 70SIC^{Cy5}. *B.* and *E.* Synchronized to FRET appearance and disappearance, respectively, for TC^{Cy3/Cy5} added to 70SIC. *C.* and *F.* Synchronized to FRET appearance and disappearance, respectively, for TC^{Cy3} added to 70SIC^{Cy5} in the presence of 4 μ M EF-G.GTP.

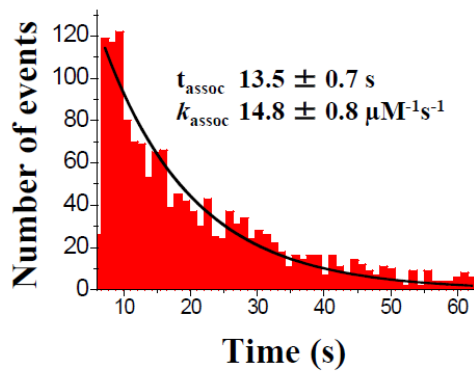
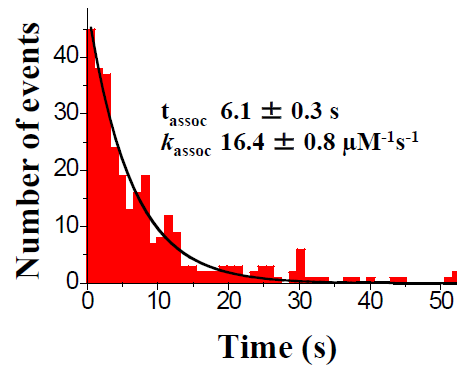
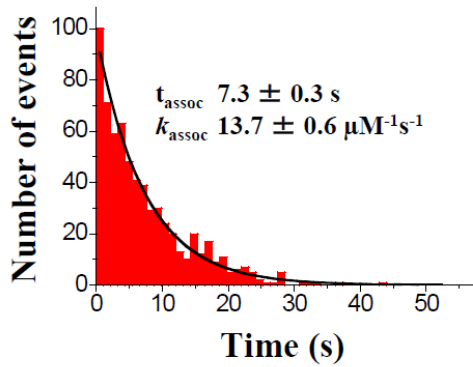
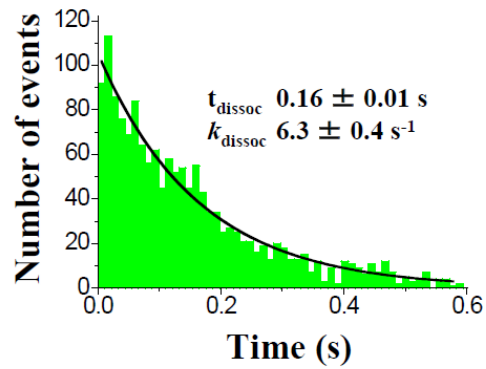
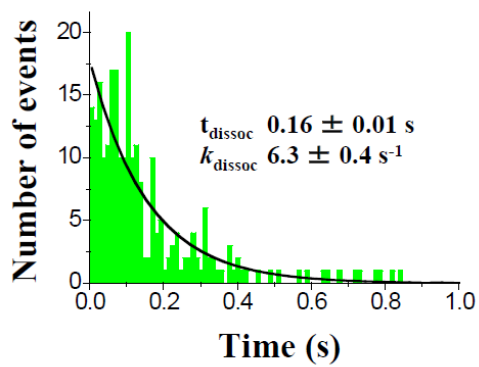
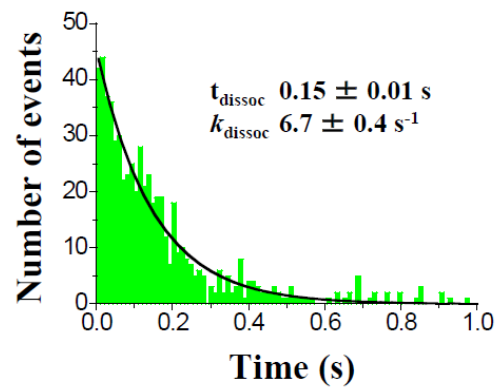
A**B****C****D****E****F**

Figure 4.6. Association (*A*, *B*, and *C*) and dissociation (*D*, *E*, and *F*) times and rate constants for TC interaction with immobilized 70SIC. *A*. and *D*. TC^{Cy3} (5 nM) and 70SIC^{Cy5}; *B*. and *E*. TC^{Cy3/Cy5} (10 nM) and 70SIC; *C*. and *F*. TC^{Cy3} (10 nM) and 70SIC^{Cy5} in the presence of EF-G (4 μ M) and 400 μ M GTP. Lines are best fits to single exponentials, giving the indicated association (t_{assoc}) and dissociation (t_{dissoc}) times and corresponding values of k_{assoc} and k_{dissoc} .

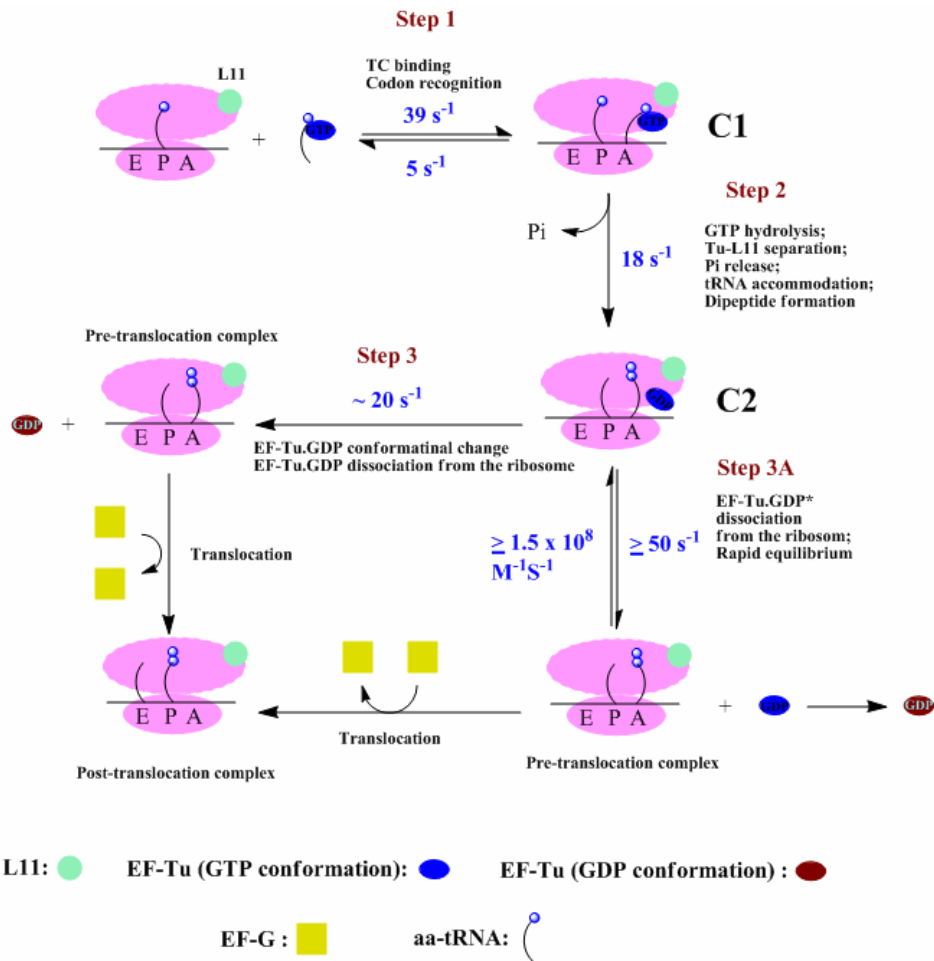


Figure 4.7. A simplified quantitative model for TC interaction with 70SIC. The rate constants shown are for reaction of TC^{QSY9} with 70SIC^{Cy3}. Rate constants for this and other TC/70SIC combinations are summarized in Table 4.3. The metastable species EF-Tu.GDP* has a conformation characteristic of EF-Tu.GTP, even though the GTP has hydrolyzed. Only upper and lower limits, respectively, can be given for K_d and k_{3A} . These limits require a rapid association rate constant ($\geq 1.5 \times 10^8 \text{ M}^{-1}\text{s}^{-1}$) for EF-Tu.GDP* binding to the PRE complex. Rate constants of this order have previously been found for TC binding to 70SIC (Gromadski, 2004; Pape, 1998). Because of uncertainty regarding the position of equilibrium in Step 3A under ensemble conditions, the simplifying assumption was made in carrying out the fitting that C₂ was dominant. Thus, the fitted value for k_3 is a lower limit.

CHAPTER 5

MONITORING TRANSLATION WITH MODIFIED

mRNAs STRATEGICALLY LABELED WITH ISOMORPHIC

FLUORESCENT NUCLEOSIDE MIMETICS

[Part of the data in this chapter is adapted with permission from (Liu, W., Shin D., Tor, Y., and Cooperman, B. S. (2013). Monitoring translation with modified mRNAs strategically labeled with isomorphic fluorescent guanosine mimetic. ACS Chem Biol 8, 2017–2023). Copyright (2013) American Chemical Society.]

5.1 Abstract

Here we examine seven mRNAs with new emissive and responsive isosteric nucleoside mimetics (thG and thA), with the goal of developing real time assays for monitoring translation-related events at nucleotide resolution. In these mRNAs the emissive nucleosides are placed site-specifically at codon positions 1, 4, 5, and 6, counting the AUG start codon as positions 1–3. All emissive mRNAs tested form initiation (70SIC), pretranslocation (PRE) and posttranslocation (POST) complexes. In most cases spectral differences are seen on binding of the mRNA to the ribosome during 70SIC formation, and on conversion of 70SIC to PRE complexes and PRE complexes to POST complexes. These differences allow measurement of the kinetics of such conversions by changes in the fluorescence of labeled mRNAs. Such measurements directly identify a specific step during PRE complex formation, provisionally assigned to codon:anticodon-loop base pair formation, that follows EF-Tu.GTP.aa-tRNA ternary complex binding to the ribosome and precedes aa-tRNA accommodation into the A-site of the ribosome. These observations not only demonstrate the functionality of mRNAs modified with the emissive nucleoside mimetic, but also the potential this mimetic offers for observing the formation and disappearance of discrete intermediates during the polypeptide elongation cycle.

5.2 Introduction

The past dozen years or so have witnessed huge progress in our understanding of ribosome function, fueled by high resolution structures (Schmeing et al., 2009a; Wilson and Doudna Cate, 2012) and by increasingly sophisticated biochemical, biophysical, and computational studies that probe the detailed workings of this complex machine (Dever and Green, 2012; Frank and Gonzalez, 2010; Wohlgemuth et al., 2011; Rodnina and Wintermeyer, 2011; Sanbonmatsu, 2012). Many of the studies directed toward understanding of the dynamics of ribosome function rely heavily on both ensemble and single molecule time-resolved observations made with functional, fluorescent-labeled derivatives of components of the protein synthesis machinery, for the most part including tRNAs, ribosomal proteins, and protein auxiliary factors such as EF-Tu and EF-G (Frank and Gonzalez, 2010; Pan et al., 2009; Chen et al., 2011a; Cooperman et al., 2011). For example, changes in the fluorescence of labeled tRNAs and labeled ribosomal proteins, combined with several other assays measuring GTP hydrolysis, dipeptide formation, P_i release, and peptidyl-tRNA reactivity toward puromycin have resulted in the formulation of quantitative kinetic schemes for the two major steps within the elongation cycle: i) ternary complex (TC, consisting of EF-Tu.GTP.aminoacyl (aa)-tRNA) binding to a posttranslocation (POST) or 70S initiation complex (70SIC) followed by accommodation of aa-tRNA within the A-site of the ribosome and peptide bond formation, leading to pretranslocation (PRE) complex formation (Pape et al., 1998; Geggier et al., 2010; Wohlgemuth et al., 2011), and ii) EF-G.GTP-catalyzed translocation of tRNAs bound in the A- and P-sites to the

P-and E-sites, respectively, along with mRNA to which they are bound, leading to conversion of PRE complex to POST complex (Savelsbergh et al., 2003; Pan et al., 2007; Munro et al., 2010; Chen et al., 2011a; Cunha et al., 2013), thus completing the cycle.

Despite the central role of mRNA in protein synthesis, the use of fluorescent mRNAs has, by contrast, been quite limited, confined almost exclusively to mRNAs derivatized at the 3'-end with fluorophores that monitor the movement of this terminus to a position at the entrance of the mRNA channel during translocation (Savelsbergh et al., 2003; Studer et al., 2003; Liu et al., 2010; Cunha et al., 2013). Although it would be of obvious interest to monitor mRNA codons that interact directly with the anticodon loops of tRNAs bound within the A, P, and E sites of the ribosome, progress in this direction has been held back by the expectation that bulky fluorophores attached to codon nucleotides within the narrow confines of the mRNA channel would either abolish or distort mRNA activity, making such derivatives unreliable probes of normal mechanism. Recently, however, new emissive and responsive nucleoside mimetics based on thieno[3,4-d]pyrimidine, which maintain normal Watson-Crick base pairing, have been described for all four RNA nucleosides (Shin, 2011 et al.; Samanta et al., 2012; Gedik and Brown, 2013), that either are isosteric with the nucleoside being mimicked [thGuanosine (thG) or thAdenosine (thA), Figure 1.5] or have the effect of converting pyrimidines into isosteres of purines (thUridine and thCytosine).

Here we describe the preparation of seven functional mRNAs containing emissive nucleoside mimetics within the initiation or the second codon that display easily measurable fluorescence changes at different stages of protein synthesis. Such changes permit monitoring of the conversion of a 70SIC first to a pretranslocation (PRE) complex and then to posttranslocation (POST) complex, at nucleotide resolution. We use such monitoring, in conjunction with other fluorescence assays, to directly identify a specific step during PRE complex formation, that follows EF-Tu.GTP.aa-tRNA ternary complex binding to the ribosome and precedes aa-tRNA accommodation into the A-site of the ribosome, and that we provisionally assign to codon:anticodon-loop base pair formation.

5.3 Results

5.3.1 Modified mRNAs

Seven short mRNAs containing a single thG or thA within the AUG initiation codon or the following second codon were prepared, and named as thG4, thG5, thG6, thA1, thA4, thA5, and thA6, respectively, according to the positions of the modification at the 5' position of initiation codon, or 5', middle, and 3'-positions of the second codon (Figure 5.1). The amino acids that these mRNAs encode at the second codon position are: Val for thG4 and thG6, Arg for thG5, and Lys for thA1, thA4, thA5 and thA6. Three additional mRNAs containing no modified nucleotides were also prepared and named as MVF, corresponding to thG4 or thG6, MRF, corresponding to thG5, and MKF,

corresponding to thA1, thA4, thA5 or thA6.

5.3.2 Formation of functional initiation and elongation complexes

Modified mRNAs were tested for their activities in different stages of translation: 70S initiation complex (70SIC) formation (Figures 5.2A–B and 5.3A), as measured by fMet-tRNA^{fMet} co-sedimentation with a 70S ribosome; pretranslocation (PRE) complex formation (Figures 5.2C–D and 5.3B), as measured by Val-tRNA^{Val} (thG4, thG6), Arg-tRNA^{Arg} (thG5), or Lys-tRNA^{Lys} (thA1, thA4, thA5, thA6) co-sedimentation with a 70SIC; and EF-G.GTP dependent translocation (Figures 5.2E–F and 5.3C), as measured by fMet-Val-puromycin (thG4, thG6), fMet-Arg-puromycin (thG5) or fMet-Lys-puromycin (thA1, thA4, thA5, thA6) formation.

The results in Figures 5.2 and 5.3 demonstrate that substantial functionality is retained on nucleoside mimetic substitution at positions 1, 4, 5, or 6. Noteworthy are the lower relative activities of thG4- and thG6-programmed ribosomes in stable PRE complex formation (Figure 5.2C), and of thA5-programmed ribosomes in stable POST complex formation (Figure 5.3C), respectively (see Section 5.4).

5.3.3 Fluorescence changes on functional complex formation

thG and thA are both ideally emissive ($\Phi = 0.46$ and 0.21 , respectively) and responsive fluorescent nucleoside mimetics (Shin et al., 2011). Although

incorporation into oligonucleotides generally lowers the quantum yield of emissive nucleosides (Sinkeldam et al., 2010), we anticipated that modified oligonucleotides shown in Figure 5.1 would retain a high level of responsiveness that would allow one to monitor mRNA binding, movement and subtle environmental changes within the ribosome during the elongation cycle. thG4, thG5, thG6, thA1, thA4, thA5 and thA6 mRNAs each have a broad excitation maximum at 340–360 nm (Figure 5.4A and C). To minimize the background fluorescence from the ribosome, 360 nm was chosen as the excitation wavelength for fluorescence experiments.

5.3.3.1 Fluorescence changes of mRNA binding to the ribosome

Each of the three mRNAs with an thG substitution within the second codon shows a negligible bathochromic shift on binding to the ribosome as part of a 70SIC but clear emission intensity changes (Figure 5.4B), presumably arising from the altered environment of emissive nucleoside mimetics on the ribosome compared to solution. The four mRNAs with an thA substitution within the initiation or the second codon also display emission intensity changes on binding to the ribosome as part of a 70SIC (Figure 5.4D). However, the data of thA-containing mRNAs are preliminary and need to be further confirmed.

5.3.3.2 Fluorescence changes of 70SIC conversion to PRE complex

Conversion of 70SIC programmed with six of the seven emissive mRNAs (all but

thA1) to the corresponding PRE complex via addition of cognate EF-Tu.GTP.aminoacyl-tRNA ternary complex (EF-Tu.GTP.aa-tRNA, denoted TC) results in Watson-Crick base pairing of the thG or thA present in the first elongator tRNA codon, so that observed changes (Figures 5.5 and 5.6; Table 5.1) reflect both generalized environmental effects of converting a 70SIC into the first PRE complex and the specific effects of codon:anticodon H-bonding at the A-site. No such changes are seen on addition of non-cognate TCs in place of cognate TCs (Figures 5.7 and 5.8). All 70SICs programmed with mRNAs with an thG or thA present in the first elongator tRNA codon, show measurable changes in fluorescence intensity on conversion to PRE complexes. In addition, the thG4- and thA4-programmed 70SIC show small hypsochromic shifts. No clear fluorescence intensity change is observed when 70SIC programmed with thA1 was mixed with cognate TC. However, an ~10% uncertainty in intensity is expected due to the background fluorescence subtraction performed (see legend of Figure 5.6). Therefore, the lack of fluorescence intensity change observed for thA1 in the static experiment is not inconsistent with the small intensity decrease seen in the kinetic experiment (Figure 5.10A).

5.3.3.3 Fluorescence changes of PRE conversion to POST complex

Conversion of a PRE complex to a POST complex via EF-G.GTP addition proceeds with maintenance of the anticodon-loop:codon Watson-Crick base pairs. For the thG4-, thG6- and thA4-programmed PRE complexes, such conversions result in

fluorescence changes that either completely (thG4 and thA4) or partially (thG6) reverse the changes seen on conversion of 70SIC to PRE complex (Figures 5.5A, C–D and 5.6B, E). thA1-programmed PRE complex to POST complex conversion shows a significant fluorescence decrease (Figures 5.6A, E). Only a small fluorescence increase was observed for both thA5- and thA6-programmed PRE complex to POST complex conversion (Figures 5.6C–E). In contrast, conversion of the thG5-programmed PRE complex to POST complex proceeds with virtually no fluorescence change (Figures 5.5B, D). These changes (summarized in Table 5.1) provide sensitive spectroscopic handles allowing us to monitor the changes in the microenvironments of specific codon nucleotides at the decoding center during the first cycle of polypeptide elongation.

5.3.4 Kinetics of PRE complex formation

We used the changes seen in Figures 5.5 and 5.6 to determine rates of PRE complex formation. Earlier work showed that 1) proflavin(prf)-labeled aa-tRNA can be used to monitor a two phase reaction of ternary complex (EF-Tu.GTP.aa-tRNA, TC) with 70SIC, initial TC binding followed by aa-tRNA accommodation into the A-site (Pape et al., 1998), that results in PRE complex formation; and 2) fMet-tRNA^{fMet}(prf) bound in the P-site monitors accommodation of aa-tRNA within the ribosome in an essentially single-phase reaction (Pan et al., 2008). Rates of thG and thA fluorescence change were determined in three parallel experiments, using either i) unlabeled

fMet-tRNA^{fMet} and unlabeled aa-tRNA^{aa}, ii) unlabeled fMet-tRNA^{fMet} and aa-tRNA^{aa}(prf), or iii) fMet-tRNA^{fMet}(prf) and unlabeled aa-tRNA (Figures 5.9 and 5.10. In ii) and iii), parallel measurements were made for the rates of proflavin fluorescence change. Rates of proflavin fluorescence change were also determined when unlabeled MVF, MRF and MKF were substituted for the corresponding emissive mRNAs (thG4 or thG6; thG5; and thA1, thA4, thA5 or thA6, respectively). All of the emissive mRNA changes proceeded as essentially single-phase reactions, with the exception of thA5, which proceeded via a two-phase reaction.

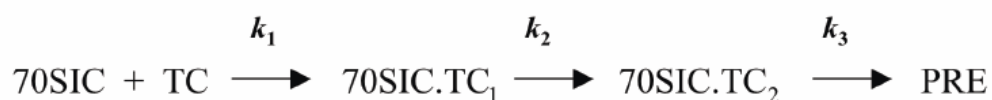
5.3.4.1 thG4- and thG6-programmed ribosomes

Below we distinguish *apparent* rate constants, which are determined by fitting the kinetic data in Figures 5.9A, and 5.9C to either a double exponential [aa-tRNA(prf) fluorescence intensity changes] or to a single exponential [both fMet-tRNA^{fMet}(prf) and thG fluorescence changes], from *microscopic* rate constants, which are determined by globally fitting all of the kinetic data obtained with a given mRNA to a posited kinetic mechanism. For both mRNAs, the measured apparent rate constants fall in the order aa-tRNA(prf)-Phase 1 (denoted k_{app1}) \gg thG (denoted k_{app2}) $>$ aa-tRNA(prf)-Phase 2 \sim fMet-tRNA^{fMet}(prf) (both denoted k_{app3}) (Table 5.2). That k_{app2} values, derived from thG fluorescence changes, differ from both k_{app1} and k_{app3} values, derived from prf-labeled tRNA fluorescence changes, demonstrates that thG-labeled mRNA provides evidence for a step in PRE complex formation not

previously seen with prf-labeled tRNAs. k_{app2} values for $^{th}G4$ and $^{th}G6$ fluorescence change were very similar to each other and in both cases were little affected by prf labeling of either fMet-tRNA^{fMet} or Val-tRNA^{Val}. Similarly, k_{app1} values were unaffected by ^{th}G substitution for unmodified G, although k_{app3} values were reduced by about one-third.

Microscopic rate constants for the two mRNAs were determined by globally fitting each set of rate measurements in Figures 5.9A and 5.9C to a simplified three-step kinetic scheme for the mixing of 70SIC and TC that results in PRE complex formation (Scheme 5.1, Table 5.4). Such fittings were carried out ignoring the quite minor changes resulting from carrying out experiments with unlabeled vs. prf-labeled forms of fMet-tRNA^{fMet} or Val-tRNA^{Val}. Interpreted in the light of earlier results (Gromadski and Rodnina, 2004a; Pan et al., 2008), steps 1 and 3 should correspond, respectively, to an initial binding of TC to 70SIC that doesn't involve codon:anticodon base pairing, and to accommodation of aa-tRNA into the A-site that is followed by peptide bond formation and EF-Tu.GDP release from the ribosome. The ^{th}G fluorescence change provides a new probe for the intervening step 2, that we presume corresponds to the base pairing step between the codon and the aa-tRNA anticodon loop. Importantly, the rate constant values k_1 – k_3 obtained with $^{th}G4$ - and $^{th}G6$ -programmed ribosomes are virtually identical to one another.

Scheme 5.1



5.3.4.2 thG5-programmed ribosomes

Results with thG5-programmed ribosomes (Figure 5.9B) differed from those discussed above in showing an apparent interaction between Arg-tRNA^{Arg}(prf) and thG5 that slowed PRE complex formation, as manifested by ~2-fold increased values of k_{app1} when MRF replaces thG5 and of k_{app2} and k_{app3} when Arg-tRNA^{Arg} replaces Arg-tRNA^{Arg}(prf) (Table 5.2). As a result, we separately fit results obtained with thG5-programmed ribosomes to Scheme 5.1 according to whether they were obtained with Arg-tRNA^{Arg}(prf) or unlabeled Arg-tRNA^{Arg} (Table 5.4).

The values obtained lead to two observations concerning thG5-programmed ribosomes. First, using unlabeled Arg-tRNA^{Arg}, k_2 and k_3 are quite similar to the values found for thG4- and thG6-programmed ribosomes, using either prf-labeled or unlabeled Val-tRNA^{Val}. Second, labeling Arg-tRNA^{Arg} with proflavin has major (~3–4-fold) and minor (1.6-fold) inhibitory effects on k_2 and k_3 , respectively.

5.3.4.3 thA4- and thA6-programmed ribosomes

Unlike Val-tRNA^{Val}(prf) and Arg-tRNA^{Arg}(prf) (Figure 5.9), Lys-tRNA^{Lys}(prf) can only be used as a good probe for the initial TC binding to the ribosomes programmed

with thA4- and thA6- containing mRNA. Thus, apparent rate constants of thA4- and thA6-programmed ribosomes are determined by fitting all of the kinetic data in Figures 5.10B and 5.10D to a single exponential. Similar to thG-programmed ribosomes, the measured apparent rate constants also fall in the order aa-tRNA(prf) (denoted k_{app1}) \gg thA (denoted k_{app2}) $>$ fMet-tRNA^{fMet}(prf) (denoted k_{app3}) (Table 5.3). The k_{app1} value for thA4 and thA6, corresponding to rate of initial TC binding to the ribosome, were a little faster (~ 1.6 fold) than the k_{app1} values for thG4 and thG6. Both k_{app2} and k_{app3} values for thA4 and thA6 were very similar to the values for thG4 and thG6 fluorescence changes. In addition, k_{app2} values for thA4 and thA6 were little affected by prf labeling of either fMet-tRNA^{fMet} or Lys-tRNA^{Val}. k_{app1} values were unaffected by thA substitution for unmodified adenosine, although k_{app3} values were reduced by about one-fourth.

Microscopic rate constants for thA4 and thA6, determined by globally fitting measurements in Figures 5.10B and 5.10D to Scheme 5.1, are listed in Table 5.4. The rate constant values k_1 – k_3 obtained with thA4- and thA6-programmed ribosomes are similar to one another. Compared with microscopic rate constants for thG4 and thG6, k_1 and k_2 for thA4 and thA6 are a little faster, while k_3 values are essentially identical.

5.3.4.4 thA1 -programmed ribosomes

Although base pairing at the ribosomal P-site between AUG codon and fMet-tRNA^{fMet} anticodon is maintained during 70SIC to PRE complex formation, a

consistent small decrease of thA1 fluorescence intensity was observed when 70SIC programmed with thA1 was rapidly mixed with corresponding cognate TC, whether fMet-tRNA^{fMet} or Lys-tRNA^{Lys} is unlabeled or labeled (Figure 5.10A). k_{app2} with unlabeled fMet-tRNA^{fMet} and Lys-tRNA^{Lys} was similar to those for thA4 and thA6, but a little slower (1.5 – 2-fold) when labeled tRNAs were used. More importantly, when 70SIC programmed with both thA1 and fMet-tRNA^{fMet}(prf) was mixed with EF-Tu.GTP.Lys-tRNA^{Lys}, k_{app2} was very similar to k_{app3} (Table 5.3). These results indicate that the thA1 response during 70SIC to PRE complex conversion monitors the tRNA accommodation. k_{app1} and k_{app3} values for thA1 were essentially identical to those for thA4 and thA6.

5.3.4.5 thA5-programmed ribosomes

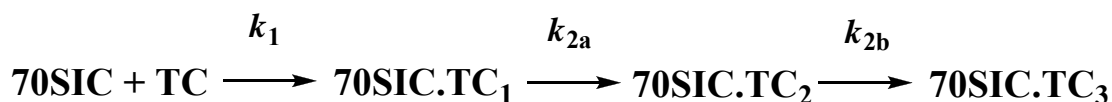
Different from all other modified mRNAs, thA5 displayed a two-phase fluorescence intensity change using either labeled or unlabeled Lys-tRNA^{Lys} and fMet-tRNA^{fMet} (Figure 5.10C and Table 5.3). The apparent rate constants of the first phase of thA5 fluorescence change using either unlabeled fMet-tRNA^{fMet} and unlabeled Lys-tRNA^{Lys}, or unlabeled fMet-tRNA^{fMet} and Lys-tRNA^{Lys}(prf) are similar to each other, but a little faster than when fMet-tRNA^{fMet}(prf) and unlabeled Lys-tRNA^{Lys} are used. The major thA5 fluorescence change occurs in the second phase, for which the apparent rate constants were 20 – 30 times lower than the fluorescence changes of thA4 and thA6. Because the same amino acid sequence is encoded in all

thA-containing mRNAs, this large rate decrease likely arises from perturbations in codon:anticodon base pairing at the middle position. Moreover, the slow second phase rate constants, which varied from 0.28 – 0.66 sec⁻¹ (Table 5.3), were in all cases comparable to k_{app3} measured by fMet-tRNA^{fMet}(prf), suggesting that base pairing at the middle codon position is rate-limiting for tRNA accommodation. Interestingly, compared with thA4 and thA6, the k_{app1} value measured by Lys-tRNA^{Lys}(prf) was also subject to a significant decrease (~ 3 fold).

Microscopic rate constants for thA5 were determined by globally fitting the measurements in Figures 5.10C to a different three-step kinetic scheme (Scheme 5.2, Table 5.4), ignoring the small changes resulting from carrying out experiments with unlabeled vs. prf-labeled forms of fMet-tRNA^{fMet} or Lys-tRNA^{Lys}. Steps 1 correspond to an initial binding of TC to 70SIC, the same as step 1 in Scheme 5.1. Different from Scheme 5.1, codon:anticodon base pairing is accomplished in two steps. Step 2 presumably corresponds to the fast base pairing at the 5' or 3' positions of the A-site codon, as measured by the fast phase of thA5 fluorescence changes; while step 3 presumably corresponds to the slow base pairing at middle codon position, as measured by the slow phase of thA5 fluorescence changes. Because tRNA accommodation is rate-limited by the full base pairing, the fMet-tRNA^{fMet}(prf) fluorescence signal change provides no information about tRNA accommodation, but is presumed to be rapid compared with the rate of step 3. The rate constant value of k_1 is modestly decreased (3 – 4 fold) compared with thA4 and thA6. Compared with the rate of full base pairing measured for thA4 and thA6, initial base pairing is ~ 2 – 6-fold

faster at the 5' or 3' positions and ~ 20-fold slower at the middle codon position.

Scheme 5.2



5.3.5 Kinetics of POST complex formation

5.3.5.1 thG-programmed ribosomes

Previous work demonstrated that fluorescence changes resulting from rapid mixing of PRE complexes containing fMet-aa-tRNA(prf) with EF-G.GTP measures the rate of translocation of fMet-aa-tRNA(prf) from the A- to the P-site of the ribosome (Savelsbergh et al., 2003; Pan et al., 2007). When PRE complexes containing thG4-labeled mRNA and fMet-Val-tRNA^{Val}(prf) are rapidly mixed with EF-G.GTP, the changes in both thG and fMet-Val-tRNA^{Val}(prf) fluorescence intensity are well fit by a single k_{app} value ($4.7 \pm 0.3 \text{ s}^{-1}$; Figure 5.11A; Table 5.5), indicating that both fluorophores are monitoring the same process. Similar results are obtained for the PRE complex containing thG6-labeled mRNA, with a slightly lower k_{app} value ($3.4 \pm 0.2 \text{ s}^{-1}$; Figure 5.11B; Table 5.5). The PRE complex programmed with thG5 had a rate constant of $6.2 \pm 1.6 \text{ s}^{-1}$ for fMet-Arg-tRNA^{Arg}(prf) fluorescence change (Table 5.5), but showed, as expected from the results presented in Figure 5.5B, almost no

change in thG fluorescence. These results demonstrate that thG-programmed ribosomes are fully functional in the translocation step that converts PRE complex to POST complex, and that in some cases this step can be monitored by changes in thG fluorescence.

5.3.5.2 thA-programmed ribosomes

According to the results in Figure 5.6, all of the four thA-containing mRNAs have a response to EF-G catalyzed translocation; however, different patterns of real-time fluorescence changes were obtained when PRE complexes containing fMet-aa-tRNA(prf) and thA were mixed with EF-G.GTP.

Change of thA1 fluorescence intensity was significantly slower than that of fMet-Lys-tRNA^{Lys}(prf) fluorescence intensity (1.3 ± 0.1 vs 4.2 ± 0.2 s⁻¹; Figure 5.12A; Table 5.5), suggesting, not unexpectedly, that thA1 fluorescence may respond to a step after PRE to POST complex conversion, possibly tRNA^{fMet} dissociation from the ribosomal E-site. Similar to thG4 and thG6, thA4 and fMet-Lys-tRNA^{Lys}(prf) fluorescent signals can be well fit to a single k_{app} value (4.4 ± 0.3 s⁻¹; Figure 5.12B; Table 5.5), indicating that thA4 monitors the same translocation process as fMet-Lys-tRNA^{Lys}(prf). In contrast, when PRE complexes containing thA5 and fMet-Lys-tRNA^{Lys}(prf) are rapidly mixed with EF-G.GTP, the observed thA5 intensity change proceeds with a apparent rate constant (2.3 ± 0.2 s⁻¹; Figure 5.12C; Table 5.5) that is much smaller than that for the major fluorescence change of

fMet-Lys-tRNA^{Lys}(prf), $13 \pm 1 \text{ s}^{-1}$ (a minor slower phase, with a rate constant of $0.94 \pm 0.16 \text{ s}^{-1}$ is observed, possibly corresponding to tRNA^{fMet} dissociation), so that, in this case, tRNA translocation measured at the D-loop proceeds more rapidly than mRNA translocation. thA6 has no fluorescence intensity change during PRE to POST complex conversion (the apparent small fluorescence intensity change of thA6 show in Figure 5.6D is likely a result of intrinsic experimental error) though fMet-Lys-tRNA^{Lys}(prf) displays a signal change with an apparent rate constant of $2.6 \pm 0.2 \text{ s}^{-1}$ (Table 5.5). These results suggest that all of the thA-programmed ribosomes are functional in translocation, and that thA substitution at different positions can be used to monitor different substeps during or after translocation.

5.4 Discussion

5.4.1 Functional activities

Modified mRNAs, site-specifically labeled with thG or thA nucleoside mimetics at the 5' position of initiation codon, or 5', middle, and 3'-positions of the second codon, were all shown to be functional in the formation of 70SIC, PRE and POST complexes (Figures 5.2 and 5.3). In general, measured activities were similar to those found with unmodified mRNAs. However, significantly lower activities were found in PRE complex formation for thG4- and thG6-programmed ribosomes and in POST complex formation for thA5-programmed ribosomes. The reasons for these lower activities are not well understood. PRE complex formation was measured at a single TC

concentration, and lower activities are most likely due to lower affinity and/or more labile binding of TC to 70SIC, as compared with MRF-programmed ribosomes. Lower activity in POST complex formation for thA5-programmed ribosome is also likely due to more labile binding of peptidyl-tRNA to the ribosome arising from the perturbation of nucleoside modification in base pairing (see Section 5.3.4.5), since thA5-programmed PRE complex is active in translocation as indicated by a rate constant of translocation similar to those of PRE complex programmed with thG- or other thA- containing mRNAs (see below, Table 5.5). The decoding center forms a tight “mould” that strongly constrains the mRNA (Ogle et al., 2001; Demeshkina et al., 2012; Demeshkina et al., 2013), so that such weakening of TC binding could result from small structural perturbations arising from both the substitution of the larger sulfur for carbon (atomic radii 1.0 Å and 0.7 Å, respectively) at purine position 8, and the loss of polar interactions resulting from carbon for nitrogen substitution at purine positions 7 and 9.

5.4.2 Fluorescence changes

Correct codon recognition in the decoding center induces local conformational changes, with base pairing at different codon positions stabilized by different rRNA and ribosomal protein residues (Ogle et al., 2001; Demeshkina et al., 2012; Demeshkina et al., 2013). In most cases, conversions between 70SIC and PRE complex or between PRE and POST complexes were accompanied by fluorescence

intensity changes (summarized in Table 5.1), with varied patterns seen for different modified mRNAs. We are unable to attribute the fluorescence intensity changes, shown in Figures 5.5 and 5.6 and summarized in Table 5.1, to specific changes in the immediate surroundings of the modified base, since they may include contributions from multiple effects, including changes in polarity, viscosity and H bonding, as well as ground and excited state processes brought about by neighboring nucleobases. Nevertheless, they provide sensitive spectroscopic handles (as summarized in Table 5.1), allowing us to monitor changes in the microenvironments of specific codon nucleotides at the decoding center during the first cycle of polypeptide elongation.

5.4.3 Kinetics

For 70SICs programmed with six of the seven mRNAs tested (thA1 excepted), fluorescence signal changes measured with thG- or thA-containing mRNAs during PRE complex formation are slower than those of initial TC binding to the ribosome and faster than tRNA accommodation, consistent with the notion that these changes monitor a common event, the formation of anticodon-codon base pairs. The similarities in the value of k_2 (obtained from global fits) for all three thG-labeled mRNAs and for thA4 and thA6 as well (Table 5.4) support this notion. It was previously indicated that EF-Tu interacts with L11 after binding to the ribosome and induces its conformational change (Wang et al., 2012). Our results suggest that this conformational change may occur as a result of cognate codon:anticodon interaction,

as part of a series of conformational changes during aa-tRNA accommodation.

During translocation, the base pairing between mRNA codon and tRNA anticodon loop is maintained, and both mRNA and tRNA move relative to the ribosome. It is well documented that tRNA movements during translocation occur in essentially two stages: first from classical states (tRNAs in A/A and P/P states, respectively) in PRE complex to hybrid states (tRNAs in A/P and P/E states, respectively), and then from hybrid states to POST complex (tRNAs in P/P and E states, respectively) (Pan et al., 2007; Zhang et al., 2009). Recently, experiments using mRNA labeled at the 3'-end showed that mRNA movements occur dominantly in coupling with ribosomal subunit rotation and tRNA movement from the hybrid state to the state in POST complex (Ermolenko and Noller, 2011), but a small signal change could be observed upon EF-G.GTP binding (Studer et al., 2003; Ermolenko and Noller, 2011). Here, utilization of emissive nucleoside mimetics programmed within the decoding codon provides the potential for directly studying mRNA movement during translocation and tRNA release from the ribosomal E-site after translocation. EF-G.GTP dependent translocation was monitored using PRE complex programmed with fMetLys-tRNA^{Lys}(prf) and thA-containing mRNAs with substitution at different positions of the first or the second codon. All PRE complexes used were functional in translocation as indicated by POST complex formation (Figure 5.3C). The fluorescence intensity change of thA4 and the simultaneous change of fMetLys-tRNA^{Lys}(prf) respond to the same translocation step, and their apparent rate constants are similar to those of PRE complexes programmed with thG4 or thG6, and

those previously reported using unmodified mRNAs (Pan et al., 2007; Ermolenko and Noller, 2011), the latter of which corresponds to the transition from hybrid state to POST complex. However, the measurements using thA1 or thA5 resulted in different results. The fluorescence intensity change of thA1 was clearly slower than that of fMetLys-tRNA^{Lys}(prf) and thA4, presumably reporting the tRNA release from the ribosomal E-site after translocation. Although the rate of thA5 fluorescence intensity change is similar to thA4, the rate of the dominant phase of fluorescence intensity change of fMetLys-tRNA^{Lys}(prf) is faster. These results can be fit in a simple model for translocation with four steps: i) EF-G.GTP binding to the ribosome; ii) translocation of tRNA on the 50S subunit seen by D-loop fluorescence change; iii) translocation of mRNA; and iv) tRNA release from the ribosomal E-site. For thG4, thG6 and thA4, steps ii) and iii) appear to proceed close to simultaneously, whereas for thA5, ii) clearly precedes iii).

5.4.4 Substitution at the middle codon position – Effects on PRE complex formation

Substitution at the middle position of the second codon (thG5 and thA5) has an inhibitory effect in all three steps that are measured here: initial TC binding to the ribosome, codon:anticodon base pairing and tRNA accommodation, with the effect more prominent for thA5. Previous results showed that aa-tRNA(prf) fluorescence change monitors initial TC binding to the ribosome in the absence of mRNA: i.e.,

without codon:anticodon interaction (Pape et al., 1998). However, the k_1 values we obtain from global fits indicate that this binding step is clearly affected by the identity of the nucleoside at the middle codon position. The mechanism of TC binding to the ribosome is still not completely understood, but our results suggest that mRNA-independent TC binding is not a pre-requisite for codon:anticodon base pairing, which is contrary to the model put forward by Pape et al. (1998).

According to the crystallographic studies of cognate TC bound to the ribosome (Demeshkina et al., 2012), codon:anticodon base pairing is monitored by highly conserved rRNA residues A1492, A1493 and/or G530. Full codon recognition requires at least three steps in principle, corresponding to the base pair formation at all three codon positions, but it is unclear whether the formation of these three base pairs is simultaneous or sequential. The interaction between the middle position of an mRNA codon and the tRNA anticodon loop was strongly inhibited by thA substitution (Table 5.3), and in a more nuanced way by thG substitution. In the latter case, a small (2-fold) decrease in the rate of base pairing with thG5 was only seen in the presence of Arg-tRNA^{Arg}(prf) (Table 5.2). We speculate that this rate effect might result from small perturbations in tRNA binding to the ribosome resulting from proflavin substitution in the D-loop of aa-tRNA that are propagated to the anticodon loop. Different from thG5, the rate of base pairing with thA5 is very slow using either labeled or unlabeled forms of Lys-tRNA^{Lys} and fMet-tRNA^{fMet} (Table 5.3), presumably due to a slowdown of base pairing at the middle codon position. A global fit for the biphasic thA5 fluorescence changes gives two values for codon:anticodon

base pairing: 40 ± 16 (minor change) and $0.44 \pm 0.07 \text{ s}^{-1}$ (major change) for k_{2a} and k_{2b} , respectively. The k_{2a} value is very close to the previously reported rate constant from tRNA fluorescence changes that was assigned to codon recognition (Pape et al., 1998). It's likely that the k_{2a} value is a reflection of environmental changes upon fast base pair formation at the 5' and/or 3' codon position. We propose that the k_{2a} value obtained for thA5 represents the normal rate for initial codon:anticodon base pair formation with unmodified codon. This is followed by a very slow base pairing step (rate constant k_{2b}) with the middle codon position, which then becomes the rate-determining step for full base pairing and subsequent tRNA accommodation. We further propose that during normal base pairing, as exemplified by the results with thA4 and thA6, the three base pairing steps occur in a series of rapid steps that we are not able to resolve, giving the appearance of a single first-order process with a rate constant of k_2 . This accounts for why k_{2a} is 2–6-fold higher than k_2 (Table 5.4).

These results are consistent with the observation that misreading by the ribosome occurs least frequently at the middle codon nucleotide (Szaflarski et al., 2008), and the tight structural constraints to which codon:anticodon base pairing at the middle position is subject within the ribosomal decoding center (Ogle et al., 2001; Demeshkina et al., 2012; Demeshkina et al., 2013). Our results indicate that a nucleoside mimetic can be utilized not only as a fluorescent probe for kinetic studies, but also as an activity probe for the functional studies of the effects of base modifications, using the sensitivity of reaction rate to base modifications.

5.5 Conclusions

Herein we report the preparation of functional modified mRNAs containing emissive nucleoside mimetics (thG or thA), and their application in elucidating the dynamics of mRNA:tRNA pair during the decoding and translocation steps of the elongation cycle of active ribosomes. Our results indicate that an thG or thA present at the 5', middle, or 3'-positions of an mRNA codon is an effective probe of codon:anticodon interaction at the ribosomal decoding center as well as for mRNA translocation within the ribosome. Such nucleoside analogues could also serve as direct reporters of various changes during translation, including mRNA:tRNA interaction during frame shifting events, or of the melting (e. g., of a downstream pseudo-knot) or transient formation (e. g., of an internal Shine-Dalgarno sequence with the 3'-end of 16S rRNA) of secondary structure.

Table 5.1. Static fluorescence spectral changes during conversions between different ribosome complexes.

	70SIC to PRE		PRE to POST	
	Δ Intensity	$\Delta \lambda_{\max}$	Δ Intensity	$\Delta \lambda_{\max}$
th G4	Increase	Blue shift	Decrease	Red Shift
th G5	Decrease	No change	No change	No change
th G6	Decrease	No change	Increase	No change
th A1	No change ^a	No change	Decrease	No change
th A4	Decrease	Blue shift	Increase	No change
th A5	Decrease	No change	Increase	No change
th A6	Decrease	No change	Increase	No change

^aDue to the necessary background subtraction in the experiments, a ~10% uncertainty in fluorescence intensity change is expected. Therefore, a slight intensity change may occur even if no apparent change is observed in static fluorescence experiments.

Table 5.2. Apparent rate constants for reactions between 70SIC programmed with thG-containing mRNAs and TC^a.

mRNA	fMet-tRNA ^{fMet}	aa-tRNA	k_{app1}^b	k_{app2}^c	k_{app3}^d
th G4	unlabeled	Val-prf	37 ± 2	8.3 ± 0.6	4.9 ± 0.3
	prf	Val	–	7.0 ± 0.3	4.1 ± 0.4
	unlabeled	Val	–	10.9 ± 0.1	–
th G6	unlabeled	Val-prf	37 ± 7	8.3 ± 0.5	5.5 ± 0.4
	prf	Val	–	8.9 ± 1.2	3.9 ± 0.1
	unlabeled	Val	–	10.5 ± 3.1	–
MVF	unlabeled	Val-prf	34 ± 1	–	7.2 ± 1.2
	prf	Val	–	–	6.2 ± 0.5
th G5	unlabeled	Arg-prf	11 ± 2	2.3 ± 0.2	1.7 ± 0.1
	prf	Arg	–	5.3 ± 0.1	3.1 ± 0.3
	unlabeled	Arg	–	4.0 ± 0.2	–
MRF	unlabeled	Arg-prf	22 ± 2	–	3.9 ± 0.1
	prf	Arg	–	–	4.8 ± 0.2

^aValues presented are average \pm average deviation from 2 independent determinations and are fits of stopped-flow data to single exponentials [k_{app2} (thG fluorescence changes) and k_{app3} (second entry tRNA^{fMet}(prf) fluorescence changes)] or double exponentials [k_{app1} and k_{app3} , first entry (tRNA^{Val}(prf) fluorescence changes)]. For thG4, thG5 and thG6, rates in the first, second and third rows were determined, respectively, in the presence of: aa-tRNA(prf) and fMet-tRNA^{fMet}; aa-tRNA and fMet-tRNA^{fMet}(prf); and aa-tRNA and fMet-tRNA^{fMet}. For MVF and MRF, rates in the first and second rows were determined, respectively, in the presence of: aa-tRNA(prf) and fMet-tRNA^{fMet}, and aa-tRNA and fMet-tRNA^{fMet}(prf).

^bRapid phase of aa-tRNA (prf) fluorescence change.

^cthG fluorescence change: upper, in presence of aa-tRNA(prf); middle, in presence of fMet-tRNA^{fMet}(prf); lower, in presence of unlabeled tRNAs.

^dUpper, slow phase of aa-tRNA (prf) fluorescence change; lower, fMet-tRNA^{fMet} (prf) fluorescence change.

Table 5.3. Apparent rate constants for reactions between 70SIC programmed with thA-containing mRNAs and TC^a.

mRNA	fMet-tRNA ^{fMet}	aa-tRNA	k_{app1}^b	k_{app2}^c	k_{app3}^d
th A1	unlabeled	Lys-prf	55 ± 10	7.3 ± 1.0	–
	prf	Lys	–	5.5 ± 0.3	6.4 ± 0.1
	unlabeled	Lys	–	11 ± 4	–
th A4	unlabeled	Lys-prf	53 ± 1	8.9 ± 0.5	–
	prf	Lys	–	9.1 ± 1.7	5.2 ± 0.6
	unlabeled	Lys	–	9.8 ± 0.7	–
th A5	unlabeled	Lys-prf	18 ± 5	13.2 ± 3.2	–
			–	0.28 ± 0.09	–
	prf	Lys	–	8.9 ± 1.2	–
			–	0.45 ± 0.08	0.43 ± 0.05
	unlabeled	Lys	–	15.0 ± 1.2	–
–	–	–	0.66 ± 0.01	–	
th A6	unlabeled	Lys-prf	62 ± 11	9.8 ± 1.6	–
	prf	Lys	–	12.0 ± 1.3	6.6 ± 0.8
	unlabeled	Lys	–	11.6 ± 1.3	–
MKF	unlabeled	Lys-prf	44 ± 3	–	–
	prf	Lys	–	–	8.1 ± 0.3

^aValues presented are average \pm average deviation from 2 independent determinations and are fits of stopped-flow data to single exponentials [k_{app1} (first entry tRNA^{Lys}(prf) fluorescence changes), k_{app2} (thA fluorescence changes) and k_{app3} (second entry tRNA^{fMet}(prf) fluorescence changes)]. For thA1, thA4, thA5 and thA6, rates in the first, second and third rows were determined, respectively, in the presence of: aa-tRNA(prf) and fMet-tRNA^{fMet}; aa-tRNA and fMet-tRNA^{fMet}(prf); and aa-tRNA and fMet-tRNA^{fMet}. For MKF, rates in the first and second rows were determined, respectively, in the presence of: aa-tRNA(prf) and fMet-tRNA^{fMet}; and aa-tRNA and fMet-tRNA^{fMet}(prf).

^b Aa-tRNA (prf) fluorescence change.

^c thA fluorescence change for thA1, thA4 and thA6: upper, in presence of aa-tRNA (prf); middle, in presence of fMet-tRNA^{fMet} (prf); lower, in presence of unlabeled tRNAs. thA fluorescence change for thA5: upper two, in presence of aa-tRNA (prf), -0.026 ± 0.005 and -0.059 ± 0.009 in amplitude changes for fast and slow phase, respectively; middle two, in presence of fMet-tRNA^{fMet} (prf), -0.016 ± 0.003 and -0.044 ± 0.007 in amplitude changes for fast and slow phase, respectively; lower two, in presence of unlabeled tRNAs, -0.030 ± 0.007 and -0.037 ± 0.010 in amplitude changes for fast and slow phase, respectively.

^d fMet-tRNA^{fMet} (prf) fluorescence change

Table 5.4. Microscopic rate constants (s^{-1}) for 70SIC reaction with TC^a.

mRNA	k_1	k_2 or k_{2a}^c	k_3 or k_{2b}^c
th G4	82 ± 9	7.2 ± 0.2	15.2 ± 0.7
th G5 ^b	45 ± 10 (45–85) ^c	1.8 ± 0.2 7.5 – 6.0	6.1 ± 1.1 9.9 ± 0.4
th G6	80 ± 11	8.4 ± 0.4	13.7 ± 1.3
th A4	123 ± 13	10.6 ± 0.3	12.0 ± 0.4
th A5 ^d	42 ± 1	40 ± 16	0.44 ± 0.07
th A6	170 ± 9	11.3 ± 0.1	15.0 ± 0.5

^aValues presented are for results in Figures 5.9, 5.10B–D that are fit to Scheme 5.1 or Scheme 5.2 (see text).

^bUpper values: Fit using fluorescence changes of Arg-tRNA^{Arg}(prf) and thG5 mRNA; lower values: Fit using fluorescence changes of fMet-tRNA^{fMet}(prf) and thG5 mRNA.

^cFor thA5.

^dThe values are mean \pm standard deviation of two fits, with and without thA5 data measured with unlabeled fMet-tRNA^{fMet} and unlabeled Lys-tRNA^{Lys}.

Table 5.5. Apparent rate constants for POST complex formation on reaction of PRE complexes programmed with thG- and thA-containing mRNAs and EF-G.GTP^a.

mRNA	k_{app} (th G or th A)	k_{app} [fMet-aa-tRNA(prf)]	k_{app} (Global fit)
th G4	3.7 ± 1.5	4.6 ± 0.1	4.7 ± 0.3
th G5	N/A ^b	6.2 ± 1.6	N/A ^c
th G6	4.1 ± 0.6	3.1 ± 0.1	3.4 ± 0.2
th A1	1.3 ± 0.1	4.2 ± 0.2	N/A ^c
th A4	3.5 ± 0.2	5.2 ± 0.3	4.4 ± 0.3
th A5	2.3 ± 0.2	13 ± 1 (0.074±0.022) ^c 0.94 ± 0.16 (0.044±0.007) ^c	N/A ^d
th A6	N/A ^b	2.6 ± 0.2	N/A ^d

^aValues presented are average \pm average deviation from 2 independent determinations and are, in most cases, fits of stopped-flow data to single exponentials [second column, fits of thG or thA fluorescence changes alone; third column, fits fMet-aa-tRNA(prf) fluorescence changes alone; and fourth column, global fits of both thG or thA and fMet-aa-tRNA(prf) fluorescence changes]. The only exception is fMet-aa-tRNA(prf) fluorescence change of PRE complex programmed with thA5, which is fit to double exponential.

^b No thA fluorescence change.

^c Values in the parentheses are amplitude changes.

^d thG or thA fluorescence change can not be globally fitted together with fMet-aa-tRNA(prf) fluorescence change.

thG4: +4
 UUA AUA AGG AUA CAU ACU AUG **GUG** UUC CGU
 fMet Val Phe Arg

thG5: +5
 UUA AUA AGG AUA CAU ACU AUG **CGU** UUC CGU
 fMet Arg Phe Arg

thG6: +6
 UUA AUA AGG AUA CAU ACU AUG **GUG** UUC CGU
 fMet Val Phe Arg

thA1: +1
 UUA AUA AGG AUA CAU ACU **AUG** AAA UUC CGU
 fMet Lys Phe Arg

thA4: +4
 UUA AUA AGG AUA CAU ACU AUG **AAA** UUC CGU
 fMet Lys Phe Arg

thA5: +5
 UUA AUA AGG AUA CAU ACU AUG **AAA** UUC CGU
 fMet Lys Phe Arg

thA6: +6
 UUA AUA AGG AUA CAU ACU AUG **AAA** UUC CGU
 fMet Lys Phe Arg

Figure 5.1. mRNAs labeled with isomorphous fluorescent nucleoside mimetics. Modification positions are shown in red.

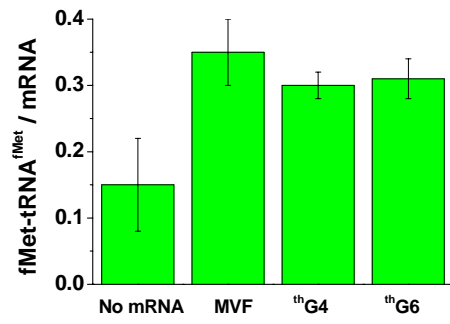
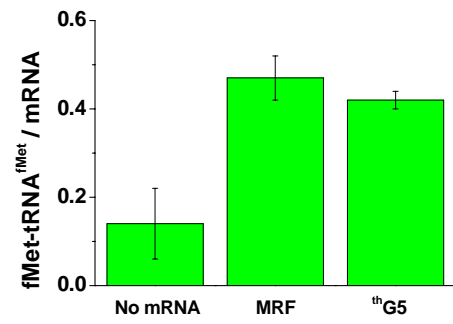
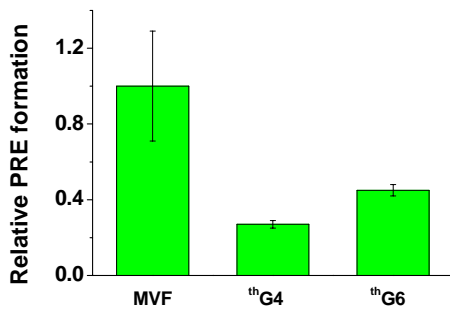
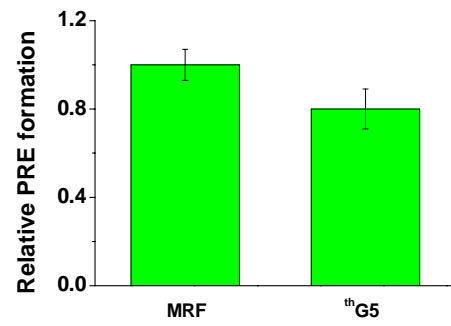
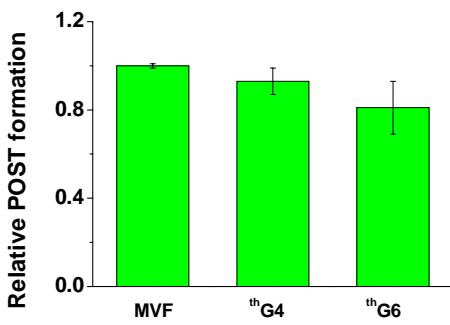
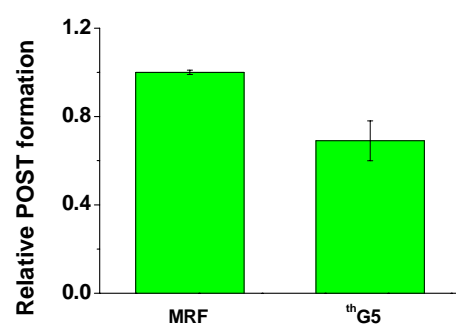
A**B****C****D****E****F**

Figure 5.2. Activities of mRNAs containing thG. Formation of various complexes with ribosomes programmed with thG4 or thG6 (A, C, E) or thG5 (B, D, F). A and B. 70SIC formation, measured as fMet-tRNA^{fMet} co-sedimented per mRNA added: ribosomes, 1.0 μM, mRNA 0.5 μM. C and D. Normalized PRE complex formation, with background in the absence of mRNA subtracted: ribosomes, 0.8 μM. E and F. Normalized POST complex formation. thG4, thG6: ribosomes, 2 μM. thG5: ribosomes 4.8 ± 0.2 μM. Control experiments were performed, as indicated, with either no added mRNA, or with added unmodified mRNA, or with no added EF-G. Values reported in C and D were relative to the corresponding unmodified mRNAs (MVF for thG4 and thG6; MRF for thG5) after subtraction of background obtained with no mRNA and normalized to the value obtained for unmodified mRNA. Values reported in E and F were obtained from Equations 2.1A and 2.1B and normalized to the value obtained for unmodified mRNA.

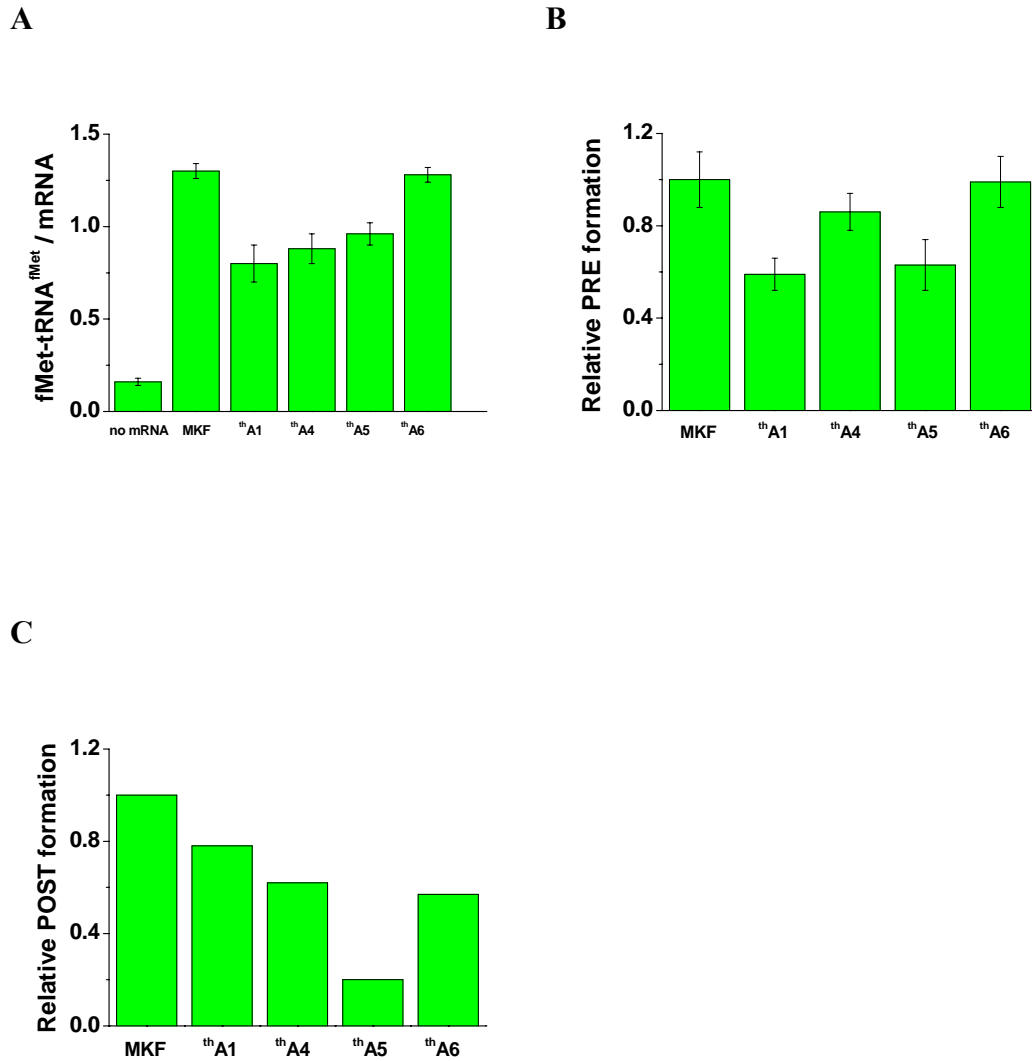


Figure 5.3. Activities of mRNAs containing thA. *A*. 70SIC formation, measured as fMet-tRNA^{fMet} co-sedimented per mRNA added: ribosomes, 1.0 μ M, mRNA 0.5 μ M. *B*. Normalized PRE complex formation, with background in the absence of mRNA subtracted: ribosomes, 0.8 μ M. *C*. Normalized POST complex formation (ribosomes, 4.8 ± 0.2 μ M). Control experiments were performed, as indicated, with either no added mRNA, or with added unmodified mRNA, or with no added EF-G. Values reported in *B* were relative to the corresponding unmodified MKF mRNA after subtraction of background obtained with no mRNA and normalized to the value obtained for unmodified mRNA. Values reported in *C* were obtained from Equations 2.1B and normalized to the value obtained for unmodified mRNA.

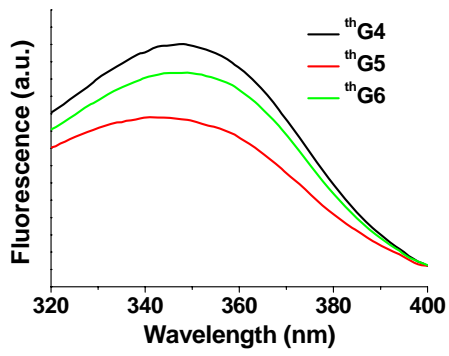
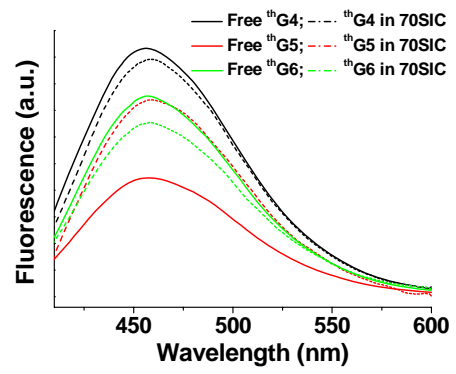
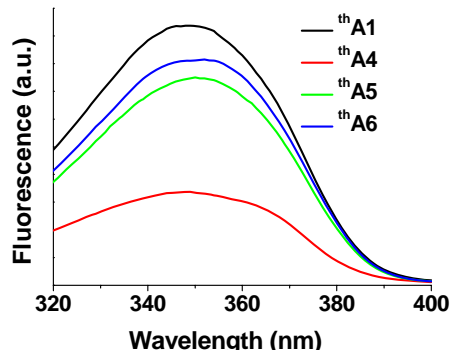
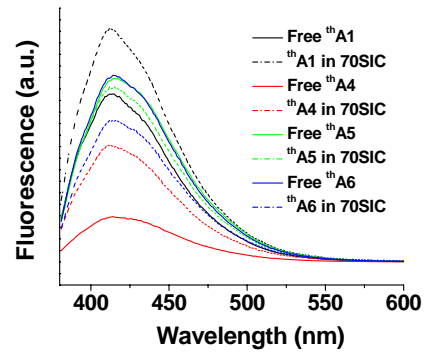
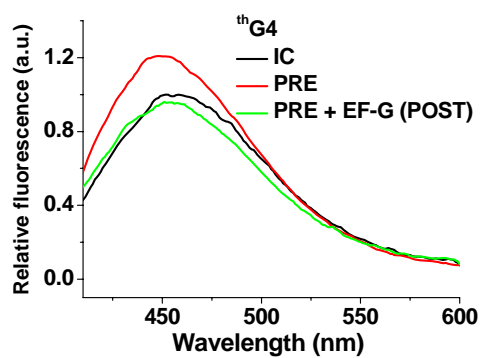
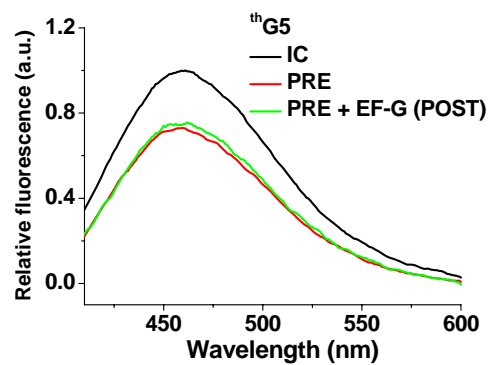
A**B****C****D**

Figure 5.4. Excitation and emission spectra of thG- and thA-containing mRNAs. *A.* Excitation spectra of free thG-containing mRNAs (0.8 μM). *B.* Slight bathochromic shift of fluorescence maximum of thG4 and thG5 but not of thG6 upon binding to the ribosome as part of a 70SIC. 70SICs programmed with thG containing-mRNAs were prepared *in situ* by using 70S (1.2 μM) and thG-containing mRNA (0.6 μM), and incubating at 37 °C for 5 min. Buffer background fluorescence was subtracted from the signals of free thG-containing mRNAs (0.6 μM). Background fluorescence from the mixture of 70S, translation factors and fMet-tRNA^{fMet} with no incubation was subtracted from the 70SIC programmed with thG-containing mRNAs. The traces shown in *B* are average of two independent determinations. *C.* Excitation spectra of free thA-containing mRNAs (0.8 μM). *D.* 70SICs programmed with thA containing-mRNAs were prepared *in situ* by using 70S (1.2 μM) and thA-containing mRNA (0.6 μM), and incubating at 37 °C for 5 min. Buffer background fluorescence was subtracted from the signals of free thA-containing mRNAs (0.6 μM). Background fluorescence from the mixture of 70S, translation factors and fMet-tRNA^{fMet} with no incubation was subtracted from the 70SIC programmed with thA-containing mRNAs.

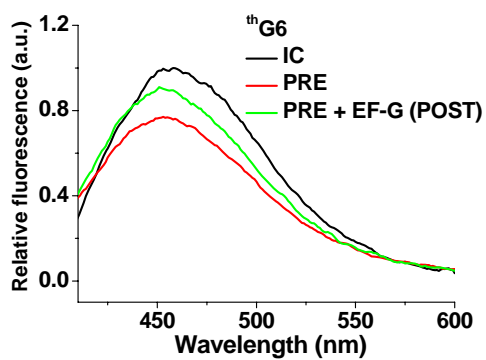
A



B



C



D

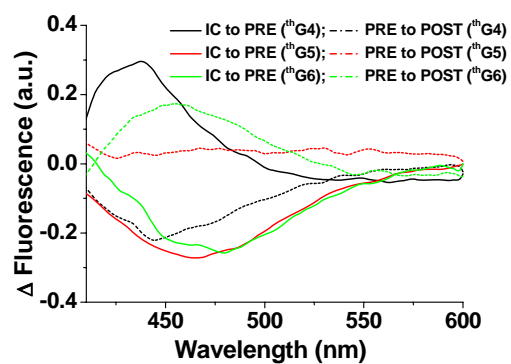
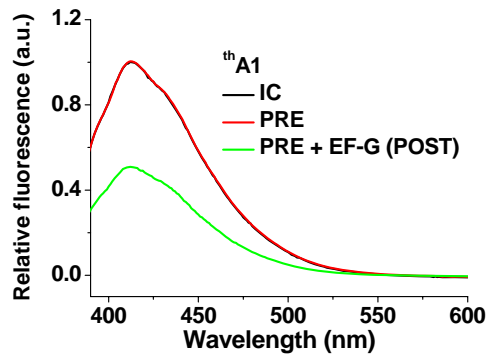
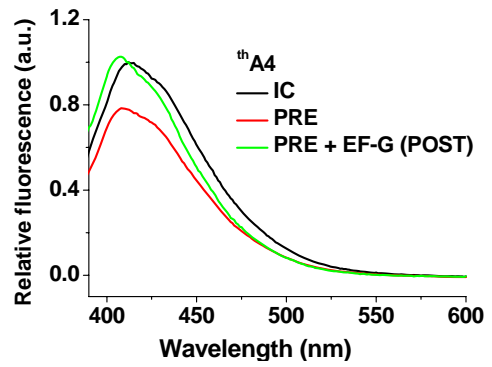


Figure 5.5. Fluorescence changes of thG-containing mRNAs. A–C. Traces are shown for 70SIC (black); PRE complex (red); POST complex (green). 70SIC traces are for purified samples. PRE complex traces shown are the average of two independently determined traces: i) PRE complex prepared *in situ* by addition of TC to 70SIC; ii) purified PRE complex used in the preparation of POST complex. To account for small concentration differences arising from the two preparation methods, the traces for purified PRE complexes were normalized to those for *in situ* generated PRE complexes, using an 8 nm window covering the fluorescence maximum to generate a normalization factor. The resulting two very similar traces were then averaged. POST complexes were prepared *in situ* from purified PRE complexes by incubation with EF-G.GTP (2.5 μM for 20 s), and traces were normalized using the same normalization factors as above. For all traces and prior to any normalization, background fluorescence of the corresponding complex made with unlabeled mRNA was subtracted from the observed fluorescence of each of the labeled ribosome complexes. Intensities are normalized to the peak intensity value of 70SIC for each mRNA. D. Fluorescence intensity changes were obtained by subtracting the spectrum of a purified complex (70SIC or PRE) from the spectrum of a complex prepared *in situ* (PRE or POST, respectively) and then normalizing the intensity differences to the peak intensity value of purified complex (70SIC or PRE, respectively).

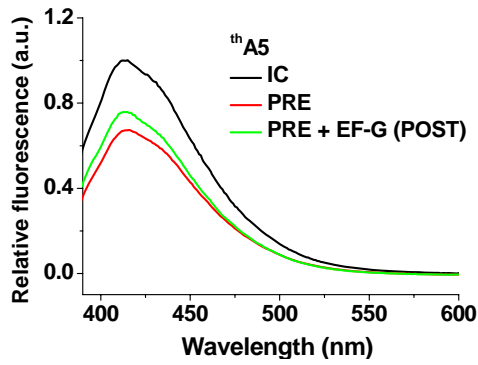
A



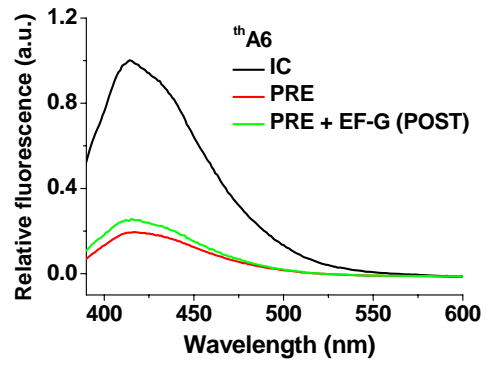
B



C



D



E

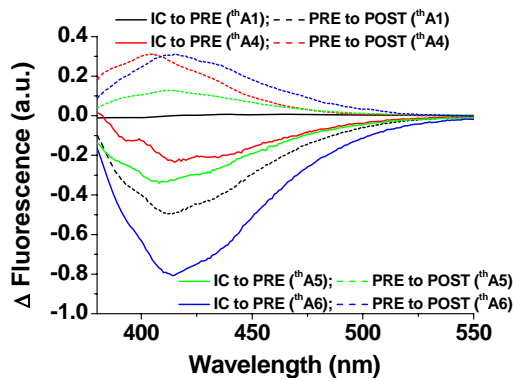


Figure 5.6. Fluorescence changes of thA-containing mRNAs. *A–D.* Traces are shown for 70SIC (black); PRE complex (red); POST complex (green). 70S IC traces are for purified samples. PRE complex traces shown are the average of two independently determined traces: i) PRE complex prepared *in situ* by addition of TC to 70SIC; ii) purified PRE complex used in the preparation of POST complex. To account for small concentration differences arising from the two preparation methods, the traces for purified PRE complexes were normalized to those for *in situ* generated PRE complexes, using an 8 nm window covering the fluorescence maximum to generate a normalization factor. The resulting two very similar traces were then averaged. POST complexes were prepared *in situ* from purified PRE complexes by incubation with EF-G.GTP (2.5 μM for 20 s), and traces were normalized using the same normalization factors as above. For all traces and prior to any normalization, background fluorescence of the corresponding complex made with unlabeled mRNA was subtracted from the observed fluorescence of each of the labeled ribosome complexes. Intensities are normalized to the peak intensity value of 70SIC for each mRNA. *E.* Fluorescence intensity changes were obtained by subtracting the spectrum of a purified complex (70SIC or PRE) from the spectrum of a complex prepared *in situ* (PRE or POST, respectively) and then normalizing the intensity differences to the peak intensity value of purified complex (70SIC or PRE, respectively).

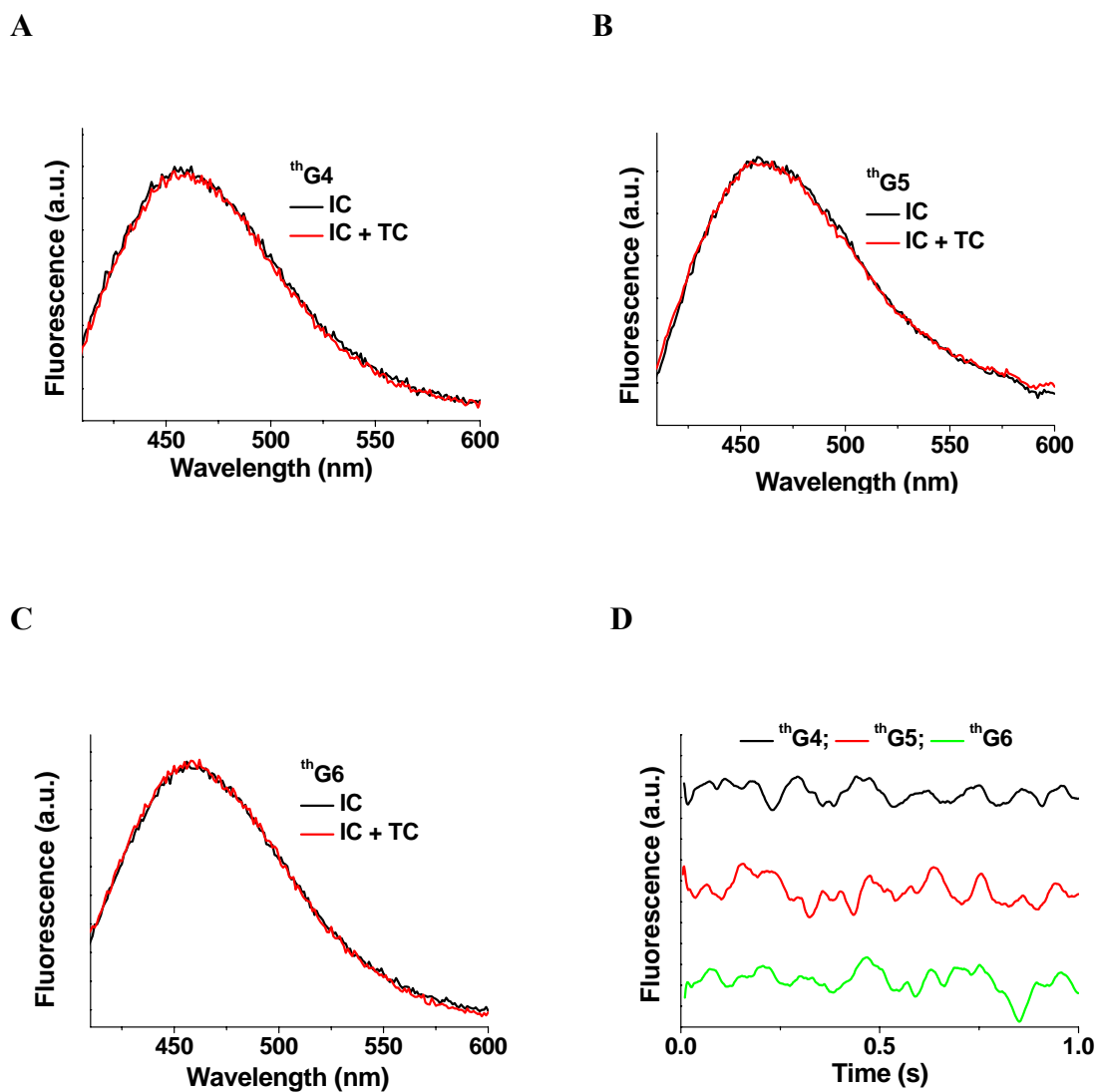


Figure 5.7. Lack of fluorescence change on adding non-cognate TCs to 70SICs programmed with thG-containing mRNAs. A–C. Traces are shown for 70SIC alone (black) and 70SIC with added non-cognate TC (red; EF-Tu.GTP.Arg-tRNA^{Arg} for thG4 and thG6, and EF-Tu.GTP.Val-tRNA^{Val} for thG5). 70S IC traces are for purified samples. For all traces, background fluorescence of the corresponding complex made with unlabeled mRNA was subtracted from the observed fluorescence of each of the labeled ribosome complexes. D. Time-resolved fluorescence changes on rapid mixing of 70SIC programmed with thG-containing mRNAs (0.1 μ M) with non-cognate TC (0.4 μ M).

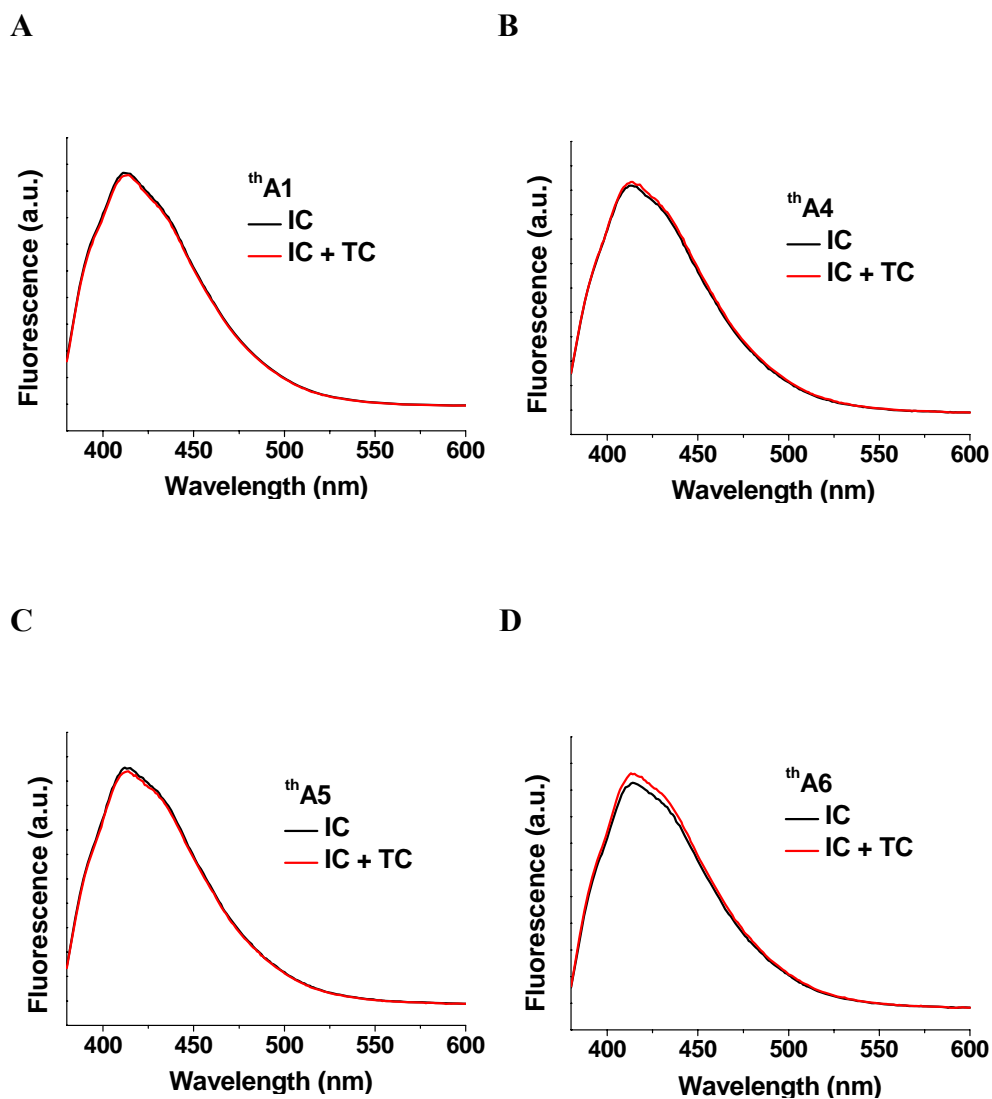


Figure 5.8. Lack of fluorescence change on adding non-cognate TCs to 70SICs programmed with ^3H -containing mRNAs. *A–D*. Traces are shown for 70SIC alone (black) and 70SIC with added non-cognate TC (red; EF-Tu.GTP.Arg-tRNA^{Arg}). 70S IC traces are for purified samples. For all traces, background fluorescence of the corresponding complex made with unlabeled mRNA was subtracted from the observed fluorescence of each of the labeled ribosome complexes.

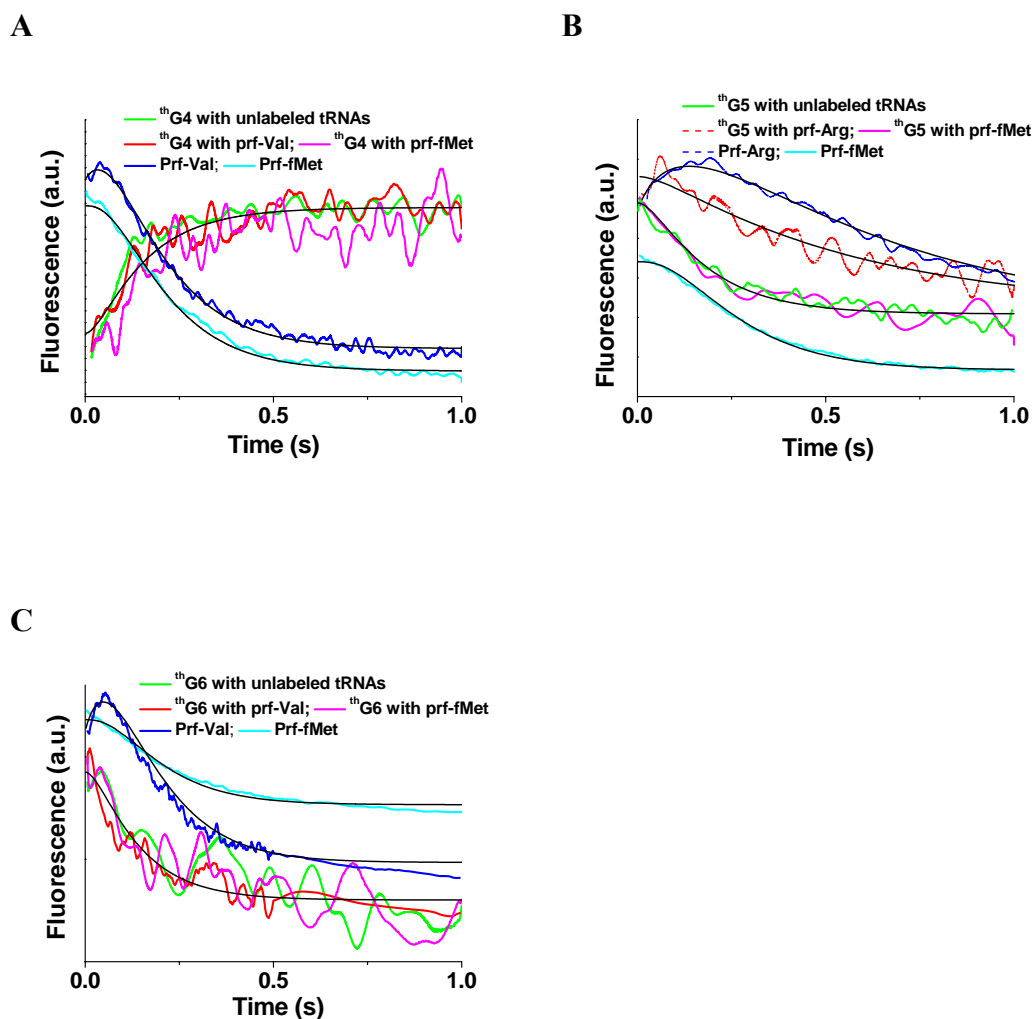


Figure 5.9. Kinetics of PRE complex formation of $^{\text{th}}\text{G}$ -containing mRNAs. Fluorescence changes on rapid mixing of 70SICs ($0.1 \mu\text{M}$) programmed with $^{\text{th}}\text{G}$ -containing mRNAs and cognate TCs ($0.4 \mu\text{M}$) compared with fluorescence changes of aa-tRNA(prf) (dark blue), present as part of the TC, or of fMet-tRNA $^{\text{fMet}}$ (prf) (cyan), present as part of the 70SIC. Rates of $^{\text{th}}\text{G}$ fluorescence change were determined using either unlabeled fMet-tRNA $^{\text{fMet}}$ and unlabeled aa-tRNA $^{\text{aa}}$ (green), unlabeled fMet-tRNA $^{\text{fMet}}$ and aa-tRNA $^{\text{aa}}$ (prf) (red), or fMet-tRNA $^{\text{fMet}}$ (prf) and unlabeled aa-tRNA $^{\text{aa}}$ (magenta). A. $^{\text{th}}\text{G4}$; B. $^{\text{th}}\text{G5}$; C. $^{\text{th}}\text{G6}$. Traces shown are the average of two independently determined traces, which, in each case were quite similar to one another. Solid black lines are global fittings to Scheme 5.1 values, using rate constant values summarized in Table 5.4. The green, magenta and cyan curves in part B was fit with the following values (in s^{-1}): $k_1 65 \pm 4$, $k_2 6.6 \pm 0.2$, $k_3 9.9 \pm 0.4$.

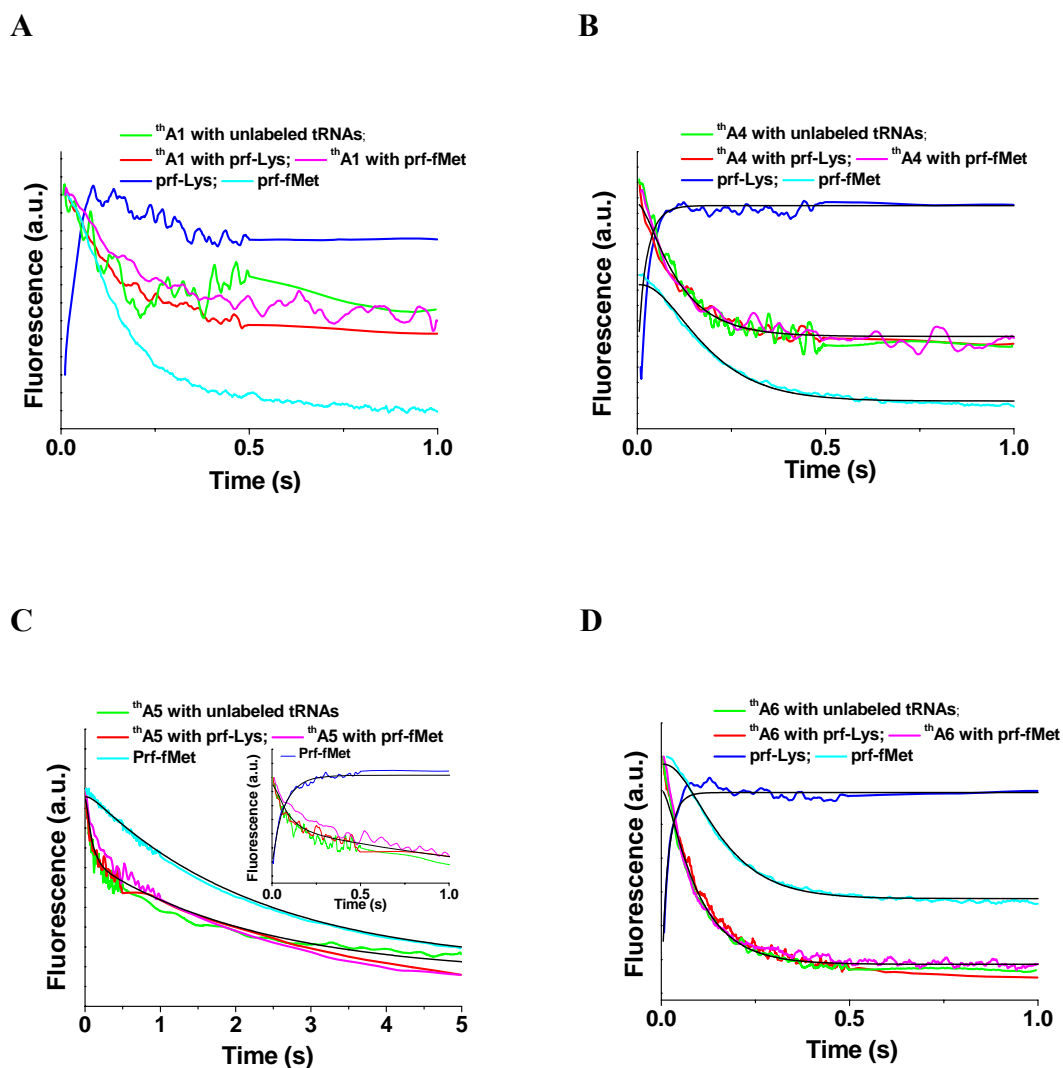


Figure 5.10. Kinetics of PRE complex formation of ^3H -A-containing mRNAs. Fluorescence changes on rapid mixing of 70SICs ($0.1 \mu\text{M}$) programmed with ^3H -A-containing mRNAs and cognate TCs ($0.4 \mu\text{M}$) compared with fluorescence changes of aa-tRNA(prf) (dark blue), present as part of the TC, or of fMet-tRNA^{fMet}(prf) (cyan), present as part of the 70SIC. Rates of ^3H -A fluorescence change were determined using either unlabeled fMet-tRNA^{fMet} and unlabeled aa-tRNA (green), unlabeled fMet-tRNA^{fMet} and aa-tRNA(prf) (red), or fMet-tRNA^{fMet}(prf) and unlabeled aa-tRNA (magenta). A. ^3H A1; B. ^3H A4; C. ^3H A5; D. ^3H A6. Traces shown are the average of two independently determined traces, which, in each case were quite similar to one another. Solid black lines in B and D are global fittings to Scheme 5.1 (^3H A4 and ^3H A6), using rate constant values summarized in Table 5.4. Solid black lines in C are global fittings to Scheme 5.2 with ^3H A5 data measured with unlabeled fMet-tRNA^{fMet} and unlabeled Lys-tRNA^{Lys} included, using rate constant values (in s^{-1}): k_1 42, k_2 40, k_3 0.44. .

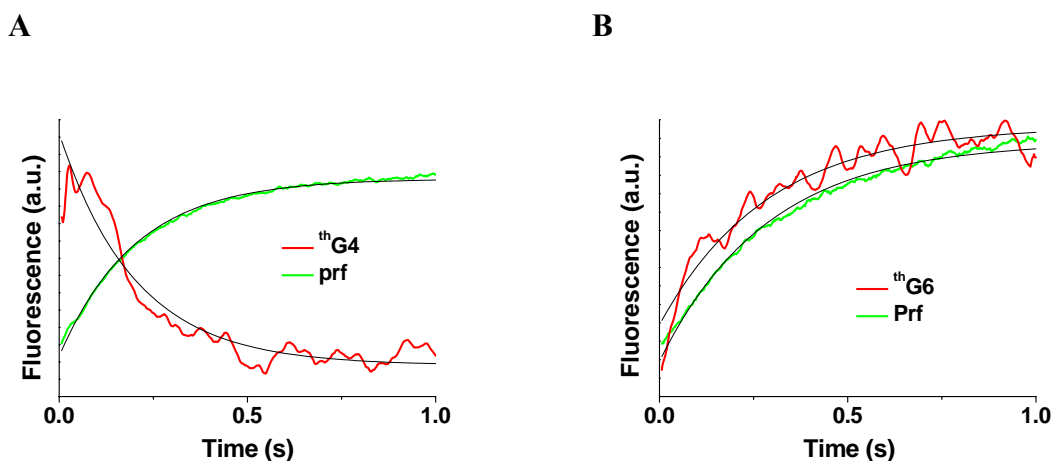


Figure 5.11. Kinetics of POST complex formation of $^{\text{th}}\text{G}$ -containing mRNAs. Fluorescence changes on rapid mixing of PRE complexes ($0.1 \mu\text{M}$) programmed with $^{\text{th}}\text{G}$ -containing mRNAs (black) and EF-G-GTP ($2 \mu\text{M}$) compared with fluorescence changes of fMetVal-tRNA $^{\text{Val}}$ (prf) (red), present as part of the PRE complex. *A.* $^{\text{th}}\text{G4}$; *B.* $^{\text{th}}\text{G6}$. Solid black lines are single exponential fits of both the $^{\text{th}}\text{G}$ and fMetVal-tRNA $^{\text{Val}}$ (prf) fluorescence intensity changes, with k_{app} of 4.7 ± 0.3 and $3.4 \pm 0.2 \text{ sec}^{-1}$ for $^{\text{th}}\text{G4}$ and $^{\text{th}}\text{G6}$, respectively. Average deviations are given for the two independent experiments.

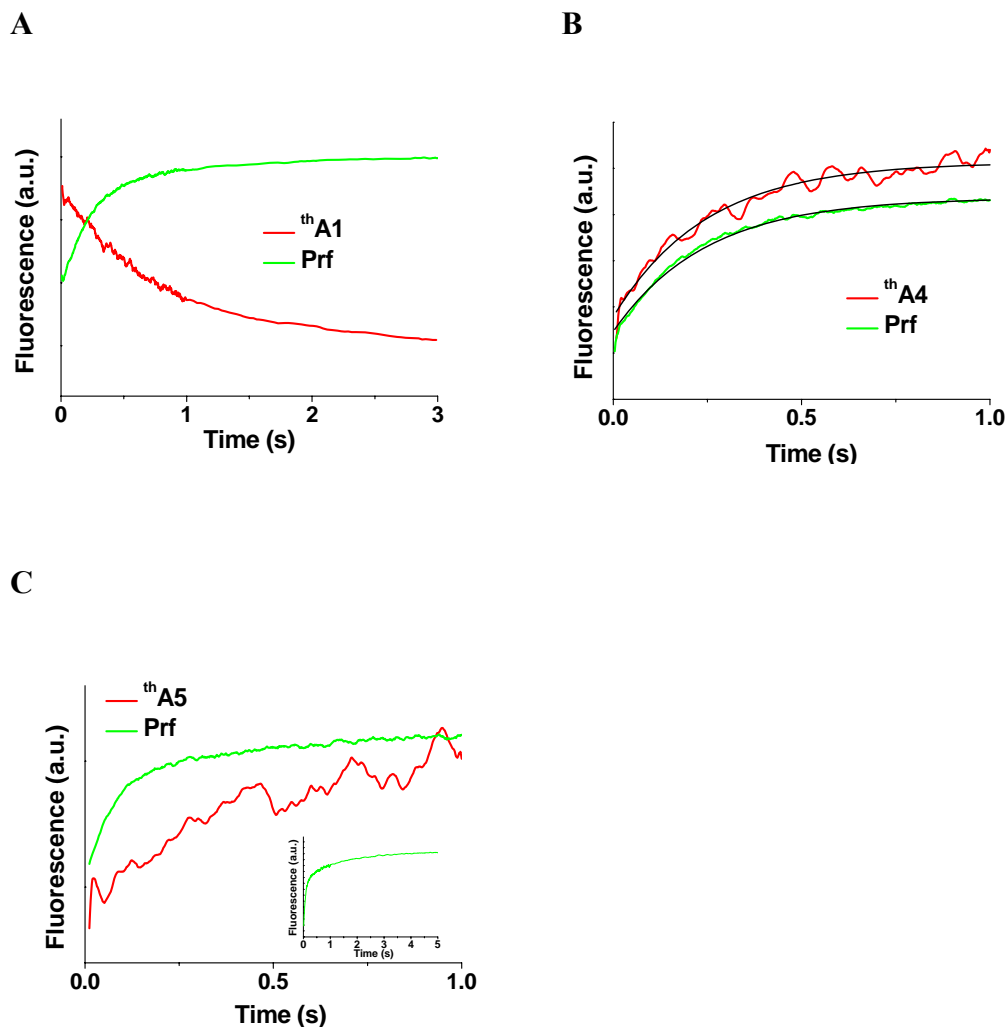


Figure 5.12. Kinetics of POST complex formation. Fluorescence changes on rapid mixing of PRE complexes ($0.1 \mu\text{M}$) programmed with thA-containing mRNAs (black) and EF-G:GTP ($2 \mu\text{M}$) compared with fluorescence changes of fMetLys-tRNA^{Lys}(prf) (red), present as part of the PRE complex. A. thA1; B. thA4; C. thA5. Solid black lines in B are single exponential fits of both the thA4 and fMetLys-tRNA^{Lys}(prf) fluorescence intensity changes, with k_{app} of $4.1 \pm 0.3 \text{ sec}^{-1}$. Average deviations are given for the two independent experiments.

APPENDIX I

MONITORING TRANSLATION WITH MODIFIED mRNAs STRATEGICALLY LABELED WITH ISOMORPHIC FLUORESCENT URIDINE AND CYTIDINE MIMETICS

I.1 Abstract

Here we examine three mRNAs, site-specifically modified at codon positions 2, 5, and 6 with new emissive and responsive isosteric nucleoside mimetics (thU and thC), with the goal of developing real time assays for monitoring translation-related events at nucleotide resolution. thU5 and thC6, but not thU2, form functional initiation (70SIC), pretranslocation (PRE) and posttranslocation (POST) complexes. Spectral differences are seen on conversion of 70SIC to PRE complexes and these differences allow measurement of the kinetics of such conversions by changes in the fluorescence of labeled mRNAs.

II.2 Introduction

Many of the studies directed toward understanding of the dynamics of ribosome function rely heavily on both ensemble and single molecule time-resolved observations made with functional, fluorescent-labeled derivatives of components of the protein synthesis machinery, for the most part including tRNAs, ribosomal proteins, and protein auxiliary factors such as EF-Tu and EF-G (Frank and Gonzalez, 2010; Pan et al., 2009; Chen et al., 2011a; Cooperman et al., 2011). Despite the central role of mRNA in protein synthesis, the use of fluorescent mRNAs has, by contrast, been quite limited, confined almost exclusively to mRNAs derivatized at the 3'-end with fluorophores that monitor the movement of this terminus to a position at the entrance of the mRNA channel during translocation (Savelsbergh et al., 2003; Studer

et al., 2003; Liu et al., 2010; Cunha et al., 2013).

In Chapter V, we describe the preparation of functional mRNAs containing emissive and responsive thGuanosine (thG) or thAdenosine (thA) mimetic based on thieno[3,4-d]pyrimidine, within the initiation or the first elongation codon. The fluorescence changes of these mRNAs permit monitoring of the conversion of a 70SIC first to a pretranslocation (PRE) complex, and a specific step corresponding to codon:anticodon-loop base pair formation was identified (Liu et al., 2013). thG and thA are isosteric with the nucleoside being mimicked; however, thUridine (thU) and thCytosine (thC) have the effect of converting pyrimidines into isosteres of purines (Shin et al., 2011). Here, we describe the preliminary characterization of three mRNAs containing emissive and responsive thU or thC within the initiation or the first elongation codon. Our results show that mRNAs carrying an thU or thC substitution within the second codon are functional in 70SIC, PRE or POST complex formation. The fluorescence changes of these two mRNAs during conversion of 70SIC to PRE complexes can be used to monitor codon:anticodon base pairing.

I.3 Results

I.3.1 Modified mRNAs

Three short mRNAs containing a single thU or thC within the AUG initiation codon or the following codon were prepared, and named as thU2, thU5 and thC6, respectively, according to the positions of the modification at the middle position of initiation

codon, or middle, and 3'-positions of the second codon (Figure I.1). All these mRNAs encode Phe at the second codon position. An additional mRNA MFTI containing no modified nucleotides was also prepared.

I.3.2 Formation of functional initiation and elongation complexes

Modified mRNAs were tested for their activities in different stages of translation: 70S initiation complex (70SIC) formation (Figure I.2A), as measured by fMet-tRNA^{fMet} co-sedimentation with a 70S ribosome; pretranslocation (PRE) complex formation (Figure I.2B), as measured by Phe-tRNA^{Phe} co-sedimentation with a 70SIC; and EF-G.GTP dependent translocation (Figure I.2C), as measured by fMet-Phe-puro formation. The results in Figure I.2 demonstrate that substantial functionality is retained on nucleoside mimetic substitution at positions 5 or 6 (thU5 and thC6). The thU substitution at the middle position of AUG codon (thU2) abolishes fMet-tRNA^{fMet} binding to the ribosome. Therefore, thU2 was not used in following studies.

I.3.3 Fluorescence changes on functional complex formation

thU and thC are both ideally emissive and responsive fluorescent nucleoside mimetics with the same quantum yields of 0.41 (Shin et al., 2011). Although incorporation into oligonucleotides generally lowers the quantum yield of emissive nucleosides (Sinkeldam et al., 2010), we anticipated that modified oligonucleotides

shown in Figure I.1 would retain a high level of responsiveness that would allow one to monitor mRNA binding and movement and subtle environmental changes within the ribosome during the elongation cycle. Excitation wavelength was chosen for thU5 (320 nm) and thC6 (340 nm) by comparing their maximum emission intensity at different excitation wavelength, to obtain the high emission intensity and minimize the background fluorescence from the ribosome (Figure I.3).

Conversion of 70SIC to PRE complex via addition of cognate EF-Tu.GTP.aminoacyl-tRNA ternary complex (EF-Tu.GTP.aa-tRNA, denoted TC) results in Watson-Crick base pairing of the thU or thC present in the first elongator tRNA codon, so that observed changes reflect both generalized environmental effects of converting a 70SIC into the first PRE complex and the specific effects of codon:anticodon H-bonding at the A-site. Conversion of thU5- or thC6-programmed 70SIC to PRE complex proceeds with a small decrease and a large increase in fluorescence intensity, respectively. Such fluorescence changes allow us to monitor changes in the microenvironments of specific codon nucleotides at the decoding center during the first cycle of polypeptide elongation.

I.3.4 Kinetics of PRE complex formation

Earlier work showed that fMet-tRNA^{fMet}(prf) bound in the P-site monitors accommodation of aa-tRNA^{aa} within the ribosome in an essentially single-phase reaction (Pan et al., 2008). Rates of fluorescence change of thU5- and

thC6-programmed ribosomes on PRE complex formation were determined using unlabeled fMet-tRNA^{fMet} and unlabeled aa-tRNA, or fMet-tRNA^{fMet}(prf) and unlabeled aa-tRNA (Table I.1; Figure I.5). In the latter experiments, parallel measurements were made for the rates of fMet-tRNA^{fMet}(prf) fluorescence change. Rates of fMet-tRNA^{fMet}(prf) fluorescence change were also determined when MFTI were substituted. Change of thC6 fluorescence was somewhat slower than that of thG6 and thA6 (see Chapter V), and tRNA accommodation measured by fMet-tRNA^{fMet}(prf) was slowed down by ~2 fold compared with unmodified MFTI mRNA. Similar to thG5 and thA5, thU substitution at the middle position of first elongation codon led to a decrease for both k_{app2} and k_{app3} compared with thC6.

I.4 Experimental

Modified mRNAs are kind gifts from Prof. Yitzhak Tor (University of California, San Diego). Functionality of mRNAs in 70SIC, PRE or POST complexes formation was tested using the same procedures as thG4 or thG6 (Section 2.2.5.2). Fluorescence experiments were performed using similar procedures to thG4 or thG6 (Section 2.2.6) with some modifications. thU5 was excited at 320 nm and fluorescence signal was collected using a 410 ± 10 nm filter. thC6 was excited at 320 nm and fluorescence signal was collected using a 410 ± 10 nm filter. Static fluorescence intensity measurements were performed using purified 70SIC and purified PRE complexes at the same concentration for both thU5 and thC6.

I.5 Conclusions

Herein we report the preliminary data showing that mRNAs containing emissive nucleoside mimetics (thU or thC) can form functional ribosomal complexes and are effective probes of codon:anticodon interaction at the ribosomal decoding center.

Table I.1. Apparent rate constants for reactions between 70SIC programmed with thU- and thC-containing mRNAs and TC^a.

mRNA	fMet-tRNA ^{fMet}	aa-tRNA	k_{app2}^b	k_{app3}^c
th U5	prf	Phe	3.2	1.0
	unlabeled	Phe	2.6	–
th C6	prf	Phe	6.7	0.67
	unlabeled	Phe	6.1	–
MFT	prf	Phe	–	2.7 ± 0.1

^aValues presented are mostly results from one independent determinations, except for MFT with fMet-tRNA^{fMet}(prf) and Phe-tRNA^{Phe}, which is average ± average deviation from two independent determinations; Values are fits of stopped-flow data to single exponentials [k_{app2} (thU or thC fluorescence changes) and k_{app3} (tRNA^{fMet}(prf) fluorescence changes)]. For thU5 and thC6, rates in the first and second rows were determined, respectively, in the presence of aa-tRNA and fMet-tRNA^{fMet}(prf) or aa-tRNA and fMet-tRNA^{fMet}. For MFT, rate was determined in the presence of: aa-tRNA and fMet-tRNA^{fMet}(prf).

^bthU and thC fluorescence change: upper, in presence of fMet-tRNA^{fMet}(prf); lower, in presence of unlabeled tRNAs.

^cfMet-tRNA^{fMet}(prf) fluorescence change.

th U2		+2							
UUA	AUA	AGG	AUA	CAU	ACU	<u>AUG</u>	UUC	UUC	CGU
						fMet	Phe	Phe	Arg
th U5:						+5			
UUA	AUA	AGG	AUA	CAU	ACU	<u>AUG</u>	<u>UUC</u>	UUC	CGU
						fMet	Phe	Phe	Arg
th C6:						+6			
UUA	AUA	AGG	AUA	CAU	ACU	<u>AUG</u>	UUC	<u>UUC</u>	CGU
						fMet	Phe	Phe	Arg

Figure I.1. mRNAs labeled with isomorphous fluorescent nucleoside mimetics. Modification positions are shown in red.

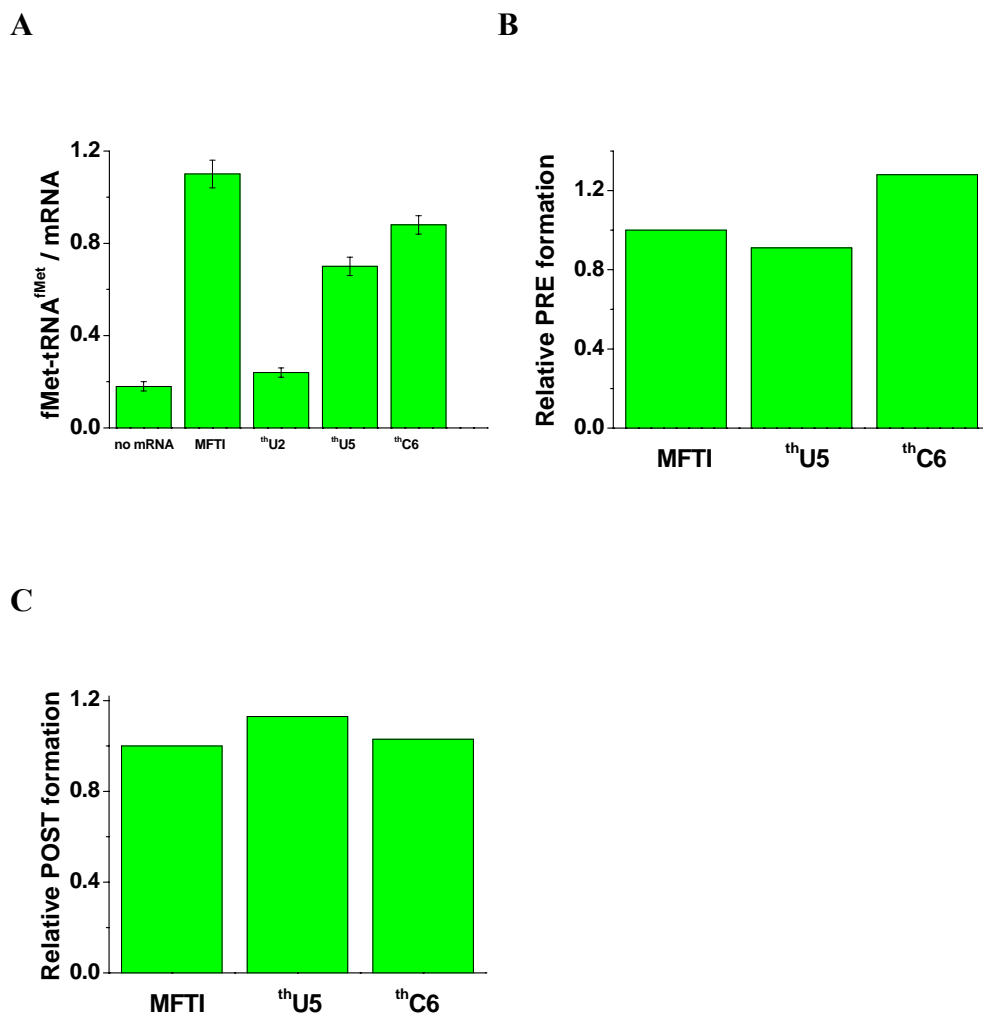


Figure I.2. Activities of mRNAs containing thU or thC. *A.* 70SIC formation, measured as fMet-tRNA^{fMet} co-sedimented per mRNA added: ribosomes, 1.0 μM, mRNA 0.5 μM. *B.* Normalized PRE complex formation, with background in the absence of mRNA subtracted: ribosomes, 0.8 μM. *C.* Normalized POST complex formation. Ribosomes, 2 μM. Control experiments were performed, as indicated, with either no added mRNA, or with added unmodified mRNA, or with no added EF-G. Values reported in *C* were after subtraction of background obtained with no mRNA and normalized to the value obtained for unmodified mRNA. Values reported in *C* were obtained from Equations 2.2A and normalized to the value obtained for unmodified mRNA.

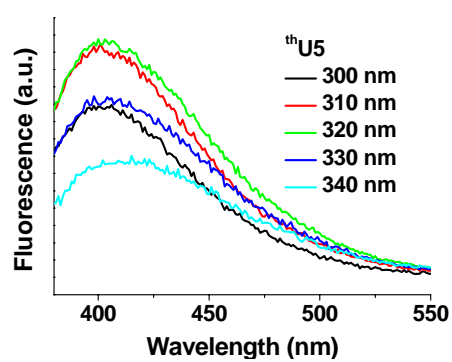
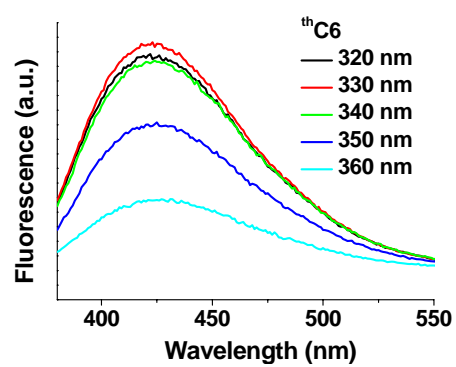
A**B**

Figure I.3. Determination of excitation wavelength for ³HU- or ³HC-containing mRNAs. Emission spectra of free ³HU5 (A) or ³HC6 (B) mRNAs (0.8 μ M) were recorded at different excitation wavelength. Background fluorescence from the buffer used was subtracted at each excitation wavelength.

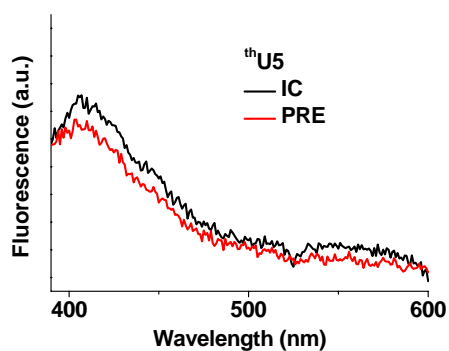
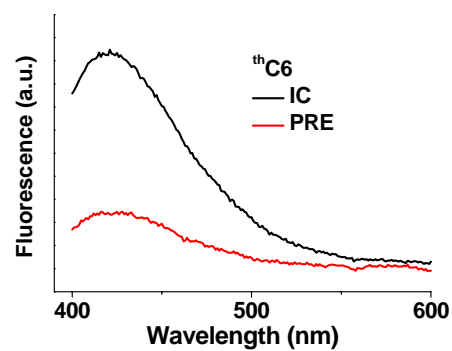
A**B**

Figure I.4. Fluorescence changes of ³H- and ³H-C-containing mRNAs. *A–B.* Traces are shown for 70SIC (black) and PRE complex (red). Both 70SIC and PRE complex traces are for purified samples. Background fluorescence of the corresponding purified complex made with unlabeled mRNA was subtracted from the observed fluorescence of each of the labeled ribosome complexes.

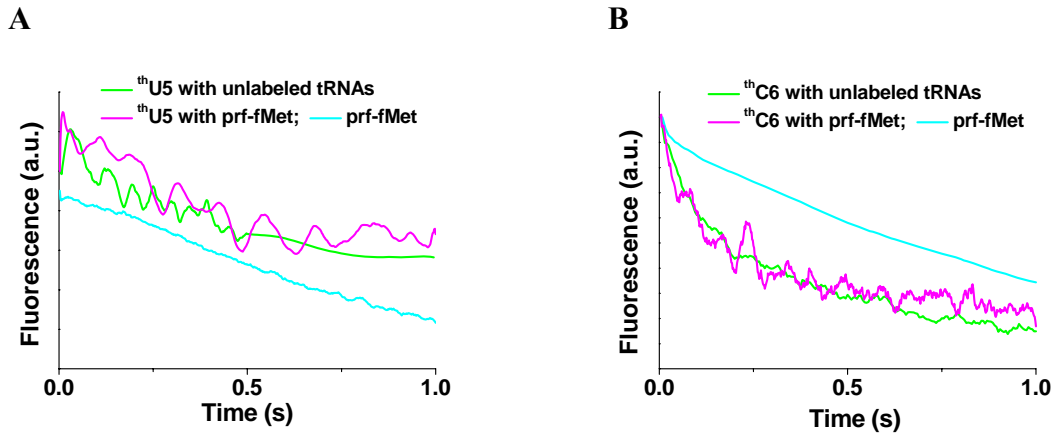


Figure I.5. Kinetics of PRE complex formation of thU- and thC-containing mRNAs. Fluorescence changes on rapid mixing of 70SICs (0.1 μ M) programmed with thU- or thC-containing mRNAs and cognate TCs (0.4 μ M) compared with fluorescence changes of fMet-tRNA^{fMet}(prf) (cyan), present as part of the 70SIC. Rates of thU or thC fluorescence change were determined using either unlabeled fMet-tRNA^{fMet} and unlabeled aa-tRNA (green), or fMet-tRNA^{fMet}(prf) and unlabeled aa-tRNA (magenta). A. thU5; B. thC6.

APPENDIX II

RIBOSOME LABELING WITH GOLD PARTICLE FOR

TRANSLATION IMAGING

II.1 Abstract

Nanoparticles have great potentials in translation imaging. Here we present preliminary results to show that ribosomal protein L1 can be specifically labeled with an Au particle. The reconstituted 70S ribosome containing Au labeled L1 is partially functional in peptide synthesis.

II.2. Introduction

Protein synthesis takes place on the ribosome. Currently, most of our understandings of the kinetics of ribosomal translation heavily relies on labeling of the ribosome, translation factors and/or tRNAs with organic fluorophores, using them for both ensemble and single molecule studies (Frank and Gonzalez, 2010; Pan et al., 2009; Chen et al., 2011a; Cooperman et al., 2011). Compared with ensemble strategy, single molecule FRET (Fluorescence Resonance Energy Transfer) method overcomes both time- and sample-dependent heterogeneity problems, and promises detection of short-lived, but functionally essential intermediates (Marshall et al., 2008; Perez and Gonzalez Jr, 2011). However, single molecule fluorescence techniques have suffered significantly from numerous requirements imposed on the probes, especially the fast photobleaching of organic dyes. Nanoparticles are ideal candidates to overcome such a limitation due to their high quantum yield, photostability and tunable absorption and emission (Gao et al., 2005; Chang and Rosenthal, 2013). Although nanoparticles have

recently been extensively used as fluorescent probes or FRET donor or acceptor in single molecule experiments (Grecco et al., 2004; Vale, 2008), only sparse attention has been paid to the ribosome translation apparatus [e.g., an Au particle was used to label L7/L12 protein on prokaryotic ribosome (Montesano-Roditis et al., 2001)]. Here it is shown that i) ribosomal protein L1 can be specifically labeled with an Au particle; ii) the L1 derivative is competent in L1 uptake by a mutant 50S ribosome subunit lacking L1; and iii) the reconstituted 70S ribosome maintains at least part of its translation function in an *in vitro* peptide synthesis system.

II.3. Results

II.3.1 L1 labeling with Au particle

The Au particle used here has a uniform diameter of 1.4 nm and molecular weight of 15 kD, bearing one maleimide group per particle on average. Mutant L1(S40C) was incubated with 2-fold excess of Au particle. After quenching of free Au particle with glutathione, the reaction mixture was analyzed by SDS-PAGE with two gels running in parallel. One gel was silver stained, which detect any protein or Au particle; and the second gel was stained by LI Silver Stain Plus kit, which only detects Au particles. Besides the band for L1(S40C) (~ 31 kD), which is only observed on the gel stained by silver, two bands around ~34–36 kD and one band at ~68 kD were observable on the gel stained by both silver and LI silver (Figure II.1). The two bands at 34–36 kD were assumed to be the Au:L1(S40C) conjugate in 1:1 ratio, and the two

resolved bands and their apparent molecular weight lower than expected (~ 46 kD) were probably because of the relative conformation of Au particle and L1(S40C) protein within the conjugate. The higher band at ~68 kD was assumed to be the Au:L1(S40C) conjugate in 1:2 ratio, resulting from a small amount of Au particle carrying two maleimide groups. In a control experiment incubating Au particle with wild type L1 [Au:L1(WT)], the resulting mixture showed bands located at 31, 34 and 64 kD on the gel stained by silver, but these bands disappeared (64 kD) or became much weaker (31 and 34 kD) on the gel stained by LI silver (Figure II.1), which may result from non-specific binding of Au particle to wild type L1 protein. These results demonstrated that ribosomal protein L1 can be specifically and stoichiometrically labeled with Au particle [L1(S40C)^{Au}] via cysteine-maleimide chemistry.

II.3.2 Reconstitution of functional 50S ribosome

Reconstitution of intact 50S subunit was performed by incubating 50S mutant lacking L1 (50S^{-L1}) with either L1(S40C)^{Au} conjugate or Au:L1(WT) mixture. The resulting 50S was purified by centrifugation through sucrose cushion, and the re-suspended 50S was analyzed on SDS-PAGE gel and stained by LI silver (Figure II.2). It was shown that L1(S40C)^{Au} can be specifically uptaken by 50S^{-L1}, even in competition with unlabeled L1(S40C). The labeling efficiency of 50S by Au (50S^{Au}) was estimated to be roughly 50% by comparing the band intensity with a “standard curve” made on the same gel using free Au (Figure II.3).

Labeled 70S ribosome by Au ($70S^{Au}$) was prepared by incubating reconstituted $50S^{Au}$ with stoichiometric 30S subunit, and the functionality of $70S^{Au}$ was evaluated in a poly(U) dependent poly(Phe) synthesis assay (Pan et al., 2009). The results in Figure II.4 showed that the activity of reconstituted $70S^{Au}$ was comparable with 70S reconstituted from 30S and unlabeled 50S subunit, and both of them are somewhat less active than intact 70S ribosome.

II.4 Experimental

The following materials were purchased from the indicated suppliers: glutathione (Sigma); Silver Stain Plus kit (Bio-Rad); LI Silver Stain kit (Nanoprobes); Nanogold monomaleimide (Invitrogen). Yeast tRNA^{Phe} was aminoacylated and AcPhe-tRNA^{Phe} was prepared as in Section 2.2.4.

II.4.1 Purification of L1 variants

Overexpression and purification of L1 variants were based on the published procedures (Stevens et al., 2012). BL21(DE3) competent cell, transformed with pET16b plasmids carrying wild type or S40C mutant L1, was grown in S.O.C. medium at 37 °C for one hour. The cell culture was plated onto LB-Agar plate with 100 µg/ml of ampicillin and grown overnight at 37 °C. Single colony on the plate was inoculated into 6 ml of LB medium with 100 µg/ml of ampicillin for overnight growth at 37 °C. Then the cell culture was transferred into 1 L of LB medium with 100 µg/ml

of ampicillin for growth until A_{260} reached $\sim 0.6\text{--}0.8$. Protein expression was started by addition of 1 mM IPTG and lasted overnight at 37 °C.

Harvested cells were resuspended in 30 ml of L1 equilibration buffer (50 mM NaH_2PO_4 pH 7.0, 300 mM NaCl) and incubated at room temperature for 30 min after addition of lysozyme (0.75 mg/ml). Cell was broken by French press twice (12,000–14,000 psi) and centrifuged (4 °C, 20k rpm with SS34 rotor, 20 min) to remove the cell debris. The supernatant was mixed with 6 ml of Co(II)-Sephrose (Talon) resin, pre-washed with 30 ml of L1 equilibration buffer, and shaken at 4 °C for 1 hour. Resins bound with L1 were pulled down by centrifugation (4 °C, 700 xg, 5 min), washed twice with 30 ml of L1 equilibration buffer, and transferred to a small gravity small column (18 mm in diameter). The column was washed with 30 ml of L1 equilibration buffer, and L1 was eluted using L1 equilibration buffer with a imidazole gradient (25 mM, 2 ml; 50 mM, 2 ml; 100 mM, 2 ml; 150 mM, 5 ml; 300 mM, 10 ml). Fractions containing L1 were confirmed by 12% SDS-PAGE and pooled for dialysis at 4 °C, first against buffer A (50 mM Tris-HCl pH 7.5, 70 mM NH_4Cl , 30 mM KCl, 7 mM MgCl_2 and 1 mM DTT) without MgCl_2 overnight and then against buffer A for 3 hours with MgCl_2 . L1 was concentrated using Amicon Ultra ultrafiltration units (MWCO: 10,000) and protein concentration was determined by Bradford assay.

II.4.2 Labeling of L1(S40C) and the 50S subunit with Au particle

L1(S40C) or wild type L1 (7 μM after exchange) was exchanged into L1

labeling buffer (20 mM NaH₂PO₄ pH 7.0, 150 mM NaCl, 1 mM EDTA) using NAP-5 column (bed volume 0.5 ml), mixed with equal volume of Au particle (21 μM) freshly dissolved in 20% DMSO, and incubated at room temperature for 2 hours in the presence of 1 mM of TCEP. Reaction was stopped by adding 1 mM of glutathione to quench all free Au particles. The samples were directly loaded onto gel or further used without any purification.

50S mutant lacking L1 (50S^{-L1}) and 30S subunit were prepared as previously described (Subramanian and Dabbs, 1980). To make reconstituted Au labeled 50S subunit (50S^{Au}), L1(S40C)^{Au} was incubated with 50S^{-L1} in 100 μl of 50S reconstitution buffer (10 mM Tris-HCl pH 7.5, 150 mM NH₄Cl, 8 mM MgCl₂, 5 mM 2-mercaptoethanol) (see Figure II.2 for amounts of the 50S subunit and L1 used) at room temperature for 1 hour. Reconstituted 50S subunit was purified by centrifugation through a sucrose cushion in 50S sucrose cushion buffer (10 mM Tris-HCl pH 7.5, 30 mM NH₄Cl, 10 mM MgCl₂, 5 mM 2-mercaptoethanol, 1.1 M sucrose) (SORVALL S120-AT2 rotor, 110K rpm, 40 min, 4 °C), and the pellets were resuspended in 50S resuspension buffer (10 mM Tris-HCl pH 7.5, 100 mM NH₄Cl, 10 mM MgCl₂, 5 mM 2-mercaptoethanol).

II.4.3 Activity of Au labeled ribosome in poly(Phe) synthesis

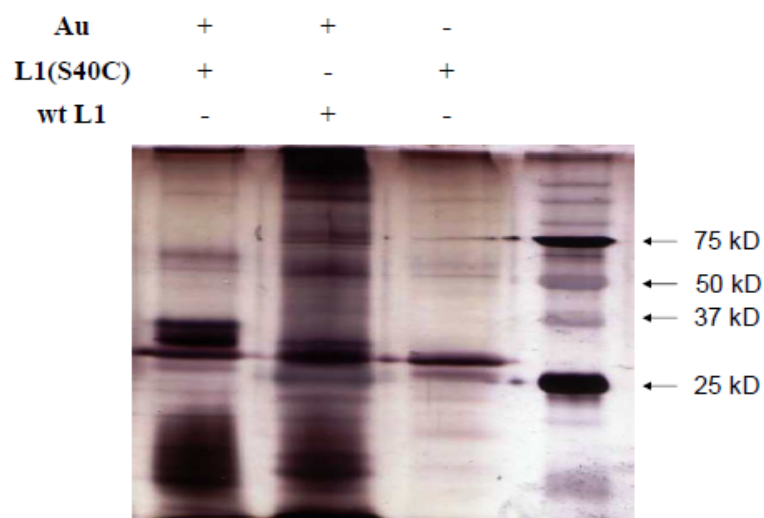
The poly(Phe) assay was carried out in buffer C (20 mM Tris-HCl pH 7.6, 200 mM NH₄Cl, 10 mM MgAc₂). All concentrations below are final concentrations after

mixing. 70S ribosome was prepared by incubating equal amounts of 50S and 30S subunits at 30 °C for 30 min. Initiation mixture was prepared by mixing 70S ribosome (0.3 μM, based on 50S or 30S subunits), poly(U) (0.3 g/L) and [³H]-AcPhe-tRNA^{Phe} (0.36 μM), and incubated at 30 °C for 30 min. Poly(Phe) synthesis was started by adding 2-mercaptoethanol (3 mM), PEP (0.4 mM), PK (4 mg/L), GTP (0.5 mM), [³H]-Phe-tRNA^{Phe} (3.6 μM) and EF-G (0.5 μM), and performed by incubating at 30 °C. Fractions (3.5 μl) were aliquoted out at different time points (0, 0.7, 2, 8, 30, 60 and 120 min), quenched with 0.3 mL of 5% TCA, and heated to 95 °C for 15 min. Filter binding was performed using a nitrocellulose filter followed by three washes with chilled 5% TCA, and the radioactivity of [³H]-Phe-tRNA^{Phe} was determined.

II.5 Conclusions

Here we report the specific and stoichiometric labeling of ribosome protein L1 with Au nanoparticle. L1(S40C)^{Au} was competent in binding to the 50S subunit, and partial activity is retained for reconstituted 70S^{Au} in *in vitro* peptide synthesis assay.

A



B

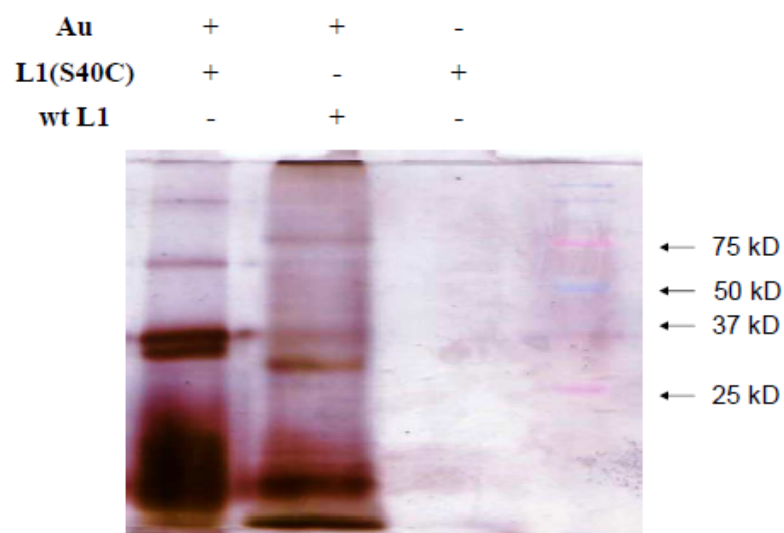
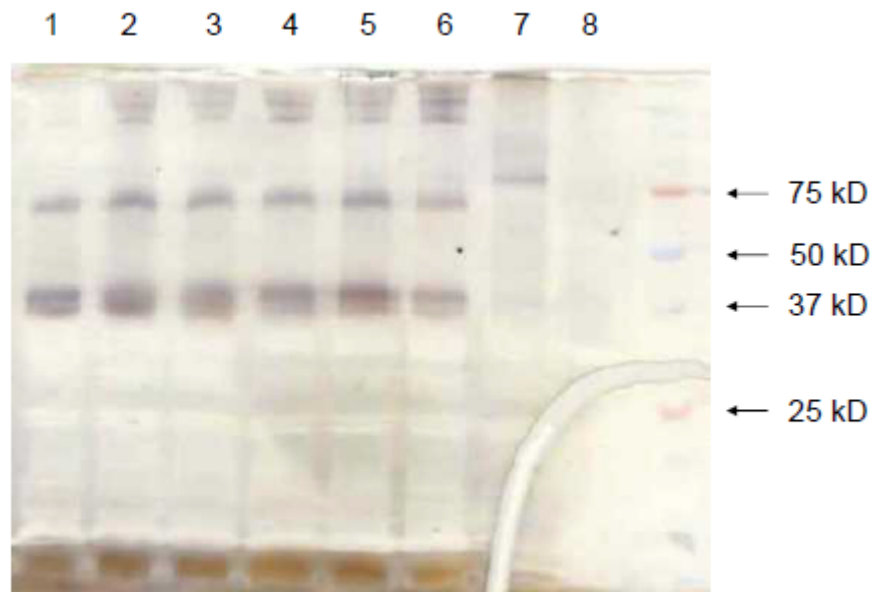


Figure II.1. Specific and stoichiometric labeling of L1 with Au nanoparticle. Au particle was incubated with either mutant L1(S40C) or wild type L1. The resulting mixtures [L1(S40C)^{Au} and Au:L1(WT), respectively] were analyzed by SDS-PAGE stained by either silver (A) or LI silver (B).



Lane	1	2	3	4	5	6	7	8
L1(S40C)^{Au}	270 pmol	270 pmol	270 pmol	270 pmol	180 pmol	120 pmol	—	—
Au:L1(WT)	—	—	—	—	—	—	270 pmol	—
L1(S40C)	—	—	100 pmol	200 pmol	90 pmol	150 pmol	—	+
50S^{-L1}	—	80 pmol	80 pmol	80 pmol	80 pmol	80 pmol	80 pmol	—
50S	80 pmol	—	—	—	—	—	—	—

Figure II.2. Reconstitution of 50S^{Au} from L1(S40C)^{Au}. L1(S40C)^{Au} or Au:L1(WT) was incubated in the presence of 50S^{-L1} or intact 50S. Unlabeled L1(S40C) was used as a reconstitution competitor for L1(S40C)^{Au} as indicated. The samples loaded onto each lane were listed in the table. The gel was stained by LI silver, which is specific for Au particle.

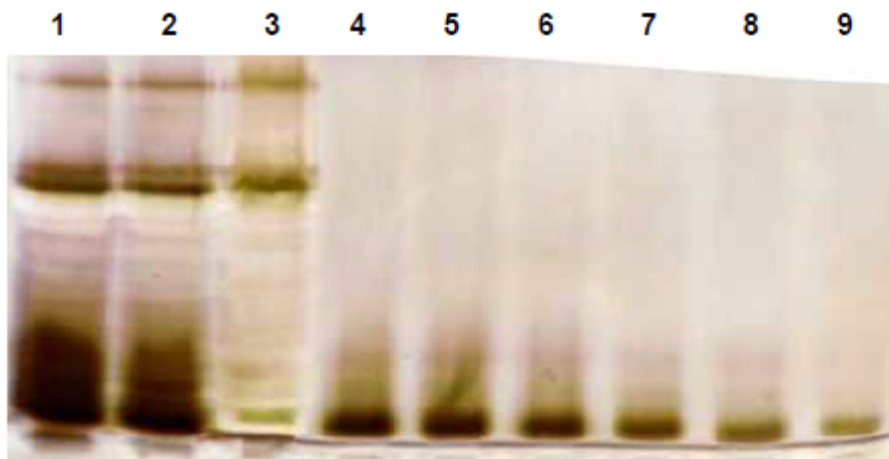


Figure II.3. Semi-quantifying of $50S^{Au}$ labeling efficiency. Samples loaded onto SDS-PAGE gel were: Lane 1, $L1(S40C)^{Au}$, 80 pmol; Lane 2, $L1(S40C)^{Au}$, 60 pmol; Lane 5, $50S^{Au}$, 43 pmol; Lane 4–9, Au particle (60, 50, 40, 30, 20, 10 pmol, respectively). The gel was stained by LI silver.

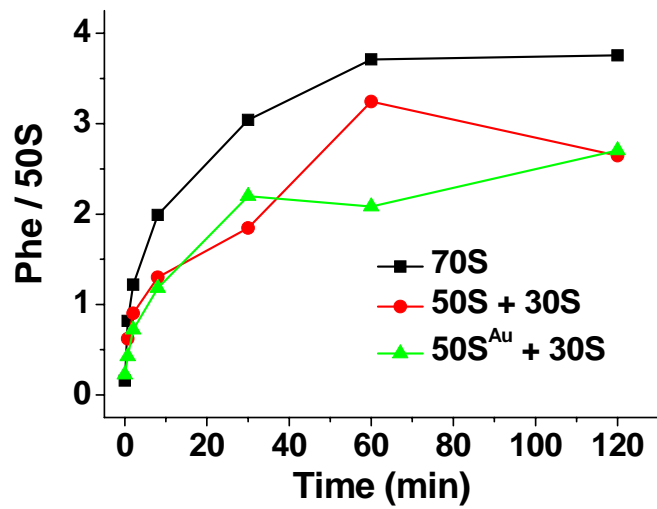


Figure II.4. Function of Au labeled ribosome subunit in peptide synthesis. Poly(U) dependent poly(Phe) synthesis was measured, as a function of time, for wild type 70S (black), reconstituted 70S from wild type 50S and wild type 30S (red), and reconstituted 70S^{Au} from 50S^{Au} and wild type 30S.

BIBLIOGRAPHY

Agirrezabala, X., Schreiner, E., Trabuco, L. G., Lei, J., Ortiz-Meoz, R. F., Schulten, K., Green, R., and Frank, J. (2012). Structural insights into cognate versus near-cognate discrimination during decoding. *EMBO J* 30, 1497–1507.

Aitken, C. E., and Puglisi, J. D. (2010). Following the intersubunit conformation of the ribosome during translation in real time. *Nat Struct Mol Biol* 17, 793–800.

Allen, G. S., Zavialov, A., Gursky, R., Ehrenberg, M., and Frank, J. (2005) The cryo-EM structure of a translation initiation complex from *Escherichia coli*. *Cell* 121, 703–712.

Anborgh, P. H., Parmeggiani, A., and Jonak, J. (1992). Site-directed mutagenesis of elongation factor Tu. The function and structure role of residue Cys 81. *Eur J Biochem* 208, 251–257.

Ban, N., Nissen, P., Hansen, J., Moore, P. B., and Steitz, T. A. (2000). The complete atomic structure of the large ribosomal subunit at 2.4 Å resolution. *Science* 289, 905–920.

Bilgin, N., and Ehrenberg, M. (1995). Stoichiometry for the elongation factor Tu:aminoacyl-tRNA complex switches with temperature. *Biochemistry* 34, 715–719.

Blanchard, S. C., Gonzalez Jr, R. L., Kim, H. D., Chu, S., and Puglisi, J. D. (2004). tRNA selection and kinetic proofreading in translation. *Nat Struct Mol Biol* 11, 1008–1014.

Boelens, R., and Gualerzi, C. O. (2002). Structure and function of bacterial initiation factors. *Curr Protein Pept Sci* 3, 107–119.

Bouadloun, F., Donner, D., and Kurland, C. G. (1983). Codon specific missense errors *in vivo*. *EMBO J* 2, 1351–1356.

Bradford, M. M. (1976). Rapid and sensitive method for the quantitation of microgram quantities of protein utilizing the principle of protein-dye binding. *Anal Biochem* 72, 248–254.

Brierley, I., and Dos Ramos, F. J. (2006). Programmed ribosomal frameshifting in HIV-1 and the SARS-CoV. *Virus Res* 119, 29–42.

Canonaco, M. A., Calogero, R. A., and Gualerzi, C. O. (1986). Mechanism of translational initiation in prokaryotes. Evidence for a direct effect of IF2 on the activity of the 30 S ribosomal subunit. *FEBS Lett* 207, 198–204.

Cetin, R., Anborgh, P. H., Cool, R. H., and Parmeggiani, A. (1998). Functional role of the noncatalytic domains of elongation factor Tu in the interactions with ligands. *Biochemistry* 37, 486–495.

Chang, J. C., and Rosenthal, S. J. (2013). Quantum-dot based single-molecule microscopy for the study of protein dynamics. *Methods Mol Biol* 1026, 71–84.

Chen, C., Stevens, B., Kaur, J., Cabral, D., Liu, H., Wang, Y., Zhang, H., Rosenblum, G., Smilansky, Z., Goldman, Y. E., and Cooperman, B. S. (2011a). Single-molecule fluorescence measurements of ribosomal translocation dynamics. *Mol Cell* 42, 367–377.

Chen, C., Stevens, B., Kaur, J., Smilansky, Z., Cooperman, B. S., and Goldman, Y. E. (2011b). Allosteric vs. spontaneous exit-site (E-site) tRNA dissociation early in protein synthesis. *Proc Natl Acad Sci USA* 108, 16980–16985.

Chen, C., Greenberg, M. J., Laakso, J. M., Ostap, E. M., Goldman, Y. E., and Shuman, H. (2012). Kinetic schemes for post-synchronized single molecule dynamics. *Biophys J* 102(6), L23–25.

Chiu, J., March, P. E., Lee, R., and Tillett, D. (2004). Site-directed, ligase-independent mutagenesis (SLIM): a single-tube methodology approaching 100% efficiency in 4 h. *Nucl Acid Res* 32, e174.

Cochella, L., and Green, R. (2005). An active role for tRNA in decoding beyond codon:anticodon pairing. *Science* 308, 1178–1180.

Cochella, L., Brunelle, J. L., and Green, R. (2007). Mutational analysis reveals two independent molecular requirements during transfer RNA selection on the ribosome. *Nat Struct Mol Biol* 14, 30–36.

Cooperman, B. S., Goldman, Y. E., Chen, C., Farrell, I., Kaur, J., Liu, H., Liu, W., Rosenblum, G., Smilansky, Z., Stevens, B., and Zhang, H. (2011). Mechanism and dynamics of the elongation cycle. In *Ribosomes: structure, function and dynamics* (Rodnina, M. V. et al., Eds.), pp339–348, SpringerWien, New York.

Crick, F. (1970). Central dogma of molecular biology. *Nature* 227, 561–563.

Cunha, C. E., Belardinelli, R., Peske, F., Holtkamp, W., Wintermeyer, W., and Rodnina, M. V. (2013). Dual use of GTP hydrolysis by elongation factor G on the ribosome. *Translation* 1, e24315.

Dale, T., Sanderson, L. E., and Uhlenbeck, O. C. (2004). The affinity of elongation factor Tu for an aminoacyl-tRNA is modulated by the esterified amino acid. *Biochemistry* 43, 6159–6166.

Demeshkina, N., Jenner, L., Westhof, E., Yusupov, M., and Yusupova, G. (2012). A new understanding of the decoding principle on the ribosome. *Nature* 484, 256–259.

Demeshkina, N., Jenner, L., Westhof, E., Yusupov, M., and Yusupova, G. (2013). New structural insights into the decoding mechanism: Translation infidelity via a G·U pair with Watson-Crick geometry. *FEBS Lett* 587, 1848–1857.

Demirci, H., Murphy, F. 4th, Murphy, E., Gregory, S. T., Dahlberg, A. E., and Jøgl, G. (2013). A structural basis for streptomycin-induced misreading of the genetic code.

Nat Commun 4, 1355.

Devaraj, A., Shoji, S., Holbrook, E. D., and Fredrick, K. (2009). A role for the 30S subunit E site in maintenance of translational reading frame. *RNA* 15, 255–265.

Dever, T.E., and Green, R. (2012). The elongation, termination, and recycling phases of translation in eukaryotes. *Cold Spring Harb Perspect Biol* 4, a013706.

Dinman, J. D. (2012). Control of gene expression by translational recoding. *Adv Protein Chem Struct Biol* 86, 129–149.

Dubnoff, J. S., and Marita, U. (1971). Isolation and properties of protein factors involved in polypeptide chain initiation in *Escherichia coli*. *Methods Enzymol* 20, 248–261.

Dunkle, J. A., Wang, L., Feldman, M. B., Pulk, A., Chen, V. B., Kapral, G. J., Noeske, J., Richardson, J. S., Blanchard, S. C., and Cate, J. H. D. (2011). Structure of the bacterial ribosome in classical and hybrid states of tRNA binding. *Science* 332, 981–984.

Edelmann, P., and Gallant, J. (1977). Mistranslation in *E. coli*. *Cell* 10, 131–137.

Ehrenberg, M., Rojas, A. –M., Weiser, J., and Kurland, C.G. (1990). How many EF-Tu molecules participate in aminoacyl-tRNA binding and peptide bond formation in *Escherichia coli* translation? *J Mol Biol* 211, 739–749.

Ermolenko, D. N., and Noller, H. F. (2011). mRNA translocation occurs during the second step of ribosomal intersubunit rotation. *Nat Struct Mol Biol* 18, 457–462.

Fei, J., Kosuri, P., MacDougall, D. D., and Gonzalez Jr., R. L. (2008). Coupling of ribosomal L1 stalk and tRNA dynamics during translation elongation. *Mol Cell* 30, 348–359.

Fischer, N., Konevega, A. L., Wintermeyer, W., Rodnina, M. V., and Stark, H. (2010). Ribosome dynamics and tRNA movement by time-resolve electron cryomicroscopy. *Nature* 466, 329–333.

Franckenberg, S., Becker, T., and Beckmann, R. (2012). Structural view on recycling of archaeal and eukaryotic ribosomes after canonical termination and ribosome rescue. *Curr Opin Struct Biol* 22, 786–796.

Frank, J., Zhu, J., Penczek, P., Li, Y., Srivastava, S., Verschoer, A., Radermacher, M., Grassucci, R., Lata, R. K., and Agrawal, R. K. (1995). A model of protein synthesis based on cryo-electron microscopy of the *E. coli* ribosome. *Nature* 376, 441–444.

Frank, J., and Agrawal, R.K. (2000). A ratchet-like inter-subunit reorganization of the ribosome during translocation. *Nature* 406, 318–322.

Frank, J. Jr, and Gonzalez, R.L. (2010). Structure and dynamics of a processive Brownian motor: the translating ribosome. *Annu Rev Biochem* 79, 381–412.

Freistroffer, D. V., Pavlov, M. Y., MacDougall, J., Buckingham, R. H., and Ehrenberg, M. (1997). Release factor RF3 in *E. coli* accelerates the dissociation of release factors RF1 and RF2 from the ribosome in a GTP dependent manner. *EMBO J* 16, 4126–4133.

Furano, A. (1975). Content of elongation factor Tu in *Escherichia coli*. *Proc Natl Acad Sci USA* 72, 4780–4784.

Gao, X. H., Yang, L. L., Petros, J. A., Marshal, F. F., Simons, J. W., and Nie, S. M.

(2005). *In vivo* molecular and cellular imaging with quantum dots. *Current Opinion in Biotechnology* 16, 63–72.

Gao, Y. –G., Selmer, M., Dunham, C. M., Weixlbaumer, A., Kelley, A. C., and Ramakrishnan, V. (2009). The structure of the ribosome with elongation factor G trapped in the posttranslocational state. *Science* 326, 694–600.

Gedik, M., and Brown, A. (2013). Computational study of the excited state properties of modified RNA nucleobases. *J PhotoChem Photobiol A* 259, 25–32.

Geggier, P., Dave, R., Feldman, M. B., Terry, D. S., Altman, R. B., Munro, J. B., and Blanchard, S. C. (2010). Conformational sampling of aminoacyl-tRNA during selection on the bacterial ribosome. *J Biol Chem* 399, 576–595.

Giedroc, D. P., and Cornish, P. V. (2009). Frameshifting RNA pseudoknots: structure and mechanism. *Virus Res* 139, 193–208.

Gonzalez, R. L., Chu, S., Puglisi, J. D. (2007). Thiostreton inhibition of tRNA delivery to the ribosome. *RNA* 13, 2091–2097.

Grecco, H. E., Lidke, K. A., Heintzmann, R., Lidke, D. S., Spagnuolo, C., Martinez, O. E., Jares-Erijman, E. A., and Jovin, T. M. (2004). Ensemble and single particle photophysical properties (Two-Photon excitation, anisotropy, FRET, lifetime, spectral conversion) of commercial quantum dots in solution and in live cells. *Microscopy Research and Technique* 65, 169–179.

Gregory, S. T., Carr, J. F., and Dahlberg, A. E. (2009). A signal relay between ribosomal protein S12 and elongation factor EF-Tu during decoding of mRNA. *RNA* 15, 208–214.

Grigoriadou, C., Marzi, S., Pan, D., Gualerzi, C. O., and Cooperman, B. S. (2007a). The translational fidelity function of IF3 during translation from the 30S initiation complex to the 70S initiation complex. *J Mol Biol* 373, 551–561.

Grigoriadou, C., Marzi, S., Kirillov, S., Gualerzi, C. O., and Cooperman, B. S. (2007b). A quantitative kinetic scheme for 70S initiation complex formation. *J Mol Biol* 373, 562–572.

Gromadski, K. B., and Rodnina, M. V. (2004a). Kinetic determinants of high-fidelity tRNA discrimination on the ribosome. *Mol Cell* 13, 191–200.

Gromadski, K. B., and Rodnina, M. V. (2004b). Streptomycin interferes with conformational coupling between codon recognition and GTPase activation on the ribosome. *Nat Struct Mol Biol* 11, 316–322.

Grunberg-Manago, M., Dessen, P., Pantaloni, D., Godefroy-Colburn, T., Wolfe, A. D., and Dondon, J. (1975). Light-scattering studies showing the effect of initiation factors on the reversible dissociation of *Escherichia coli* ribosomes. *J Mol Biol* 94, 461–478.

Gualerzi, C. O., and Pon, C. L. (1990). Initiation of mRNA translation in prokaryotes. *Biochemistry* 29, 5881–5889.

Gustilo, E. M., Vendeix, F. AP., and Agris, P. F. (2008). tRNA's modifications bring order to gene expression. *Curr Opin Microbiol* 11, 134–140.

Hauryliuk, V., Hansson, S., and Ehrenberg, M. (2008). Cofactor dependent conformational switching of GTPases. *Biophys J* 95, 1704–1715.

Hetrick, B., Lee, K., and Joseph, S. (2009). Kinetics of stop codon recognition by release factor 1. *Biochemistry* 48, 11178–11184.

Hirashima, A. and Kaji, A. (1973). Role of elongation factor G and a protein factor on the release of ribosome from messenger ribonucleic acid. *J Biol Chem* 248, 7580–7587.

Hirokawa, G., Iwakura, N., Kaji, A., and Kaji, H. (2008). The role of GTP in transient splitting of 70S ribosomes by RRF (ribosome recycling factor) and EF-G (elongation factor G). *Nucleic Acids Res* 36, 6676–6687.

Jenner, L., Demeshkina, N., Yusupova, G., and Yusupov, M. (2010). Structural rearrangements of the ribosome at the tRNA proofreading step. *Nat Struct Mol Biol* 7, 1072–1078.

Johansson, M., Zhang, J., and Ehrenberg, M. (2012). Genetic code translation displays a linear trade-off between efficiency and accuracy of tRNA selection. *Proc Natl Acad Sci USA* 109, 131–136.

Kaltschmidt, E., and Wittmann, H. G. (1970). Ribosomal proteins. XII. Number of proteins in small and large ribosomal subunits of *Escherichia coli* as determined by two-dimensional gel electrophoresis. *Proc Natl Acad Sci USA* 67, 1276–1282.

Karimi, R., Pavlov, M. Y., Buckingham, R. H., and Ehrenberg, M. (1999). Novel roles for classical factors at the interface between translation termination and initiation. *Mol Cell* 3, 601–609.

Kaur, J., Raj, M. & Cooperman, B. S. (2011). Fluorescent labeling of tRNA dihydrouridine residues: mechanism and distribution. *RNA*, 17, 1393–1400.

Kavaliauskas, D., Nissen, P., and Knudsen, C. R. (2012). The busiest of all ribosomal assistants: elongation factor Tu. *Biochemistry* 51, 2642–2651.

Kemkhadze, K. S., Odintsov, V. B., Semenov, Y. P., and Kirillov, S.V. (1981). *FEBS Lett* 125, 10–14.

Kjeldgaard, M., and Nyborg, J. (1992). Refined structure of elongation factor EF-Tu from *Escherichia coli*. *J Mol Biol* 23, 721–742.

Kornberg, R. D. (2007). The molecular basis of eucaryotic transcription. *Cell Death Differ* 14, 1989–1997.

Korostelev, A., Asahara, H., Lancaster, L., Laurberg, M., Hirschi, A., Zhu, J., Trakhanov, S., Scott, W. G., Noller, H. F. (2008). Crystal structure of a translation termination complex formed with release factor RF2. *Proc Natl Acad Sci USA* 105, 19684–19689.

Kothe, U., and Rodnina, M. V. (2006). Delayed release of inorganic phosphate from elongation factor Tu following GTP hydrolysis on the ribosome. *Biochemistry* 45, 12767–12774.

Kurland, C. G. (1979). Reading frame errors on ribosomes. In *Nonsense Mutations and Trna Suppressors* (Celis, J. E., and Smith, J.D., Eds.), pp.97–108, London: Academic Press.

Lagerkvist, U., and Waldenstrom, J. (1964). Structure and function of transfer RNA. I. Species specificity of transfer RNA from *E.coli* and yeast. *J Mol Biol* 8, 28–37.

Lake, J. A. (1976). Ribosome structure determined by electron microscopy of *Escherichia coli* small subunits, large subunits and monomeric ribosomes. *J Mol Biol* 105, 131–159.

Laurberg, M., Asahara, H., Korostelev, A., Zhu, J., Trakhanov, S., and Noller, H. F. (2008). Structural basis for translation termination on the 70S ribosome. *Nature* 454, 852–857.

Laurentiis, E. I. D., Mo, F., and Wieden, H. –J. (2011). Construction of a fully active Cys-less elongation factor Tu: Functional role of conserved cysteine 81. *Biochim Biophys Acta* 1814, 684–692.

Laursen, B. S., Sørensen, H. P., Mortensen, K. K., and Sperling-Petersen, H. U. (2005). Initiation of proteins synthesis in bacteria. *Microbio Mol Biol Rev* 69, 101–123.

Lee, T. –H., Blanchard, S. C., Kim, H. D., Puglisi, J. D., and Chu, S. (2007). The role of fluctuation in tRNA selection by the ribosome. *Proc Natl Acad Sci USA* 104, 13661–13665.

Lee, Y. S., and Dutta, A. (2009). MicroRNAs in cancer. *Annu Rev Pathol* 4, 199–227.

Liu, H., Pan, D., Pech, M., and Cooperman, B. S. (2010). Interrupted catalysis: the EF4 (LepA) effect on back-translocation. *J Mol Biol* 396, 1043–1052.

Liu, H., Chen, C., Zhang, H., Kaur, J., Goldman, Y. E., and Cooperman, B. S. (2011). The conserved protein EF4 (LepA) modulates the elongation cycle of protein synthesis. *Proc Natl Acad Sci USA* 108, 16223–16228.

Liu, W., Shin D., Tor, Y., and Cooperman, B. S. (2013). Monitoring translation with modified mRNAs strategically labeled with isomorphous fluorescent guanosine mimetic. *ACS Chem Biol* 8, 2017–2023.

Luirink, J., von Heijne, G., Houben, E., and de Gier, J.W. (2005). Biogenesis of inner membrane proteins in *Escherichia coli*. *Annu Rev Microbiol* 59, 329–355.

Marshall, R. A., Aitken, C. E., Dorywalska, M., and Puglisi, J. D. (2008). Translation at the single-molecule level. *Annu Rev Biochem* 77, 177–203.

Medintz, I. L., Goldman, E. R., Lassman, M. E., and Mauro, J. M. (2003). A fluorescence resonance energy transfer sensor based on maltose binding proteins. *Bioconjugate Chem* 14, 909–918.

Milón, P., Konevega, A. L., Gualerzi, C. O., and Rodnina, M. V. (2008). Kinetic checkpoint at a late step in translation initiation. *Mol Cell* 30, 712–720.

Milón, P., Maracci, C., Filonava, L., Gualerzi, C. O., and Rodnina, M. V. (2012). Real-time assembly landscape of bacterial 30S translation initiation complex. *Nat Struct Mol Biol* 19, 609–615.

Mishra, P. P., Qureshi, M. T., Ren, W., and Lee, T. -H. (2010). Codon-dependent tRNA fluctuations monitored with fluorescence polarization. *Biophys J* 99, 3849–3858.

Moazed, D., Samaha, R. R., Gualerzi, C., and Noller, H. F. (1995). Specific protection of 16 S rRNA by translational initiation factors. *J Mol Biol* 248, 207–210.

Montesano-Roditis, L., Glitz, D. G., Traut, R. R., and Stewart, P. L. (2001). Cryo-electron microscopic localization of protein L7/L12 within the *Escherichia coli* 70 S ribosome by difference mapping and nanogold labeling. *J Biol Chem* 276, 14117–14123.

Munro, J. B., Altman, R. B., O'Connor, N., and Blanchard, S. C. (2007). Identification of two distinct hybrid state intermediates on the ribosome. *Mol Cell* 35, 505–517.

Nishikura, K. (2006). Editor meets silencer: crosstalk between RNA editing and RNA interference. *Nat Rev Mol Cell Biol* 7, 919–931.

Nissen, P., Kjeldgaard, M., Thriup, S., Polekhina, G., Reshetnikova, L., Clark, B., and Nyborg, J. (1995). Crystal structure of the ternary complex of Phe-tRNA^{Phe}, EF-Tu and a GTP analog. *Science* 270, 1464–1472.

Nissen, P., Thriup, S., Kjeldgaard, M., and Nyborg, J. (1999). The crystal structure of Cys-tRNA^{Cys}-EF-Tu-GDPNP reveals general and specific features in the ternary complex and in tRNA. *Structure* 7, 143–156.

Ogle, J. M., Brodersen, D. E., Clemons W. M. Jr, Tarry, M. J., Carter, A. P., and Ramakrishnan, V. (2001). Recognition of cognate transfer RNA by the 30S ribosomal subunit. *Science* 292, 897–902.

Pan, D., Kirillov, S., Zhan, C., Hou, Y. & Cooperman, B. S. (2006). Rapid ribosomal translocation depends on the conserved 18-55 base pair in P-site transfer RNA. *Nat Struct. Mol Biol* 13, 354–359.

Pan, D., Kirillov, S. V., and Cooperman, B. S. (2007). Kinetically competent intermediates in the translocation step of protein synthesis. *Mol Cell* 25, 519–525.

Pan, D., Zhang, C., Kirillov, S., Hou, Y., and Cooperman, B. S. (2008). Perturbation of the tRNA tertiary core differentially affects specific steps of the elongation cycle. *J Biol Chem* 283, 18431–18440.

Pan, D., Qin, H., and Cooperman, B. S. (2009). Synthesis and functional activity of tRNAs labeled with fluorescent hydrazides in the D-loop. *RNA* 15, 346–354.

Pape, T., Wintermeyer, W., and Rodnina, M. V. (1998). Complete kinetic mechanism of elongation factor Tu-dependent binding of aminoacyl-tRNA to the A site of the *E. coli* ribosome. *EMBO J* 17, 7490–7497.

Pape, T., Wintermeyer, W., and Rodnina, M. V. (2000). Conformational switch in the decoding region of 16S rRNA during aminoacyl-tRNA selection on the ribosome. *Nat Struct Biol* 7, 104–107.

Perla-Kajan, J., Lin, X., Cooperman, B. S., Goldman, E., Jakubowski, H., Knudsen, C. R., and Mandeck, W. (2010). Properties of *Escherichia Coli* EF-Tu mutants designed for fluorescence resonance energy transfer from tRNA molecules. *Protein Eng Des Sel* 23, 129–136.

Perez, C. E., and Gonzalez Jr, R. L. (2011). *In vitro* and *in vivo* single-molecule fluorescence imaging of ribosome-catalyzed protein synthesis. *Curr Opin Chem Biol* 15, 1–11.

Polekhina, G., Thirup, S., Kjeldgaard, M., Nissen, P., Lippmann, C., and Nyborg, J. (1996). Helix unwinding in the effector region of elongation factor EF-Tu-GDP. *Structure* 4, 1141–1151.

Qin, H., Grigoriadou, C., and Cooperman, B. S. (2009). Interaction of IF2 with the ribosomal GTPase-associated center during 70S initiation complex formation. *Biochemistry* 48, 4699–4706.

Rodnina, M. V., Fricke, R., and Wintermeyer, W. (1994). Transient conformational states of aminoacyl-tRNA during ribosome binding catalyzed by elongation factor Tu. *Biochemistry* 33, 12267–12275.

Rodnina, M. V., and Wintermeyer, W. (1995a). GTP consumption of elongation factor Tu during translation of heteropolymeric mRNAs. *Proc Natl Acad Sci USA* 92, 1945–1949.

Rodnina, M. V., Fricke, R., Kuhn, L., and Wintermeyer, W. (1995b). Codon-dependent conformational change of elongation factor Tu preceding GTP hydrolysis on the ribosome. *EMBO J* 14, 2613–2619.

Rodnina, M.V., and Wintermeyer, W. (2011). The ribosome as a molecular machine: the mechanism of tRNA-mRNA movement in translocation. *Biochem Soc Trans* 39, 658–662.

Rosenblum, G., Chen, C., Kaur, J., Cui, X., Goldman, Y. E. & Cooperman, B. S. (2012). Real-time assay for testing components of protein synthesis. *Nucleic Acids Res* 40, e88.

Roy, R., Hohng, S., and Ha, T. (2008). A practical guide to single-molecule FRET. *Nat. Methods* 5, 507–516.

Sacerdot, C., Chiaruttini, C., Engst, K., Graffe, M., Milet, M., Mathy, N., Dondon, J., and Springer, M. (1996). The role of the AUU initiation codon in the negative feedback regulation of the gene for translation initiation factor IF3 in *Escherichia coli*. *Mol Microbio* 21, 331–346.

Sakakibara, Y., Abeysirigunawardena, S. C., Duc, A-C. E., Dremann, D. N., and Chow, C. S. (2012). Ligand- and pH-induced conformational change of RNA domain helix 69 revealed by 2-Aminopurine fluorescence. *Angew Chem Int Ed Engl* 51, 12095–12098.

Samanta, P. K., Manna, A. K., and Pati, S. K. (2012). Thieno analogues of RNA nucleosides: a detailed theoretical study. *J Phys Chem B* 116, 7618–7626.

Sanbonmatsu, K.Y. (2012). Computational studies of molecular machines: the ribosome. *Curr. Opin. Struct. Biol.* 22, 168–174.

Savelsbergh, A., Katunin, V.I., Mohr, D., Peske, F., Rodnina, M.V., and Wintermeyer, W. (2003). An elongation factor G-induced ribosome rearrangement precedes tRNA-mRNA translocation. *Mol Cell* 11, 1517–1523.

Schmeing, T. M., Voorhees, R. M., Kelley, A. C., Gao, Y, Murphy, F. V., Weir, J. R., and Ramakrishnan, V. (2009a). The crystal structure of the ribosome bound to EF-Tu and aminoacyl-tRNA. *Science* 326, 688–694.

Schmeing, T. M., and Ramakrishnan, V. (2009b). What recent ribosomal structures have revealed about the mechanism of translation. *Nature* 461, 1234–1242.

Schrader, J. M., Chapman, S. J., and Uhlenbeck, O. C. (2009). Tuning the affinity of aminoacyl-tRNA to elongation factor Tu for optimal decoding. *Proc Natl Acad Sci USA* 108, 5215–5220.

Schrader, J. M., Chapman, S. J., and Uhlenbeck, O. C. (2011). Tuning the affinity of aminoacyl-tRNA to elongation factor Tu for optimal decoding. *Proc Natl Acad Sci USA* 108, 5215–5220.

Schuette, J. –C., Mruphy IV, F. V., Kelley, A. C., Weir, J. R., Giesebrecht, J., Connell,

S. R., Loerke, J., Mielke, T., Zhang, W., Penczek, P. A., Ramakrishnan, V., and Spahn, C. MT. (2009). GTPase activation of elongation factor EF-Tu by the ribosome during decoding. *EMBO J* 28, 755–765.

Shimizu, Y., Inoue, A., Tomari, Y., Suzuki, T., Yokogawa, T., Nishikawa, K., and Ueda, T. (2001). Cell free translation reconstituted with purified components. *Nat Biotechnol* 19, 751–755.

Shin, D., Sinkeldam, R. W., and Tor, Y. (2011). Emissive RNA alphabet. *J Am Chem Soc* 133, 14912–14915.

Shin, Y. C., Yoon, J. H., Jang, T. H., Kim, S. Y., Do Heo, W., So, I., Jeon, J. H. & Park, H. H. (2012). Crystal structure of Rab6A'(Q72L) mutant reveals unexpected GDP/Mg²⁺ binding with opened GTP-binding domain. *Biochem Biophys Res Commun* 424, 269–273.

Shine, J., and Dalgarno, L. (1974). The 3'-terminal sequence of *Escherichia coli* 16S ribosomal RNA: complementarity to nonsense triplets and ribosome binding sites. *Proc Natl Acad Sci USA* 71, 1342–1346.

Sinkeldam, R. W., Greco, N. J., and Tor, Y. (2010). Fluorescent analogs of bimolecular building blocks: design, properties and applications. *Chem Rev* 110, 2579–2619.

Srivatsan, S. G., Greco, N. J., and Tor, Y. (2008). A highly emissive fluorescent nucleoside that signals the activity of toxic ribosome-inactivating proteins. *Angew Chem Int Ed Engl* 47, 6661–6665.

Stark, H., Rodnina, M. V., Rinke-Appel, J., Brimacombe, R., Wintermeyer, W., and Heel, M. V. (1997). Visualization of elongation factor Tu on the *Escherichia coli* ribosome. *Nature* 389, 403–406.

Stark, H., Rodnina, M. V., Wieden, H. –J., Zemlin, F., Wintermeyer, W., and Heel, M. V. (2002). Ribosome interaction of aminoacyl-tRNA and elongation factor Tu in the codon-recognition complex. *Nat Struct Biol* 9, 849–854.

Stevens, B., Chen, C., Farrell, I., Zhang, H., Kaur, J., Broitman, S. L., Smilansky, Z., Cooperman, B. S., and Goldman, Y. E. (2012). FRET-based identification of mRNAs undergoing translation. *PLoS One* 7, e38344.

Studer, S.M., Feinberg, J.S., and Joseph, S. (2003). Rapid kinetic analysis of EF-G-dependent mRNA translocation in the ribosome. *J Mol Biol* 327, 369–381.

Subramanian, A. R., and Dabbs, E. R. (1980). Functional studies on ribosomes lacking protein L1 from mutant *Escherichia coli*. *Euro J Biochem* 112, 425–430.

Szaflarski, W., Vesper, O., Teraoka, Y., Plitta, B., Wilson, D. N., and Nierhaus, K. H. (2008). New features of the ribosome and ribosomal inhibitors: non-enzymatic recycling, misreading and back-translocation. *J Mol Biol* 380, 193–205.

Tedin, K., Moll, I., Grill, S., Resch, A., Graschopf, A., Gualerzi, C. O., and Blasi, U. (1999). Translation initiation factor 3 antagonizes authentic start codon selection on leaderless mRNAs. *Mol Microbio* 31, 67–77.

Tsai, A., Petrov, A., Marshall, R. A., Korlach, J., Uemura, S., and Puglisi, J. D. (2012). Heterogeneous pathways and timing of factor departure during translation initiation. *Nature* 487, 390–393.

Uemura, S., Aitken, C. E., Korlach, J., Flusberg, B. A., Turner, S. W., and Puglisi, J. D. (2010). Real-time tRNA transit on single translating ribosomes at codon resolution.

Nature 464, 1012–1017.

Vale, R. D. (2008). Microscopes for Fluorimeters: The Era of Single Molecule Measurements. *Cell* 135, 779–785.

Valle, M., Sengupta, J., Swami, N. K., Grassucci, R. A., Burkhardt, N., Nierhaus, K. H., Agrawal, R. K., and Frank, J. (2002). Cryo-EM reveals an active role for aminoacyl-tRNA in the accommodation process. *EMBO J* 21, 3557–3567.

Valle, M., Zavialov, A., Li, W., Stagg, S. M., Sengupta, J., Nielsen, R. C., Nissen, P., Harvey, S. C., Ehrenberg, M., and Frank, J. (2003a). Incorporation of aminoacyl-tRNA into the ribosome as seen by cryo-electron microscopy. *Nat Struct Biol* 10, 899–1074.

Valle, M., Zavialov, A., Sengupta, J., Rawat, U., Ehrenberg, M., and Frank, J. (2003b). Locking and unlocking of ribosomal motions. *Cell* 114, 123–134.

Vanzi, F., Vladimirov, S., Knudsen, C. R., Goldman, Y. E., and Cooperman, B. S. (2003). Protein synthesis by single ribosomes. *RNA* 9, 1174–1179.

Veigel, C., Wang, F., Bartoo, M. L., Sellers, J. R., and Molloy, J. E. (2002). The gated gait of the processive molecular motor, myosin V. *Nat Cell Biol* 4, 59–65.

Vicens, Q., and Westhof, E. (2003) RNA as a drug target: the case of aminoglycosides. *Chembiochem* 4, 1018–1023.

Villa, E., Sengupta, J., Trabuco, L. G., LeBarron, J., Baxter, W. T., Shaikh, T. R., Grassucci, R. A., Nissen, P., Ehrenberg, M., Schulten, K., and Frank, J. (2009). Ribosome-induced changes in elongation factor Tu conformation control of GTP hydrolysis. *Proc Natl Acad Sci USA* 106, 1063–1068.

Voet, D., Voet, J. G., and Pratt, C. W. (2006). *Fundamentals of biochemistry: life at the molecular level*, 2nd edn (New York: Wiley).

Voorhees, R. M., Schmeing, T. M., Kelley, A. C. and Ramakrishnan, V. (2010). The mechanism for activation of GTP hydrolysis on the ribosome. *Science* 350, 835–838.

Wahl, M. C., Will, C. L., and Lührmann, R. (2009). The spliceosome: design principles of a dynamic RNA machine. *Cell* 136, 701–718.

Wang, L., Yang, F., Zhang, D., Chen, Z., Xu, R. M., Nierhaus, K. H., Gong, W., and Qin, Y. (2012). A conserved praline switch on the ribosome facilitates the recruitment and binding of trGTPases. *Nat Struct Mol Biol* 19, 403–411.

Wang, Y., Qin, H., Kudaravalli, R. D., Kirillov, S. V., Dempsey, G. T., Pan, D., Cooperman, B. S., and Goldman, Y. E. (2007). Single-molecule structural dynamics of EF-G-ribosome interaction during translocation. *Biochemistry* 46, 10767–10775.

Watson, J. D., and Crick, F. H. (1953a). Genetical implications of the structure of deoxyribonucleic acid. *Nature* 171, 964–967.

Watson, J. D., and Crick, F. H. (1953b). Molecular structure of nucleic acids; a structure for deoxyribose nucleic acid. *Nature* 171, 737–738.

Weixlbaumer, A., Jin, H., Neubauer, C., Voorhees, R. M., Petry, S., Kelley, A. C., and Ramakrishnan, V. (2008). Insights into translational termination from the structure of RF2 bound the ribosome. *Science* 322, 953–956.

Whitford, P. C., Geggier, P., Altman, R. B., Blanchard, S. C., Onuchic, J. N., and Sanbonmatsu, K. Y. (2010). Accommodation of aminoacyl-tRNA into the ribosome involves reversible excursions along multiple pathways. *RNA* 16, 1196–1204.

Wilson, D.N., and Doudna Cate, J.H. (2012). The structure and function of the eukaryotic ribosome. *Cold Spring Harb Perspect Biol* 4, a011536.

Wimberly, B. T., Brodersen, D. E., Clemons, W. M., Morgan-Warren, R. J., Carter, A. P., Vornrhein, C., Hartsch, T., and Ramakrishnan, V. (2000). Structure of the 30S ribosomal subunit. *Nature* 407, 327–339.

Wohlgemuth, I., Pohl, C., and Rodnina, M. V. (2010). Optimization of speed and accuracy of decoding in translation. *EMBO J* 29, 3701–3709.

Wohlgemuth, I., Pohl, C., Mittelstaet, J., Konevega, A.L., and Rodnina, M.V. (2011). Evolutionary optimization of speed and accuracy of decoding on the ribosome. *Philos Trans R Soc Lond B Biol Sci* 366, 2979–2986.

Xie, Y., Dix, A. V., and Tor, Y. (2009). FRET enabled real time detection of RNA-small molecule binding. *J Am Chem Res* 131, 17605–17614.

Xie, Y., Dix, A. V., and Tor, Y. (2010). Antibiotic selectivity for prokaryotic vs. eukaryotic decoding site. *Chem Commun* 46, 5542–5544.

Yonath, A. (2010). Polar bears, antibiotics, and the evolving ribosome. *Angew Chem Int Ed* 49, 4340–4354.

Yusupov, M. M., Yusupova, G. Z., Baucom, A., Lieberman, K., Earnest, T. N., Cate, J. H. D., and Noller, H. F. (2001). Crystal structure of the ribosome at 5.5 Å resolution. *Science* 292, 883–896.

Yusupova, G., Jenner, L., Rees, B., Moras, D., and Yusupov, M. (2006). Structural basis for messenger RNA movement on the ribosome. *Nature* 444, 391–394.

Zaher, H. S., and Green, R. (2009a). Fidelity at the molecular level: lessons from protein synthesis. *Cell* 136, 746–762.

Zaher, H. S., and Green, R. (2009b). Quality control by the ribosome following peptide bond formation. *Nature* 457, 161–166.

Zaher, H. S., and Green, R. (2011). A primary role for release factor 3 in quality control during translation elongation in *Escherichia coli*. *Cell* 147, 396–408.

Zhang, W., Dunkle, J.A., and Cate, J.H.D. (2009). Structures of the ribosome in intermediate states of ratcheting. *Science* 325, 1014–1017.

Zhou, J., Lancaster, L., Trakhanov, S., and Noller, H. F. (2012). Crystal structure of release factor RF3 trapped in the GTP state on a rotated conformation of the ribosome. *RNA* 18, 230–240.